Development of Fe-Based Nanocomposites for Water Treatment and Methane Generation

ラマダン，エム，エム，エルジャマル

出版情報：Kyushu University, 2021, 博士（学術）, 課程博士
バージョン：
権利関係：

九州大学
KYUSHU UNIVERSITY

Ph.D. Thesis on

Development of Fe-Based Nanocomposites for Water Treatment and Methane Generation

by

Ramadan M. M. Eljamal

Department of Advanced Environmental Science and Engineering,
Interdisciplinary Graduate School of Engineering Sciences,

Kyushu University, Fukuoka,

Japan

September 2021

Development of Fe-Based Nanocomposites for Water Treatment and Methane Generation

A THESIS SUBMITTED IN PARTIAL FULLFILMENT OF THE

REQUIRMENTS FOR THE DEGREE OF

Doctor of Philosophy (Ph.D.)

By

Ramadan M. M. Eljamal

Department of Advanced Environmental Science and Engineering,

Interdisciplinary Graduate School of Engineering Sciences,

Kyushu University,

Japan

Abstract

Nanoscale zero-valent iron (Fe^0) has been proved as one of the effective materials for water treatment and environmental applications. However, Fe^0 particles tend to aggregate rapidly due to their magnetic properties. The aggregation of Fe^0 particles decreases their efficiency when they used to treat the contaminated water. Therefore, the first project of the current thesis aimed to produce Fe^0 particles with excellent properties (less aggregation and high reactivity). To achieve this goal, Fe^0 particles were stabilized using four different polymers, including polyacrylamide (PAA), carboxymethyl cellulose (CMC), Polyethylene sorbitan monolaurate (PSM) and polyvinylpyrrolidone (PVP), aiming to find the best polymer for stabilizing Fe^0 particles.

The Fe^0 particles were characterized before and after being stabilized using scanning electron microscopy coupled to energy dispersive x-ray spectroscopy, x-ray diffraction and fourier transform infrared analyses for surface investigation and mechanisms detection. Besides, transmission electron microscopy was used to examine the surface morphology of Fe^0 before and after the stabilization process. This was followed by investigating the performance of Fe^0 and the stabilized Fe^0 for the removal of nitrate and phosphorus from the contaminated water. Nitrate and phosphorus were chosen as targeted contaminates due to their different removal mechanism by Fe^0. These polymers were used at different mass ratios varied between 0.04 and 0.40 % to acquire the optimal mass ratio with Fe^0 particles for achieving the highest removal of nitrate and phosphorus along with improving the particle characteristics of Fe^0.

Among four polymers used in this study, PVP was the best for stabilizing Fe^0 particles to achieve 97.7% removal of nitrate compared to 55.6% using the non-stabilized particles. But, for phosphorus removal, PAA was the best among the others for offering Fe^0 with the highest adsorption capacity in which the removal of phosphorus reached 97 % using the stabilized Fe^0 particles with PAA, and 76.3% using the non-stabilized particles. However, when it comes to remove two different contaminates by two different mechanisms such as nitrate and phosphorus using Fe^0, PAA was the best among the others to stabilize Fe^0 for enhancing both nitrate and phosphorus removal with a removal efficiency of 99% and 97%, respectively.

The second project of this thesis covers the use of the coated Fe^0 in anaerobic digesters to improve methane production rate. The Fe^0 particles were modified through surface coating using $Mg(OH)_2$ as a coating layer following thermal deposition method. $Mg(OH)_2$ was chosen to coat Fe^0 particles due to its superior performance in controlling and slowing the corrosion reaction of Fe^0. The coated Fe^0 particles with $Mg(OH)_2$ were applied in the anaerobic digesters to increase methane generation by stimulating methanogens bacteria. The characteristics of the coated Fe^0 were investigated using different techniques including TEM, SEM-EDX and XRD. Different coating ratios of $Mg(OH)_2$ to Fe^0 were used in the anaerobic digesters to acquire the optimum coating ratio for achieving high methane production rate. Also, the effect of different dosages and dosing time factor of the coated/Fe^0 were investigated. Results showed that the coated Fe^0 improved biogas and methane production by 25% and 46.6%, respectively with respect to the control and bare/Fe^0. Moreover, when it scaled up in a lab-scale semi-continuous system, methane production was enhanced by 120% with respect to the control by the addition of 25mg of coated/Fe^0 particles per gVS.

In the third project of this thesis, Fe^0 was used to accelerate the conversion of waste sludge to aerobic granules and increase the removal efficiency of contaminants from wastewater using Sequencing Batch Reactors system (SBR). Two sequencing batch reactors (SBR) were simultaneously and automatically operated in a cyclic batch mode for sixty days with adding 10 mg/L of Fe^0 particles to the influent wastewater tank of SBR2, whereas SBR1 was operated as a control. The reactors were fed with synthetic wastewater (3 liters per cycle and each cycle lasted for 6 hr.) and acclimated with seed sludge collected from a full-scale municipal wastewater treatment plant in Istanbul. The removal efficiency of COD, ammonia and phosphate increased with the time in the reactors, and almost complete removal was observed after the formation of aerobic granules. The addition of Fe^0 to SBR2 on day 24th slightly increased the removal efficiency of contaminants from wastewater and stimulated the production of Extracellular Polymeric Substances (EPS) including protein and carbohydrate by 23% and 42%, respectively. Moreover, Fe^0 has shorted the formation of anaerobic granules in SBR2. Finally, microbial community analysis showed that the addition of Fe^0 to SBR2 increased the growth rate of some bacterial species such as Rhizobiales and Xanthomonadales and decreased others such as Clostridiales, confirming that the effect of Fe^0 particles on bacterial growth was genera dependent.

Acknowledgements

The whole praise, prostrations and supplications are to Allah who aided me in every moment and helped me in finishing this work.

The studies presented in this dissertation were completed and submitted in partial fulfillment of the requirements for the degree of Doctor of Philosophy (Ph.D.) from Kyushu University, Interdisciplinary Graduate School of Engineering Sciences, Department of Advanced Environmental Science and Engineering.

I would like to express my sincere gratitude to Prof. Osama Eljamal for his supervision, guidance, support, and countless efforts in achieving this work, many thanks.

I would like to thank the readers of this dissertation Prof. Yuji Sugihara, Prof. Aya Hagishima, prof. Jun Tanimoto and Assoc. Prof. Osama Eljamal for assessing this thesis and giving valuable review comments and questions.

Also, I want to thank Prof. Aya Hagishima for her support, help, and cooperation throughout this study, my sincere gratitude to her.

I am indebted to Prof. Gulsum Yilmaz my internship supervisor at Istanbul University for her strong support and cooperation.

I should be thankful to prof. Yuji Sugihara for his support in carrying out and achieving this work.

I would like to thank prof. Jun Tanimoto, the director of Green Asia program which I belong to, and all staff in Green Asia program for their support and cooperation.

Finally, I would like to thank Dr. Ahmed Kahlil for his cooperation and assistance in achieving this work and also would like to thank all my colleagues for their cooperation.

Ramadan M. M. Eljamal

Table of Contents

Abbreviation

Abbreviation	Definition	Page
Fe^0	Nanoscale zero-valent iron	2
VFAs	volatile fatty acids VFAs	5
TEM	Transmission electron microscopy	9
SEM	Scanning electron microscopy	9
XRD	X-ray diffraction analysis	9
FTIR	Fourier transform infrared	9
EPS	Extracellular polymerics substances	10
SBRs	Sequencing batch reactors	10
CMC	Carboxymethyl cellulose sodium salt, high viscosity	14
PAA	Polyacrylamide	14
PSM	Polyethylene sorbitan monolaurate	14
PVP	Polyvinylpyrrolidone	14
DDIW	Deoxygenated deionized water	16
OLR	Organic loading ratio	19
CFU	Colony-forming unit	20
NGSM	Next Generation Sequencing (NGS)–Based Metagenomics	22
TS	Total solids	22
TVS	Total volatile solids	22
COD	Chemical oxygen demand	22
MLSS	Mixed liquor suspended solids	23
MLVSS	Mixed liquor volatile suspended solids	23
SVI	Sludge volume index	23
GC	Gas chromatograph	23
TCD	Thermal conductivity detector	23
EDX	Energy dispersive X-ray	36
IEP	Isoelectric point	49
q_s	Maximum adsorption capacities	53

Abbreviation	Definition	Page
AD	Anaerobic digestion	64
A	Methane production potential	93
μ_m	Maximum methane production	93
λ	lag phase	93
Y_{pre}	Predicted methane values	93
Y_{exp}	Experimental methane values	93
%Δ	Difference between predicted and experimental values	93
PAA/Fe^0	Polyacrylamide/iron nanoparticles	44
CMC/Fe^0	Carboxymethyl cellulose/iron nanoparticles	48
PVP/Fe^0	Polyvinylpyrrolidone/iron nanoparticles	50
PSM/Fe^0	Polyethylene sorbitan monolaurate/iron nanoparticles	52
AGS	Aerobic granular sludge	100
SMP	Soluble microbial products	107
CAMP	Crassulacean Acid Metabolism plants	123
HRT	Hydraulic retention time	126

List of Figures

List of Tables

CHAPTER 1

INTRODUCTION

Chapter 1: Introduction

Nowadays, the world is suffering from increasing and exacerbating several environmental problems such as water pollution and environmental wastes. In response to that, researchers all over the world are working to solve the problems or find alternative solutions for such problems. Water pollution and environmental wastes are the most environmental problems that need to be solved. Recently, nanotechnology has been involved in the environmental fields to treat the contaminated water and accelerate finding renewable source of energy from the environmental wastes. Nanoscale zero-valent iron (Fe^0) has emerged as one of the most efficient materials, which can be used to treat contaminated water and to recover a renewable source of energy from environmental wastes. Therefore, this chapter starts with a background overview on the synthesis, modification, application, and limitation of Fe^0 nanoparticles. Also, discusses the role of Fe^0 nanoparticles in solving water pollution and improving the production of biofuels as a renewable source of energy, followed by the research objectives and the framework of the current dissertation.

1.1. Problem statement

Nowadays, the world is suffering from the significant consumption of clean water sources. Globally, the utilization of water supplies is doubled every 15 years because of the population growth. Along with increasing the consumption of clean water, water pollution is increasing all over the world due to the increased population and industrial activities, contributing to decrease the availability of clean water for human beings. For instance, various pollutants already reached water supplies in many areas in different countries, including heavy metals and emerging contaminants of pharmaceuticals. For these reasons, human societies are threatened by the risk of water pollution, in addition to the large decrease in the available freshwater sources. The World Health Organization (WHO) has declared that over than 40% of the world population use rare water resources. Thus, more than two billion people have no enough pure water access [1]. Specifically, over 780 million people suffer in finding clean drinking water sources. Nitrate and phosphorus are the most discharged contaminants to water bodies and are known as nutrient pollution. They come from animal waste, industrial process, septic systems, and agricultural runoff. The contamination of water bodies by these

contaminants causes several human health issues and environmental problems. For the environmental problems, the high release of phosphorus and nitrogen causes harmful effects of eutrophication to several water bodies around the world. The oxygen depletion, biodiversity reduction, lower light transmission and generation of algal blooms occur in the lakes and rivers when the concentration of phosphorus exceeds 0.02 mg/L at which eutrophication starts [2]. Regarding human health, nitrate (NO_3^-) contamination converts into nitrite NO_2^-, which in turn causes many diseases such as blue baby syndrome, liver damage, and cancer [3]. Therefore, it has become an urgent need to treat contaminated waters such as household and industrial wastewater to compensate for the lack of clean water sources. Interestingly, due to the high content of organic matter in the household wastewater, treatment of wastewater could provide a renewable source of energy by integrating the anaerobic digestion process to the treatment system. Converting the organic matters to methane gas through anaerobic digestion during the treatment process generates energy which will be a solution for the depletion of nonrenewable sources of energy. However, the low conversion rate of organic matter to methane by anaerobes is the main challenge that affects the performance of the anaerobic digestion process. Therefore, the main target of this dissertation is to treat the polluted water along with accelerating the production of biofuels as a renewable source of energy to maintain the environmental sustainability and human societies.

1.2. Background overview

It is a must to overview the background of the nanotechnology from synthesis to environmental applications to treat the contaminated water and accelerate finding an environmentally friendly source of energy.

1.2.1. Nanotechnology

Nanotechnology is the process used to produce materials at a level of nanoscale, ranging from 1 to 100 nm. Nowadays, nanotechnology includes different applications in different fields such as molecular engineering, environmental engineering, catalysis, electronics, semiconductors, molecular biology, surface science, etc. With this technology, materials can be fabricated in the nanoscale size with different physiochemical properties. These properties make the nanomaterials appropriate for different applications in many fields.

There are two main approaches that can be used to fabricate the nanomaterials, including the bottom-up and top-down approaches. The bottom-up approach uses to fabricate organic and inorganic composites by constructing the atoms to each other or molecules to each other. In the bottom-up approach chemical reactions can be used to fabricate the desired nanocomposites. Many chemical reactions can be included in the bottom-up approach, including reduction reaction, emulsion reactions, thermal deposition reaction, etc. On the other hand, the top-down approach can be used to break down the bulk materials to nano-scale dimensions. In the top-down approach, blocks of materials are broken by the means of mechanical techniques such as the use of high energy ball milling for nanoparticles production. Recently, the fabricated nanomaterials either using top-down or bottom-up approaches have been used in the environmental applications for many environmental remediation processes.

1.2.2. Application of nanotechnology for water treatment and energy generation

The application of nanotechnology in water treatment can take different forms such as sorption, membrane process, etc. Nanotechnology in the form of nanoparticles can be used to remove the harmful pollutants from water through different physical and chemical reactions, including adsorption, reduction, oxidation, and ions exchange. For instance, nanostructured graphene oxide has been used to remove the emerging contaminates (pharmaceutical) from water through the adsorption process [4].

Also, different types of nanomaterials including surfactant-modified zeolites [5], chitosan nanofibers [6], carbon nanotube [7], iron [8] and iron bimetallic nanoparticles [9], have been used to treat the contaminated water with different contaminates. Moreover, nanomaterials can be applied during the treatment process of the municipal wastewater as trace elements to improve the production of biofuels as a renewable source of energy [10].

Furthermore, nanomaterials can be applied to enhance the generation of biofuels using different types of environmental wastes such as food wastes, livestock manures, waste sludges, etc. The process which is used to generate biofuels from such feedstocks is known as the anaerobic digestion process.

In the anaerobic microbiological digestion process microorganisms generate energy and grow by hydrolyzing and metabolizing organic material in an oxygen-free environment resulting in the production of biogas. The anaerobic digestion process includes four stages, each requiring a specific group of microorganisms as described in Fig.1-1.
In the first stage of hydrolysis, the non-soluble and colloidal organic matter will be converted to soluble organic compounds.

Then, in the second stage of acidogenesis, the soluble organic compounds will be target for the acidifying bacteria to generate volatile fatty acids (VFAs) and CO_2. After that, in the acetogenesis, the generated volatile fatty acids in the previous stage of acidogenesis will be utilized to produce acetic acid and H_2.

Finally, in the methanogenesis stage, acetate, CO_2, and H_2 will be utilized generate to CO_2 and CH_4 gases as the final products of anaerobic digestion process.

So far, the low conversion rate of organic matter to methane during anaerobic digestion is the main limitation of applying this technology as dependable/renewable source of energy. To accelerate and improve the performance of anaerobic digestion process, nanomaterials have been used during the anaerobic digestion process as additives to accelerate the hydrolysis process of organic matter to be easily degraded for biogases generation. For instance, recently, CuO [11], ZnO [12], TiO_2, SiO_2, Al_2O_3 [13], and CeO_2 [14], and Fe_3O_4 [15] have been used to increase methane generation rate. The use of the nanomaterials had slight effect or sometimes negative effect on the performance of anaerobic digestion and biogas generation. Therefore, it a must to investigate the role of other nanomaterials to enhance the anaerobic digestion process, aiming to find an appropriate additive for methane production enhancement.

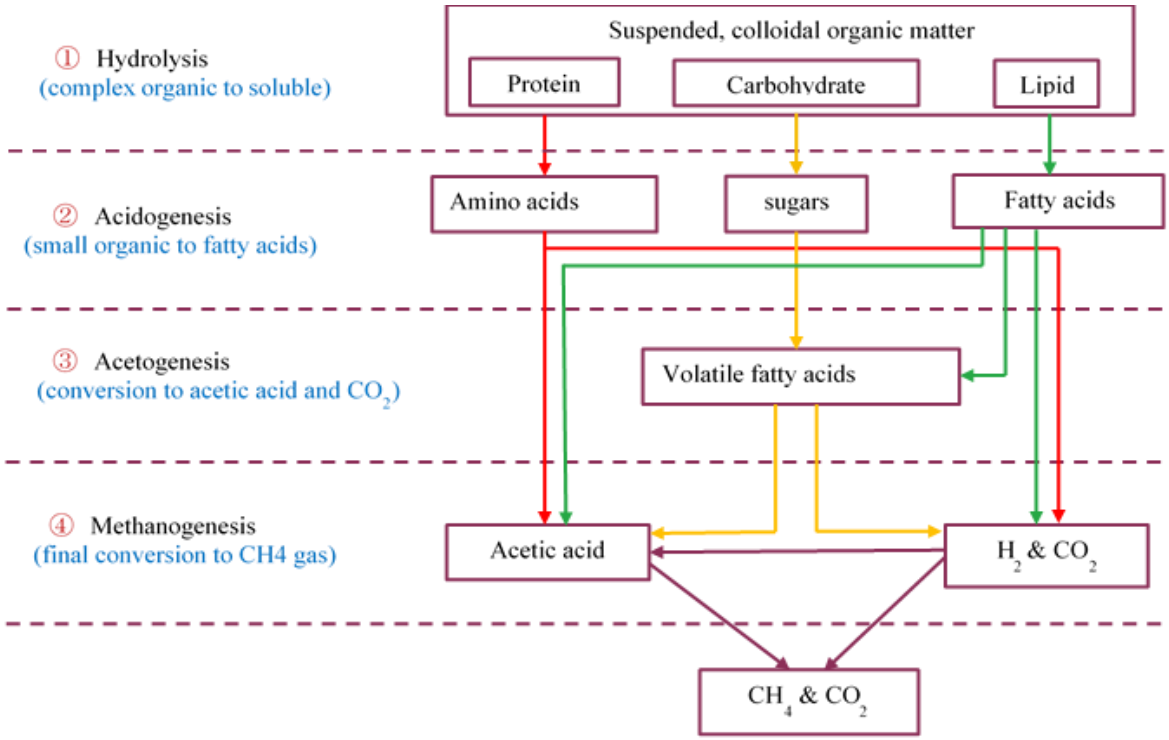

Fig. 1-1. Simplified schematic representation of the anaerobic degradation process

1.3. Nanoscale zerovalent iron (Fe^0)

Nanoscale zero-valent iron is one of the most used materials in water treatment. The extensive use of Fe^0 in environmental applications is mainly due to its unique properties, including small particle size, large surface area, high reducing power. More importantly, Fe^0 is a multifunctional material as it can react with the contaminants in water by different mechanisms, including adsorption, reduction, oxidation, precipitation and coprecipitation mechanisms. Moreover, Fe^0 is an excellent additive which can be added to the anaerobic digesters to improve the anaerobic digestion process through different mechanism. These mechanisms include the role of Fe^0 as an essential nutrient in stimulating the microorganisms in the anaerobic digesters for high conversion of organic matter to biogas. Besides, the addition of Fe^0 to the anaerobic digesters could improve the alkalinity by maintaining the pH value within the optimum range during the anaerobic digestion process. Also, Fe^0 as electron doner could accelerate the conversion of CO_2 to methane during the anaerobic digestion process.

1.3.1. Synthesis of Fe^0

The synthesis of Fe^0 particles can be accomplished using either top-down or bottom-up methods for nanomaterials fabrications as described in section 1.2.1. The top-down is a physical approach which is used to produce the Fe^0 particles by the physical means such as grinding ball milling, lithography, and abrasion. On the other hand, in the bottom-up approach, the Fe^0 is produced by implementing chemical reactions such as the reduction reaction. Most of these physical or chemical methods were emerged as attempts to increase the effectiveness of the produced Fe^0 particles along with reducing the production cost. One of the most used methods to prepare Fe^0 is the chemical reduction of iron ions by a strong reductant such as sodium borohydride. This method was used to synthesis Fe^0 particles in this dissertation, and the method is well explained in chapter 2. The use of chemical reduction method is easy and simple to be conducted in laboratories and can be controlled to reduce the particle size during the synthesis process.

1.3.2. Limitation of Fe^0 application

Despite the numerous features of Fe^0 particles, the particles still have many drawbacks that affect their real application. The aggregation of Fe^0 particles is the main obstacle that affects their performance when applied for environmental remediation. The reasons behind the aggregation of Fe^0 particles are summarized in the following points: 1) Ostwald ripening; its one of the reasons which indicate the dissolution of the small particles during the synthesis stages of Fe^0 particles. And then, the dissolved particles will be taken by the large particles, forming large aggregates. 2) Arrested precipitation: it includes the deposition of small particles on the nucleation centers during the synthesis process. 3) Particle interactions: the interactions between the formed particles caused by different forces, including van der Waals forces, magnetic and electric dipolar interactions, are also leading reasons behind the aggregation phenomena [16, 17]. The aggregation of Fe^0 particles reduces their specific surface area and mobility, thereby decreasing particle reactivity.

1.3.3. Modification of Fe^0 particles

Since the last decade, several attempts have been conducted to modify the Fe^0 surface to prevent particle aggregation and improve particle reactivity. These attempts include three main methods, including the use of supports [18], metals [19, 20], and surfactants [21]. Concerning the use of supports, numerous studies have been conducted to investigate the role of supporting and carrying Fe^0 particles using efficient supports such as activated carbon and graphene oxide in preventing particle aggregation [22]. Carrying Fe^0 particles on an inert supporter accelerates the removal rate of pollutants as the supporter serves as anti-aggregation, which improves the electron transfer for the reducible contaminants and surface area for high adsorption capacity [23].

For Fe^0 modification using second metal, several studies reported the use of second metal to break down the necklace-like structure of Fe^0 particles and show the particles with high dispersibility and reactivity. Coating or dipping Fe^0 particles with other metal has proven to improve its reactivity for the removal of several pollutants [24]. For instance, Takami et al. [25] investigated the role of copper addition in improving the reactivity of Fe^0 for phosphorus removal and found a remarkable improvement in the reactivity comparing with bare/Fe^0.

For surfactants, the surfactants can be used to disperse Fe^0 particles. Surfactants offer several advantages compared with using other metals and supports. Surfactants contribute to decreasing the size of Fe^0 particles, reducing zeta (ζ) potential for high stable dispersion, shifting isoelectric point to acidic medium, and decreasing agglomeration through steric and electrostatic stabilization. Surfactants are organic polymers that can be used to stabilize Fe^0 particles without posing any adverse effect on the local environment in the practical application. Moreover, surfactants can breakdown the aggregated particles through different mechanisms. Some surfactants can be used to alter the surface charge of Fe^0 to create an electrostatic repulsion between the particles to produce highly dispersed particles. Some other surfactants prevent the particle aggregation by creating a network around the particles. In terms of particle reactivity, it was reported that, stabilization of Fe^0 particles with various surfactants showed the particles with high reactivity. For instance, when it comes to TCE dichlorination, the stabilized Fe^0 was much reactive than that bare Fe^0 [26].

Additionally, Joo et al. [27] reported that the stabilized Fe^0 with carboxymethyl cellulose (CMC) offered higher removal efficiency for both lindane and atrazine under aerobic and anaerobic conditions. In a field study, the stabilized Fe^0 particles with CMC were found to be more efficient than bare-Fe^0 for treating a contaminated zone with PCE, TCE, and PCBs in northern Alabama [28]. In this field study, the stabilized Fe^0 degraded more than 88% of TCE over 596 days. In another field study, the emulsified Fe^0 particles were able to travel up to 2.1 m by pneumatic injection method [29]. It is worthy to mention that most of the field studies were conducted using stabilized Fe^0 particles. There are several reasons behind the use of the stabilized Fe^0 in the field studies. These reasons include the availability, high cost-effective, high viscosity, excellent physicochemical properties, and easy operation of the surfactants.

1.4. Research objectives

The main objective of the current thesis is to improve the reactivity, physiochemical properties, and reaction mechanisms of Fe^0 particles for various environmental applications, including water treatment and energy/methane generation. To do so, the plan has been drawn to achieve the following goals of the dissertation.

Firstly, it has been schemed to investigate the effect of various surfactants on the enhancement of Fe^0 reaction mechanisms. The target was to screen several surfactant to improve the reactivity of Fe^0 regarding two main mechanisms, including reduction and adsorption mechanisms, which are very common mechanisms to remove a wide verity of contaminants from water. Nitrate and phosphate were selected as a targeted contaminants to represent the reduction and adsorption mechanisms, respectively.

Secondly, the plan included to use of Fe^0 nanoparticles in the anaerobic digesters to improve the production of methane gas from waste sludge, which was used as a feedstock. To achieve this goal, the fresh Fe^0 particles were subject to the coating process using the thermal deposition method. The coating process was conducted to control/slow the corrosion reaction of Fe^0 particles and make them suitable additives in the anaerobic digesters. $Mg(OH)_2$ was used to coat the bare/Fe^0 particles due to its outstanding role in this process.

Thirdly, this dissertation has included a plan to design a sequencing batch reactor system to be automatically operated to treat the contaminated wastewater alongside with converting the waste sludge to aerobic granules, which will further be used to remove organic/inorganic pollutants from water. The above points are general explanations for three projects which have been implemented in this thesis. Here are in detail the main steps to achieve the above-mentioned objectives.

In the first project:

- To synthesize bare/Fe^0 particles with testing their performance in nitrate and phosphate removal under different conditions.
- To synthesis a stabilized/Fe^0 particles using four different polymers, including carboxymethyl cellulose sodium salt, high viscosity, polyacrylamide, Polyethylene sorbitan monolaurate and polyvinylpyrrolidone, in order to investigate their role in preventing the particle aggregation and find out the best one for improving the reaction mechanisms of Fe^0.
- To investigate the reactivity of the stabilized/Fe^0 for nitrate and phosphorus removal under various conditions.
- To fully characterize the Fe^0 particles before and after the stabilization process using different techniques, including TEM, SEM-EDX, XRD, and FTIR.

In the second project:

- To synthesize bare/Fe^0 particles and investigate their performance in improving methane generation rate from waste sludge during anaerobic digestion process.
- To coat the bare/Fe^0 particles using $Mg(OH)_2$ as a coating layer to control the reactivity of bare/Fe^0 particles.
- To investigate the role of the coated/Fe^0 particles with $Mg(OH)_2$ in improving biogas/methane generation rate form waste sludge.
- To investigate different factors that affect the enhancement of methane generation by the added Mg/Fe^0 nanoparticles such as the coating ratio of Mg to Fe^0, Dosing time of Mg/Fe^0 in the reactors, pH, etc.
- To demonstrate the effect of Mg/Fe^0 on bacterial growth during anaerobic digestion.

- Long-term investigation of methane generation using lab-scale semi-continuous system was carried out, to assess the feasibility and the productivity of methane production from waste sludge by the addition of Mg/Fe^0 nanoparticles.

In the third project:

- To develop sequencing batch reactor (SBR) for wastewater treatment and aerobic granules formation.
- To investigate the effect of Fe^0 addition in the sequencing batch reactor system on the removal efficiency of contaminants from wastewater and the conversion efficiency of waste sludge to aerobic granules as well.
- To demonstrate the role of the addition of Fe^0 on the generation of Extracellular polymerics (EPS) substance in the reactor.
- To highlight the effect of Fe^0 addition on the growth of bacterial species in the reactor.

1.5. Dissertation framework

This thesis has a framework consist of six chapters that explains the way of improving the reactivity of Fe^0 particles and their applications in different environmental issues. In general, problem identification, literature survey, dissertation's objectives, synthesis of Fe^0 particles, modification of Fe^0 particles, application of stabilized Fe^0 in water treatment, synthesis of coated Fe^0 with $Mg(OH)_2$, application of bare and coated Fe^0 in improving methane generation, material characterizations, analyses, batch experiments, mechanisms, and the role of Fe^0 in converting the waste sludge to aerobic granules were the main frameworks of this thesis. Hence, the framework was organized as follows:

Chapter 1 presents information concerning water pollution problems followed by an overview on the use of nanotechnology as a promising track of science to solve such problem. Also, this chapter covers the fabrications methods of Fe^0 particles, potential use of Fe^0 nanoparticles in environmental remediation, limitation of Fe^0 application and the modification of Fe^0 particles. Finally, the chapter showed the objectives which have been implemented in this thesis.

Chapter 2 presents the methodology of the implemented works including reagents, protocols, procedures, material characterization, operation of the treatment systems, measurements of bacterial growth, and synthesis procedures of iron-based nanoparticles.

Chapter 3 presents the main limitations of Fe^0 particles that affect their use in the real application for pollutants removal from water. Also, this chapter shows the stabilization of Fe^0 particles as one of the effective, low-priced, environmentally friendly approaches to solve the limitation of Fe^0 particles and increase their performance when they used in real application to remove contaminants from water. In this regard, four different polymers were used to overcome the drawbacks of Fe^0 particles to efficiently remove nitrate and phosphorus from contaminated waters.

Chapter 4 presents a new technique used in this research to increase the production rate of methane gas. The new approach includes the use of Fe^0 coated with $Mg(OH)_2$ as an additive to improve the anaerobic digestion process of waste sludge. The experiments were performed in a batch mode and then scaled up to a semi-continuous system. The results of these experiments were explained, compared to that of Fe^0, and the previously reported in the literature.

Chapter 5 presents an introduction about aerobic granulation technology as a new approach that can be used to convert the waste sludge to aerobic granules. And the limitation of this technology as it requires long time for full granulation. Also, the chapter showed the operation process of the sequencing batch reactor system and the methodology used in the work. Finally, the chapter presented the role of Fe^0 particles in accelerating the formation of aerobic granules and contaminants removal from wastewater using a sequencing batch reactor system (SBRS).

Finally, Chapter 6 presents the significant findings obtained from three projects on water treatment and energy generation with providing valuable recommendations for future research investigation. Additionally, the chapter displays the future research plan, expected results, and impacts.

CHAPTER 2

MATERIALS AND METHODS USED IN RESEARCH WORKS

Chapter 2: Materials and methods used in research works

This Chapter presents the methodology of the implemented works including reagents, protocols, procedures, material characterization, operation of the treatment systems, measurements of bacterial growth, and synthesis procedures of iron-based nanoparticles.

2.1. Chemicals

In chapter 3, Ferric chloride hexahydrate ($FeCl_3.6H_2O$, >99.0%, Junsei Chemical Co., Japan), sodium borohydride ($NaBH_4$, >98.0%, Sigma-Aldrich Inc., USA) and ethanol (C_2H_5OH, 99.5%, Wako Co., Japan) were used for the synthesis of Fe^0 particles. Sodium nitrate ($NaNO_3$ > 99.0% Junsei Chemical Co., Japan) and potassium dihydrogen phosphate (KH_2PO_4, 99.5%, Kanto Chemical Co., Japan), were used to prepare reactant stock solutions. Hydrochloric acid (HCl, 35–37%, Wako Co., Japan) and sodium hydroxide (NaOH , 97%, Wako Co., Japan) were used for pH adjustments. Carboxymethyl cellulose sodium salt, high viscosity (CMC, MP Biomedicals, LLC, France), polyacrylamide (PAA, Sigma-Aldrich Co., USA), Polyethylene sorbitan monolaurate (PSM, Sigma-Aldrich Co., USA) and polyvinylpyrrolidone (PVP, Sigma-Aldrich Co., USA) were used for the stabilization process of Fe^0.

In chapter 4, Magnesium nitrate hexahydrate $(Mg(NO)_3)_2{\cdot}6H_2O$, >99.0%, Sigma-Aldrich Inc., USA) and Sodium hydroxide (NaOH, >97.0%, Wako Co., Japan) were utilized to prepare $Mg(OH)_2$ shell to be used for coating process of Fe^0. Ethanol solution (C_2H_5OH, >99.5%, Wako Co., Japan) was used to disperse Fe^0 particles before being coated with $Mg(OH)_2$. The other material concerning the synthesis of Fe^0 particles were prepared using deoxygenated deionized water (DDIW, 18.2 MΩ·cm, Milli-Q filter). The waste sludge was collected from a municipal wastewater treatment plant in Fukuoka city, Japan and utilized as a feedstock for methane generation and Standard Plate Count Agar (APHA) CM0463 (OXOID LTD., England) was used for estimating bacterial growth.

In chapter 5, the seed sludge was collected from a full-scale wastewater treatment plant in Istanbul and used to form the aerobic granules. Fe^0 particles were added to SBR2 on day 24th (purity 98%, particle size 70 nm, surface area 15 $m^2\ g^{-1}$) to stimulate the growth of bacteria and increase the removal of contaminants in the SBRS.

The reactors were fed with synthetic wastewater to simulate the real wastewater and had the following chemical composition: glucose 165 mg L^{-1}; sodium acetate trihydrate 345 mg L^{-1}; meat extract 64 mg L^{-1}; peptone 100 mg L^{-1}; urea 32 mg L^{-1}; starch 75 mg L^{-1}; $KHPO_4$ 31.5 mg L^{-1}; $MgSO_4.7H_2O$ 6 mg L^{-1}; NH_4Cl 95 mg L^{-1}; KH_2PO_4 10 mg L^{-1}; $CaCl_2.2H_2O$ 5 mg L^{-1} and 0.3 mL L^{-1} of the trace elements. The trace elements were prepared using the following chemical compounds: ethylenediaminetetraacetic acid (EDTA), 52.5 g L^{-1}; $MnCl_2.7H_2O$, 3.97 g L^{-1}; (NH_4) $6MoO_{24}$, 1.21 g L^{-1}; $ZnSO_4.7H_2O$, 2.2 g L^{-1}; $CoCl_2.6H_2O$, 1.61 g L^{-1}; $CuSO_4.5H_2O$, 1.57 g L^{-1}. PBS solution was prepared by dissolving 0.656 g of $Na_3PO_412H_2O$, 1.104 g of $NaH_2PO_4H_2O$, 1.052 g of NaCl and 0.149 g of KCl in 2 L and then was used to analyze the Extracellular polymeric substances (EPS). Resin was used for cation exchange and added to the sludge samples for the analysis of EPS.

2.2. Synthesis of bare Fe^0 particles

The bare Fe^0 particles were synthesized following the bottom-up approach through the chemical reduction reaction as described in the following equation.

$$2FeCl_3.6H_2O + 6NaBH_4 + 18H_2O \rightarrow 2Fe^0 + 21H_2 + 6B(OH)_3 + 6NaCl \quad (1).$$

Briefly, the reactants of ferric chloride hexahydrate ($FeCl_3.6H_2O$, 25 g/L) and sodium borohydride ($NaBH_4$, 22 g/L) were prepared using DDIW and purged with nitrogen for 10 min. After that, sodium borohydride solution was added into ferric chloride solution dropwise using a peristaltic pump at a flow rate of 20 mL/min^{-1} in four neck flask reactor as described in Fig. 2.1.

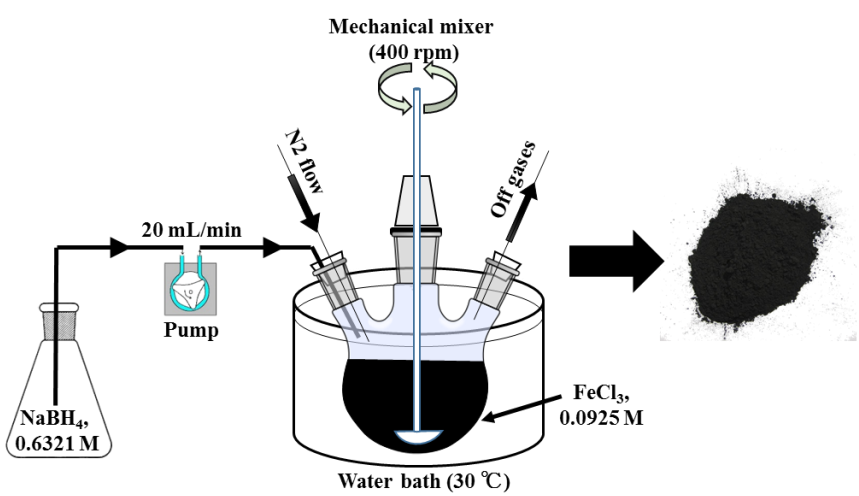

Fig. 2-1. The configuration of Fe^0 synthesis process.

During the synthesis process, N_2 gas was continuously provided to prevent particle oxidation and maintain anoxic conditions in the reactor. The other synthesis parameters such as temperature, reaction mixing speed and aging time were set at 30 ± 0.5 °C, 400 rpm, and 5 min, respectively. As soon as the aging time completed, the slurry of Fe^0 particles was washed using DDIW, dried, and separated using a vacuum filtration system. These procedures were based on the optimized synthesis conditions of Fe^0 particles accomplished in our previous work [30].

2.3. Synthesis of stabilized Fe^0 particles

The very same procedures which mentioned above in section 2.2 were used to prepare the stabilized Fe^0 particles with only adding and mixing the polymer with $FeCl_3$ solution. A specific concentration of each polymer (0.04, 0.08, 0.12, 0.2, and 2) was first mixed with $FeCl_3$ for half an hour before starting the reduction process using $NaBH_4$. Then, aging time was given for 5 min and the stabilized particles were washed using DDIW, dried, and separated using vacuum filtration system.

2.4. Synthesis of coated/Fe^0 particles

To prepare iron coated with $Mg(OH)_2$, the synthesized Fe^0 particles were dispersed in ethanol solution using ultrasonication at a concentration of 1 g/L following the controlled thermal deposition method [31]. In the synthesis procedure of the coated/Fe^0, 0.1 g of Fe^0 particles were dispersed in 100 mL of ethanol solution for 30 min using ultrasonication at a temperature of 50 °C. Thereafter, Mg^{2+} coating ions and OH^- were sequentially injected into Fe^0/ethanol solution at a flow rate of 2 mL/min. Mg^{2+} and OH^- solutions were prepared with a certain concentration and their injected volumes were varied to achieve different coating ratios on the surface of Fe^0 and maintain their molar ratios as described in the following equation.

$$Mg^{2+} + 2\,OH^- \rightarrow Mg(OH)_2\ (Mg^{2+}/OH: 0.5) \quad (2)$$

A continuous flow of nitrogen was provided during the coating process and after 1 h of aging time, the coated Fe^0 with $Mg(OH)_2$ was washed with ethanol, filtrated and dried using a vacuum filtration system.

2.5. Characterization

The synthesized bare, stabilized, and coated Fe^0 particles were characterized using different techniques. Transmission electron microscopy (TEM, JEM-ARM 200 F, JEOL Co., Japan) was used to examine the surface morphology, size, and particle dispersion. The average particle size and size distribution were also measured by ImageJ analysis for the obtained TEM images. Scanning electron microscopy coupled to energy dispersive X-ray spectroscopy (SEM-EDS, JCM-6060LA/VI, JEOL Co., Japan) was used to detect the elements proportions. X-ray diffraction analysis (XRD, TTR, Rigaku, Tokyo, Japan) was conducted to investigate the to investigate the surface components. XRD analysis was conducted using Cu Kα radiation (λ = 1.5418 Å) with an operating scanning range from 3° to 90° at a speed of 30° min^{-1}. The crystalline size was calculated using Scherrer's formula, $D = K\lambda / \beta\cos\theta$, where D is average crystalline size, K is the Scherrer's constant, λ is the wavelength of the incident copper X-ray (λ = 1.5418 Å), β is the full width at half maximum (FWHM) for all of the observed peaks, and θ is the angle of diffraction (Bragg's angle). Fourier transform infrared (FTIR) was used to identify the functional groups on the surface, particularly for the stabilized Fe^0 particles.

2.6. Evaluation methods of particle reactivity

2.6.1. Batch test for water treatment

In chapter 3, batch experiments were carried out to evaluate the performance of Fe^0 particles before and after being stabilized towards the removal of nitrate and phosphorus. Nitrate batch experiments were implemented by adding 0.25 g of bare or stabilized Fe^0 particles in 200 mL aqueous solution of nitrate with an initial concentration of 300 mg/L. Phosphorus batch experiments were conducted by adding 0.25 g bare or stabilized Fe^0 particles in 200 mL aqueous solution of phosphorus with an initial concentration of 100 mg/L. Nitrate and phosphorus solutions were purged using nitrogen gas to maintain anoxic conditions before adding the nanoparticles. Afterwards, the solutions were placed on the magnetic stirrer with mixing speed of 1000 rpm at the ambient temperature. At specific times, 2 mL of solution sample were withdrawn and filtered through a 0.22 μm membrane filter for the analysis process to evaluate the removal efficiency of nitrate and phosphorus.

When it comes to pH effect or to the effect of any other factor, the same experimental procedures were used with only changing the variable parameter. For instance, to study the effect of pH, nitrate and phosphorus solutions were adjusted using NaOH and HCl for four different pH values (3, 7, 9 and 12). The maximum uptake capacity and the efficiency of nitrate and phosphorus removal were determined by the following formulas, respectively.

$$q_t = (\mathrm{V}(Co - Ce))/m \quad (3)$$

$$\%E = (Co - Ce)/Co * 100 \quad (4)$$

where, where, q_t (mg/g) is the maximum uptake capacity at a specific time; V (L) is the total volume of the reactants; Co and Ce (mg/L) are the initial and final concentrations of contaminant; m (g) is the mass of adsorbent and E% is the removal efficiency of the contaminant.

2.6.2. Batch test for energy methane generation

Biochemical methane potential test (BMPT) was conducted to evaluate the effect of Fe^0-based particles on energy methane generation during the anaerobic digestion process. The BMPTs were implemented to evaluate the production rate of methane gas using the waste sludge as a feedstock. Fe^0 and coated/Fe^0 particles with three different coating ratios of $Mg(OH)_2$ shell (0.05, 0.5, 1%) were used and added to bioreactors using different concentrations ranged between 10 to 500 mg/L.

Another BMPTs were carried out to evaluate crucial paraments which affect anaerobic digestion process such as dosing time of the used nanoparticles and pH of the anaerobic digesters. The BMPT was performed using 200 mL serum vials with a working volume of 150 mL. After filling the bioreactors, they were bubbled with nitrogen for 2 min to eradicate the effect of oxygen and stablish the anerobic conditions. The bioreactors were then sealed with rubber stoppers and aluminum caps and placed in the incubator for fermentation at 40 ± 1 °C with constant agitation of 150 rpm. Regularly, biogas volume was determined using the water displacement method, followed by methane analysis using GC.

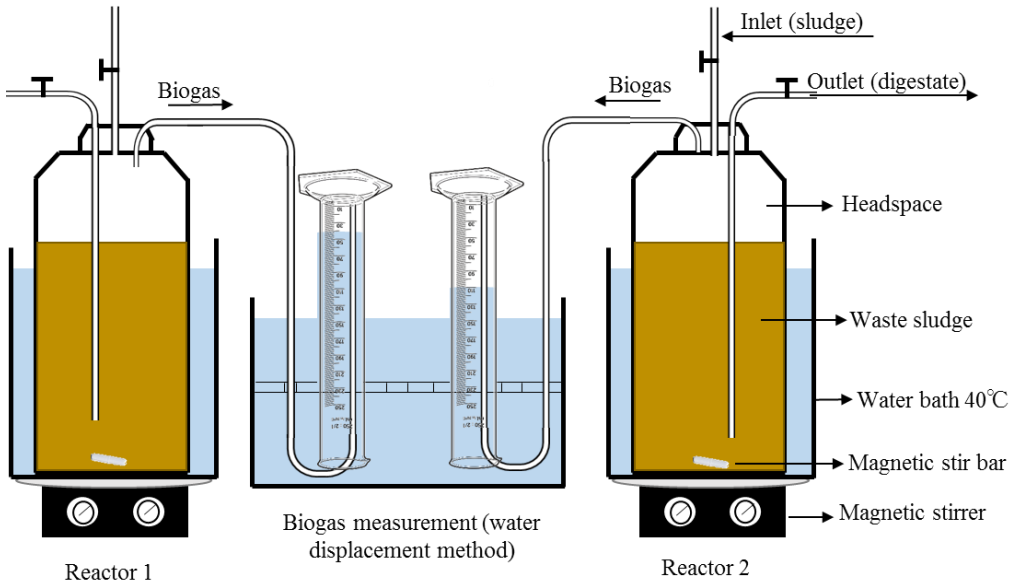

Fig. 2-2. The configuration of the semi-continuous system for biogas/methane generation.

2.6.3. Lab-scale semi-continues system for methane generation

Long-term investigation of methane generation using lab-scale semi-continuous system was carried out, to assess the feasibility and the productivity of methane production from waste sludge by the addition of $MgFe^0$ nanoparticles. Two bioreactors (R1&R2) were run with a working volume of 1000 mL of waste sludge. The reactors were operated for 24th days as a batch mode, and the semi-continuous operation was started on day 24th, in which 70 mL of waste sludge were fed every day to each reactor (Organic loading ratio (OLR) = 0.285gVS/L.d) and this was equivalent to the effluent volume of the rectors. Additionally, 25 mg of coated Fe^0 particles per gVS were added with the fed volume of waste sludge to R2, whereas R1 operated as a control. The reactors were put in water bath at 40℃ and continuously stirred using a magnetic stirrer. The produced biogas volume was regularly measured using the water displacement method, and methane volume was determined by analyzing the biogas compositions using gas chromatography.

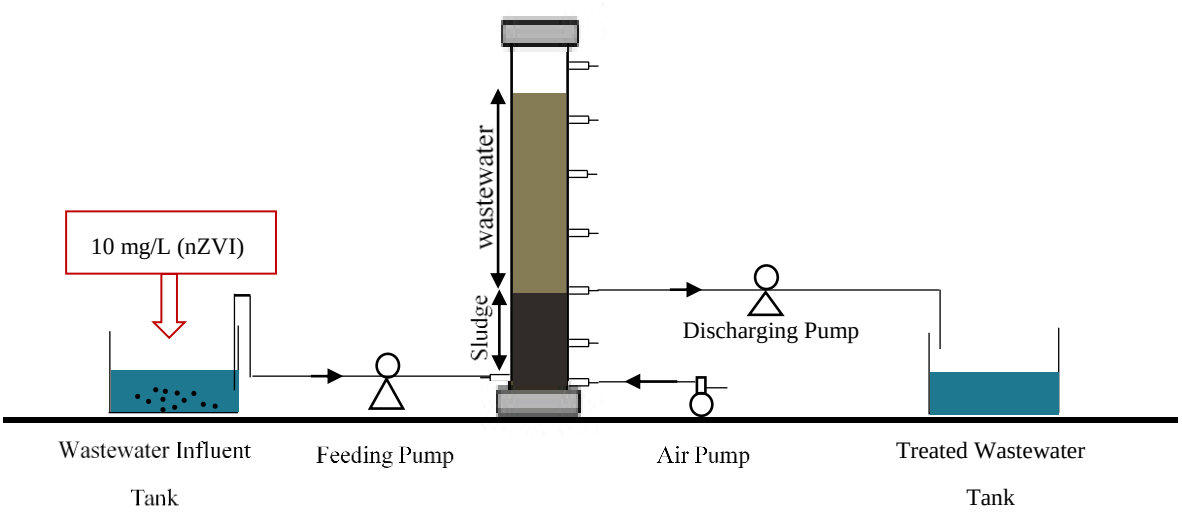

Fig. 2-3. The configuration of SBRS for wastewater treatment and granulation process.

2.6.4. Sequencing batch reactor system (SBRS)

To evaluate the effect Fe^0 particles on the conversion speed of waste sludge to aerobic granules and the removal efficiency of contaminants from wastewater, two symmetrical lab-scale sequencing batch reactors (SBRs) were simultaneously operated for sixty days with adding 10 mg/L of Fe^0 particles to the influent wastewater tank of SBR2, whereas SBR1 was operated as a control. The reactors had an internal diameter of 12 cm and a length of 60 cm, providing a working volume of 5 L as described in Fig2-2. The reactors were fed with synthetic wastewater and acclimated with 2 L of seed sludge collected from a full-scale municipal wastewater treatment plant in Istanbul.

The reactors were operated in a cyclic batch mode (4 cycles per day and each cycle lasted for 6 hr.) to treated 3 L of wastewater in each cycle. The cycle consisted of four successive phases: (1) 60 min static feeding, (2) 283 min aerobic reaction, (3) 2 min settling, (4) 15 min decanting. The third phase of settling was 1 hr. on the first day and gradually reduced to 2 min to promote the formation of aerobic granules. The settling time was slowly reduced within 23 days to avoid biomass loss from the reactors. The remaining cycle time from the settling phase was conveyed to the aeration phase.

Air was introduced via a diffuser tube aerator at the bottom of the reactor during the aeration phase. The reactors were operated automatically using three digital timers at room temperature 25 ± 3 °C.

2.7. Measurements of bacterial growth

2.7.1. Direct counting of bacterial colonies

In chapter 4, the bacterial growth rate was assessed by the direct counting of colonies using the colony-forming unit (CFU) technique [1, 32]. In detail, 1 mL of the original mixed culture was withdrawn from anaerobic digester and diluted by making serial dilutions (1:10, 1:100,1:1000 etc.) to ensure a countable plate. The molten agar (15 mL) was used and poured into the plate. After that, 1 ml of the diluted sample was cultivated in the molten agar using a sterile pipette. The bacterial colonies were carefully counted after 24 hr. of incubation at 37 °C and each colony was considered as a CFU. The number of bacterial cells present in the test sample was calculated using the formula: CFU = CFU* dilution factor *1/aliquot [33].

2.7.2. Extracellular polymeric substances analysis (EPS)

EPSs are the metabolic products generated by bacteria in the SBRS, representing their growth rate. Also, EPSs play a crucial role in the formation of aerobic granules in the SBRS. Therefore, it was necessary to analyze the main components of EPSs (protein and carbohydrate) in the SBRS. The analysis of EPSs was performed four times during the operation of SBRS, particularly on days 12, 30, 44, and 52. In detail, a specific sample volume was withdrawn from SBR1 & SBR2 based on the MLVSS concentration in each reactor. Then, samples were centrifuged at 9000 rpm for 15 min. After centrifuging, the supernatant was filtered using 0.45 and 0.22 microfilter, respectively, to analyze the soluble microbial products (SMP) of protein and carbohydrate.

On the other hand, EPSs components of protein and carbohydrate in soild precipitated sludge was measured following the chemical treatment method. In the chemical treatment, 30 mL of PBS solution (which was prepared by mixing 0.656 g of $Na_3PO_412H_2O$, 1.104 g of $NaH_2PO_4H_2O$, 1.052 g of NaCl, and 0.149 g of KCl in 2 L) was added to the precipitated sludge or granules and then centrifuged at 9000 rpm for 15 min. After centrifuging, the precipitate was mixed with an additional 100 mL of PBS solution and 35 g of resin and placed on the mixer for 3 hr. at 700 rpm.

Then, the supernatant of the resin-sludge solution was filtered using 0.45 and 0.22 microfilter, respectively to analyze the EPSs content. Finally, EPSs concentration of carbohydrate was obtained according to the anthrone-sulfuric acid method [34]. In detail, 2 mL of sample, 5 mL sulfuric acid, and 0.5 μm phenol were mixed and left 10 min for reaction. After that, the mixed solution was heated for 10 min at 30 °C and analyzed using T60UV-Visble Spectrophotometer at a wavelength of 480 nm. Whereas, EPSs concentration of protein was analyzed by following Lowry method [35, 36]. In detail, 100 μm of sample and100 μm of NaOH were mixed and heated for 10 min at 100 °C and then left 10 min for cooling before adding 100 μm Folin solution. After that, protein concentration was analyzed using T60UV-Visble Spectrophotometer at a wavelength of 750 nm.

2.7.3. Bacterial community analysis

Next Generation Sequencing (NGS)–Based Metagenomics were conducted to identify microbial community in the SBRS. The nested PCR approach was used to amplify microbial rDNAs. In the first round qPCRs were implemented using the Bact8f-Bact1541r primer set. Whereas, the Bact342f-Bact534r primer set was applied for the second round PCR. For Next Generation Sequencing (NGS)–Based Metagenomics, the protocol includes primer pair sequences for the V3 and V4 regions of the 16S rRNA, to create a single amplicon of 460 bp. It also includes overhang adapter sequences appended to the primer pair sequences for compatibility with the Illumina index and sequencing adapters. The Illumina adapter overhang nucleotide sequences-16SrRNA specific sequences,

5TCGTCGGCAGCGTCAGATGTGTATAAGAGACAG-CCTACGGGNGGCWGCAG 3 and5-GTCTCGTGGGCTCGGAGATGTGTATAAGAGACAG-GACTACHVGGGTATCTAATCC-3,

were for the forward and for the reverse primer, respectively. The first PCR was performed using Biospeedy® Proof Reading DNA Polymerase 2x Reaction Mix (Bioeksen Ltd. Co., Turkey) and 200 nm of each primer. The following program was performed on a Biorad CFX Connect Instrument (Bio-Rad Inc., U.S.A.): 95 °C for 3 min, 25 cycles of 95 °C for 30 s, 55 °C for 30 s, 72 °C for 30 s and 72 °C for 5 min. The PCR product was run on agarose gel to verify the size (550 bp) and purified using Biospeedy TM PCR Product Purification Kit (Bioeksen Ltd. Co., Turkey).

2.8. Water analysis

In chapter 3, nitrate and phosphorus were analyzed using UV–Vis spectrophotometer (DR 3900, Hach Co., USA). For nitrate analysis, dimethylphenol method was used to determine nitrate concentration at 345 nm. On the other hand, phosphorus was analyzed using USEPA PhosVer 3 at 880 nm which is the ascorbic acid method [37].

In chapter 4, Total solids (TS), Total volatile solids (TVS), and chemical oxygen demand (COD) were analyzed before and after the fermentation process following the standard methods [38]. The ORP (Oxidation–Reduction Potentials) and pH were measured using a pH meter (TPX-999si, Toko Co., Japan). Ferrous (Fe^{2+}) and Total iron concentrations were analyzed using 1,10-phenanthroline and USEPA FerroVer iron methods, respectively [39]. Subsequently, ferric iron (Fe^{3+}) concentration was directly estimated as: (Fe^{3+} (mg/L) = Total iron − Ferrous iron).

In chapter 5, the effluent of the SBRS was analyzed using T60UV- Visible Spectrophotometer for chemical oxygen demand (COD), nitrate (NO, nitrite (NO–N), orthophosphate (PO–P). Whereas ammonia (NH–N) concentration was analyzed using UV–Vis spectrophotometer (DR 3900, Hach Co., USA). Additionally, the mixed liquor suspended solids (MLSS), mixed liquor volatile suspended solids (MLVSS) and sludge volume index (SVI after 5 and 30 min) were analyzed inside the SBRS to evaluate the granulation presses according to Standard Methods [38].

2.9. Biogas analysis

In chapter 4, Gas chromatograph (GC, GL Sciences Inc., Japan) equipped with a thermal conductivity detector (TCD) was used to analyze the composition of the produced biogas.
In detail, 1 ml of the biogas was taken from the headspace of anaerobic digesters and immediately injected into the injector unit of GC for the separation process using a Hamilton gas-tight syringe (GL Sciences Inc., Japan).

The temperatures of the detector, injector, and oven were 60 °C, 80 °C, and 60 °C, respectively. The temperature of the injector was determined to be enough for making flash vaporization for the injected sample. But the temperatures of column and detector were determined to be enough for separating the gas mixture at the column stage and avoiding any condensation for the separated sample in the detector unit.

The argon gas was used as a mobile phase to push and carry the analyte through the column at a flow rate of 30 mL/min.

CHAPTER 3

STABILIZATION OF Fe^0 PARTICLES FOR WATER TREATMENT

Chapter 3: Stabilization of Fe^0 particles for water treatment

This chapter presents a literature survey about the limitations of Fe^0 particles when used on a large scale for pollutants removal from water and modifications used in literature to enhance the performance of Fe^0 particles, followed by the objectives conducted in this study on using polymeric stabilization to overcome the drawbacks of Fe^0 particles.

3.1. Introduction

Nanotechnology techniques have proven their efficiency for treating contaminated water with heavy metals, organic, inorganic, and chlorinated compounds [40-42]. Fe^0 (nanoscale zero-valent iron) is one of the efficient nanomaterials used for decontamination of the contaminated water. Fe^0 was wildly studied in lab-scale systems and applied in different sites to treat contaminated water in different zones [43]. The increasing interest in using Fe^0 for water treatment is mainly due to its strong reducing power ($E_0 = -0.44$ V). This feature makes Fe^0 capable of removing the reducible contaminants such as nitrate and chromium hexavalent [30]. Moreover, Fe^0 offers a large adsorption capacity for adsorbing various types of contaminants such as phosphorus [44]. In economic terms, Fe^0 is a cost-effective material, easy to produce, and easy to apply using various techniques, including a permeable reactive barrier (PRB) and injection wells [45].

Despite the above-mentioned features of Fe^0, there are several drawbacks of Fe^0 that require further investigation to be solved, including its high tendency of aggregation. The aggregation of Fe^0 is mainly occurs due to the magnetic attraction between the particles. The aggregation of Fe^0 particles limits the available surface area, which causes large drop in the reactivity towards the targeted contaminants [46].This problem significantly reduces the effectiveness of Fe^0 particles when used in practical applications.

Besides this aggregation phenomenon, Fe^0 is a very reactive material and rapidly gets oxidized if exposed to the surrounding media such as water and oxygen. The oxidation of Fe^0 particles is another problem that significantly deteriorates particle reactivity. In the literature, many efforts conducted to resolve these limitations and show Fe^0 particles with good characteristics and high reactivity.

Generally, three main methods have been used to improve the reactivity, mobility, stability, dispersibility, and longevity of Fe^0.

First, numerous studies have used a second metal to break down the neckline structure of Fe^0 particles and show the particles with high dispersibility and reactivity. Coating or dipping Fe^0 particles with other metal has proven to improve its reactivity for the removal of several pollutants [24]. For instance, Takami et al. [25] investigated the role of copper addition in improving the reactivity of Fe^0 for phosphorus removal and found a remarkable improvement in the reactivity comparing with bare/Fe^0.

Second, supporting and carrying Fe^0 particles using efficient supports such as activated carbon and graphene oxide is another way that can be used to prevent particle aggregation [22]. Carrying Fe^0 particles on an inert supporter accelerates the removal rate of pollutants as the supporter serves as anti-aggregation, which improves the electron transfer for the reducible contaminants and surface area for high adsorption capacity [23].

Third, Particles of nZVI have aggregated structures that can be dispersed through the stabilization process using different surfactants. Surfactants offer several advantages compared with using other metals and supporters. Surfactants contribute to decreasing the size of Fe^0 particles, reducing zeta (ζ) potential for high stable dispersion, shifting isoelectric point to acidic medium, and decreasing agglomeration through steric and electrostatic stabilization. Surfactants are organic polymers that can be used to stabilize Fe^0 particles without posing any adverse effect on the local environment in the practical application. Moreover, surfactants can breakdown the aggregated particles through different mechanisms. Some surfactants can be used to alter the surface charge of Fe^0 to create an electrostatic repulsion between the particles to produce highly dispersed particles. Some other surfactants prevent the particle aggregation by creating a network around the particles.

In terms of particle reactivity, it was reported that, stabilization of Fe^0 particles with various surfactants showed the particles with high reactivity. For instance, when it comes to TCE dichlorination, the stabilized Fe^0 was much reactive than that bare Fe^0 [26]. Additionally, Joo et al. [27] reported that the stabilized Fe^0 with carboxymethyl cellulose (CMC) offered higher removal efficiency for both lindane and atrazine under aerobic and anaerobic conditions.

In another field study, the stabilized Fe^0 particles with CMC were found to be more efficient than bare/Fe^0 for treating a contaminated zone with PCE, TCE, and PCBs in northern Alabama [28]. In this field study, the stabilized Fe^0 degraded more than 88% of TCE over 596 days. In another field study, the emulsified Fe^0 particles were able to travel up to 2.1 m by pneumatic injection method [29]. It is worthy to mention that most of the field studies were conducted using stabilized Fe^0 particles.

There are several reasons behind the use of the stabilized Fe^0 in the field studies. These reasons include the availability, high cost-effective, high viscosity, excellent physicochemical properties, and easy operation of the surfactants. However, the research efforts are low in removing the pollutants using the stabilized Fe^0 particles.

To the best of the author's knowledge, there are no reports on the effect of surfactants on the adsorption and reduction mechanisms of Fe^0 particles. Thereby, this work aimed to answer the following questions by finding the suitable polymer for each. What is the suitable polymer that can improve the reduction process of contaminants by Fe^0 particles? Which one can improve the adsorption process of contaminants by Fe^0? What if we need to remove two or three contaminants by different mechanisms? Can we find a polymer to enhance both the reduction and adsorption mechanisms of Fe^0 particles?

Following the main target of current research, four different polymers were used during the synthesis process to stabilize Fe^0 particles, including PAA, PVP, CMC, and PSM. Two different contaminants (nitrate & phosphorus) were chosen as targeted contaminants due to their various removal mechanisms by Fe^0 particles. Nitrate was used to evaluate the reducing power of Fe^0 particles as nitrate can be removed or transformed by the released electrons from the core of Fe^0 particles. On the other hand, phosphorus was chosen to assess to adsorption ability of Fe^0 particles as phosphorus mainly can be removed from water by the direct adsorption on the surface of Fe^0 particles.

The goals of this research were achieved by synthesizing Fe^0 particles following the pre-aggregation method. With this approach, each polymer was separately impregnated with ferric iron ions before starting the reduction process to produce dispersed zero-valent iron particles. It was followed by conducting deepen characterization for Fe^0 particles before and after being stabilized with the used polymers.

In another field study, the stabilized Fe^0 particles with CMC were found to be more efficient than bare/Fe^0 for treating a contaminated zone with PCE, TCE, and PCBs in northern Alabama [28]. In this field study, the stabilized Fe^0 degraded more than 88% of TCE over 596 days. In another field study, the emulsified Fe^0 particles were able to travel up to 2.1 m by pneumatic injection method [29]. It is worthy to mention that most of the field studies were conducted using stabilized Fe^0 particles.

There are several reasons behind the use of the stabilized Fe^0 in the field studies. These reasons include the availability, high cost-effective, high viscosity, excellent physicochemical properties, and easy operation of the surfactants. However, the research efforts are low in removing the pollutants using the stabilized Fe^0 particles.

To the best of the author's knowledge, there are no reports on the effect of surfactants on the adsorption and reduction mechanisms of Fe^0 particles. Thereby, this work aimed to answer the following questions by finding the suitable polymer for each. What is the suitable polymer that can improve the reduction process of contaminants by Fe^0 particles? Which one can improve the adsorption process of contaminants by Fe^0? What if we need to remove two or three contaminants by different mechanisms? Can we find a polymer to enhance both the reduction and adsorption mechanisms of Fe^0 particles?

Following the main target of current research, four different polymers were used during the synthesis process to stabilize Fe^0 particles, including PAA, PVP, CMC, and PSM. Two different contaminants (nitrate & phosphorus) were chosen as targeted contaminants due to their various removal mechanisms by Fe^0 particles. Nitrate was used to evaluate the reducing power of Fe^0 particles as nitrate can be removed or transformed by the released electrons from the core of Fe^0 particles. On the other hand, phosphorus was chosen to assess to adsorption ability of Fe^0 particles as phosphorus mainly can be removed from water by the direct adsorption on the surface of Fe^0 particles.

The goals of this research were achieved by synthesizing Fe^0 particles following the pre-aggregation method. With this approach, each polymer was separately impregnated with ferric iron ions before starting the reduction process to produce dispersed zero-valent iron particles. It was followed by conducting deepen characterization for Fe^0 particles before and after being stabilized with the used polymers.

In this regard, TEM, XRD, SEM-EDX, and FTIR were used to show the physiochemical properties of bare and stabilized Fe^0 particles and clarifying the adsorption mechanisms between the used polymers and Fe^0 particles. Polymers were examined during the synthesis process by considering various concentrations to acquire the optimal mass ratio with Fe^0 particles for achieving the highest removal rate of nitrate and phosphorus, followed by investigating crucial parameters that affect the removal of nitrate and phosphorus like contaminants concentrations and pH. Furthermore, adsorption isotherm and kinetic models were used to describe the adsorption mechanism and removal kinetic of nitrate and phosphorus by the bare and stabilized Fe^0. The present work of current chapter could have a significant contribution in the aspect of water treatment using nanotechnology material based on integrating Fe^0 particles with PAA as an effective polymer among the rest.

3.2. Batch experiments targeted nitrate and phosphorus removal

Batch experiments were conducted to investigate the effect of different polymers on the reactivity of Fe^0 for nitrate and phosphorus removal. More details were presented in chapter 2, section 2.6.1, explaining the reaction conditions of nitrate and phosphorus removal by bare and stabilized Fe^0.

3.3. Characterization of bare and stabilized Fe^0 particles

3.3.1. Morphology and dispersibility of Fe^0 particles

The morphological structure of Fe^0 particles was examined before and after the stabilization process using transmission electron microscopy. The shape and size of bare Fe^0 particles are shown in Fig. 3-1a. The particles were aggregated and appeared as necklace-like structure. It is the behavior of Fe^0 particles, which rapidly tend to form aggregates due to the magnetic attraction and the thermodynamic processes during the synthesis process. [47, 48]. To breakdown the necklace-like structure of bare Fe^0 particles, CMC was used as an anionic polymer to alter the surface charge of Fe^0 particles. CMC presented the Fe^0 particles with an excellent structure and low particle size. As shown in Fig.3-1b, CMC/Fe^0 particles were spherical, dispersed and not aggregated with an average particle size of 10 nm.

The improvement in the morphological structure of Fe^0 particles was attributed to the role of CMC in creating a strong electrostatic repulsion between the particles. Additionally, TEM images were taken for the stabilized Fe^0 particles with PAA as shown in Fig.3-1c.The stabilized PAA/Fe^0 particles were clearly trapped by the polymer matrix, therefore, the aggregation of Fe^0 was hindered by the stiffness of the polymer matrix. Fig. 3-1d shows the TEM image and size distribution of Fe^0 particles stabilized with PVP. The PVP/Fe^0 particles were spherical, darker, and dispersed. The dark color of PVP/Fe^0 indicates heavier atomic mass, whilst the grey color of bare/Fe^0 indicates lighter atomic mass, illustrating the reason behind the improved reactivity towards nitrate removal using such polymer.

PSM was used as an emulsifier to prevent the particle aggregation and make them as an oil droplet. The TEM image of the stabilized PSM/Fe^0 showed that the particles had a clear core-shell structure without forming any aggregates. The clouds of PSM were well observed around the particles, and the particles were completely separated and dispersed as shown in Fig. 3-1e. The average particle size of bare and the stabilized types of Fe^0 was in the following order; CMC/Fe^0 (9.53 nm) < bare/Fe^0 (65.4 nm) < PAA/Fe^0 (106.4 nm) < PSM/Fe^0 (106.6 nm) < PVP/Fe0(108.8 nm), indicating that CMC was the most efficient polymer for producing the particles with very low sizes.

It was observed that the stabilization of Fe^0 particles using PSM, PVP and PAA did not decrease the size largely as it was observed by using CMC. It could be attributed to the deposition of polymer molecules on the surface of Fe^0 particles during the synthesis process. Whereas CMC as anionic polymer provided a negative surface charge which led to improve the repulsive force between the particles to increase the dispersibility of Fe^0 particles and decrease their sizes.

In conclusion, anionic polymers such as CMC prevent particle aggregation through the electrostatic mechanism by altering the surface charge, and they are the best for producing the Fe^0 with small sizes. On the other hand, non-ionic polymers such as PAA, PVP, and PSM prevent particle aggregation through the steric mechanism by the deposition of polymer molecules on the surface of Fe^0.

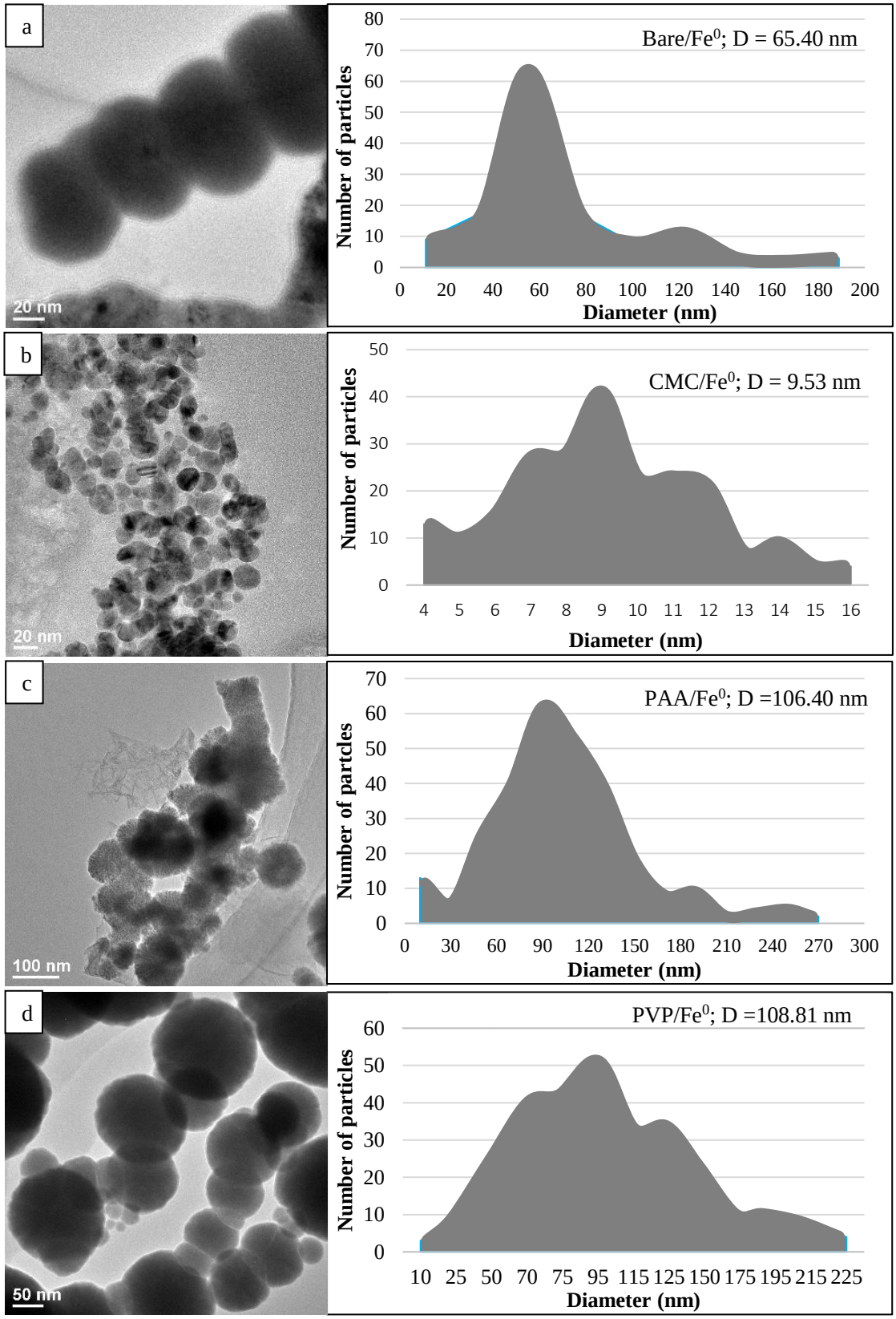
a
20 nm
Bare/Fe0; D = 65.40 nm
Number of particles
Diameter (nm)
b
20 nm
CMC/Fe0; D = 9.53 nm
Number of particles
Diameter (nm)
c
100 nm
PAA/Fe0; D =106.40 nm
Number of partcles
Diameter (nm)
d
50 nm
PVP/Fe0; D =108.81 nm
Number of particles
Diameter (nm)

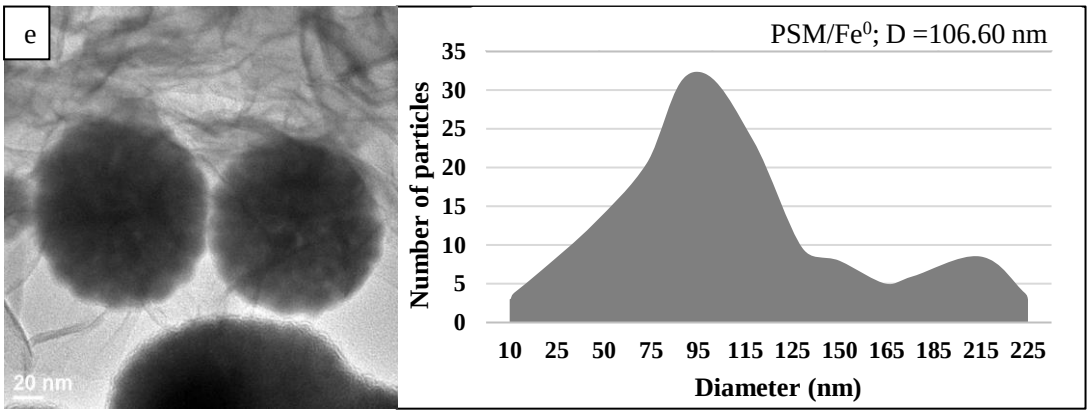

Fig. 3-1. TEM images and size analyses of Fe^0 particles; a) bare/Fe^0; b) CMC/Fe^0; c) PAA/Fe^0; d) PVP/Fe^0; and e) PSM/Fe^0

3.3.2. Surface composition

To investigate surface composition of Fe^0 particles before and after the stabilization process with four different polymers, XRD analysis was performed in the range from 0 to 90° (2θ). Fig.3-2 displays XRD spectrum for the bare and stabilized Fe^0. Results showed the formation of Fe^0 at 44.8°, 65.3° and 82.3° (2θ). The sharp peak of Fe^0 at 44.8° (2θ) indicates the high crystallinity and purity of the produced Fe^0. In the pure sample of Fe^0, the atoms were well arranged in a specific periodic manner. Therefore, during the analysis of Fe^0, X-ray scattered in a certain direction, which led to obtaining a sharp peak at 44.8 (2θ), indicating the pure and crystalline structure of bare/Fe^0.

On the other hand, the stabilization of Fe^0 particles with CMC, PVP, PAA, and PSM resulted in disrupting the periodic arrangement of iron atoms, which led to scattering X-ray in many directions. Thereby, the sharp peak of the bare/Fe^0 significantly decreased, confirming the amorphous structure of Fe^0 after being stabilized. As shown in Fig.3-2, XRD patterns of PAA/Fe^0, PVP/Fe^0, and PSM/Fe^0 exhibited more amorphous structure than CMC/Fe^0 and bare/Fe^0 following the order of PAA/Fe^0 > PVP/Fe^0 > PSM/Fe^0 > CMC/Fe^0 > bare/Fe^0. The amorphous structure of the stabilized Fe^0 could be also attributed to the finer sizes of the primary Fe^0 particles. Lin et al. [49], reported that the diffraction peaks largely decreased when the primary sizes of Fe^0 were less than 5 nm.

This fact was confirmed by calculating the crystalline size of bare and stabilized Fe^0 using Scherrer's equation. The results proved that the less crystalline size the more amorphous structure.

The crystalline size of bare and stabilized Fe^0 followed the order of PAA/Fe^0 (1.1 nm) < PVP/Fe^0 (1.7 nm) < PSM/Fe^0 (5.1 nm) < CMC/Fe^0 (6 nm) < bare/Fe^0 (10 nm) which is corresponding with XRD diffractograms. The amorphous structure of stabilized Fe^0 with detecting new compounds such as Fe_3C and $FeCO_3$ confirmed the adsorption of polymers on the surface of Fe^0 through chemical bonds.

Fig. 3-3 displays XRD patterns of bare and stabilized Fe0 particles after the reaction with nitrate and phosphorus under specific conditions (200 mL of nitrate (300mg/L), 200 mL of phosphorus (100 mg/L), 0.25 g of adsorbent). Results showed that the XRD patterns of the spent nanoparticles confirmed the combination of nitrate and phosphorus with Fe^0 through the chemical bonds. Phosphorus and nitrate adsorbed directly onto the surface of iron whereas, no links were observed between phosphorus, nitrate, and polymers, confirming the role of polymers to improve the reactivity only by enhancing the properties of Fe^0.

Surface properties of bare and stabilized Fe^0 were also investigated by SEM-EDX analysis. In this investigation, EDX analysis was applied for the SEM images to determine the elemental proportions and elemental mapping on the surface of Fe^0 particles. EDX spectrum indicated the presence of Fe and O as the main elemental components of bare/Fe^0. Iron and oxygen were detected on the surface with a weight percent of 93.7 and 6.3, respectively. Also, EDX analysis was performed for the stabilized Fe^0 with PAA. The results confirmed the presence of Fe, O, and C with a weight percent of 42.6, 31.6, and 25.7, respectively. In case of the stabilized Fe^0 with CMC, EDX showed Fe, C, O, and Na as the main elemental components on the surface of CMC/Fe^0. These elements were detected with a weight percent of 36, 32.9, 30.0, and 0.62, respectively

For the stabilized Fe^0 with PSM and PVP, EDX analysis confirmed the presence of C, O, and Fe as shown in Fig.3-4. The detection of C on the surface of Fe^0 particles after the stabilization process proved the adsorption of polymers on the surface of Fe^0 particles. Furthermore, the elemental mapping analysis indicated that the polymers nanoparticles were uniformly and well dispersed throughout the surface of Fe^0 particles.

The thermogravimetric analysis of the stabilized Fe^0 showed that the weight loss mainly occurred at temperature in the range from 25–200 °C, implying that the chemical decomposition of polymers starts when the sample was heated above 25 °C [50]

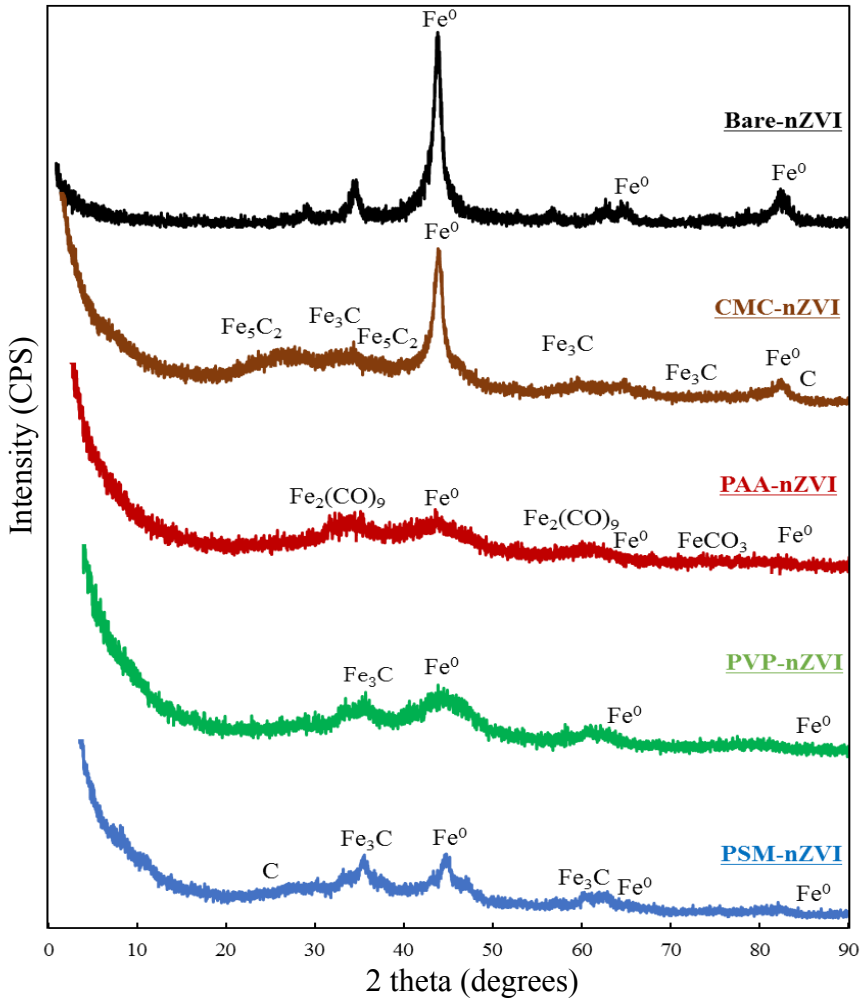

Fig. 3-2. XRD results of bare/Fe^0, CMC/Fe^0, PAA/Fe^0, PVP/Fe^0, and PSM/Fe^0

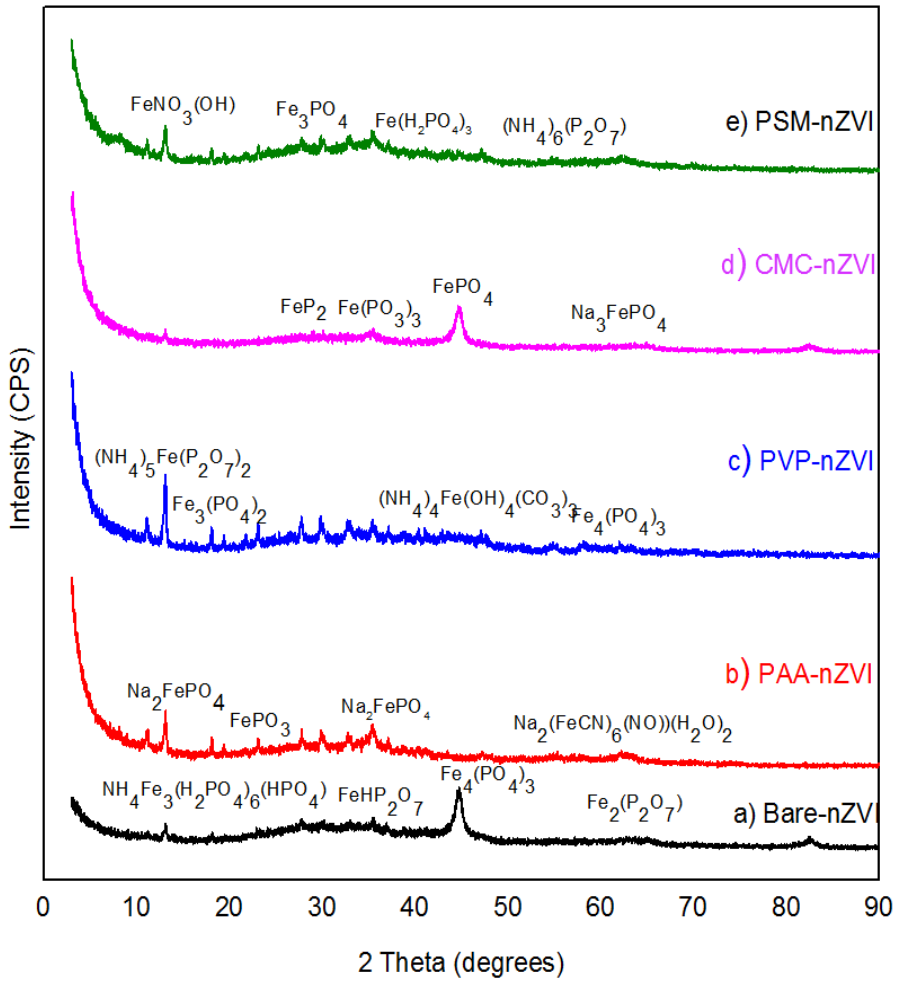

Fig.3-3. XRD results of bare/Fe^0, PAA/Fe^0, PVP/Fe^0, CMC/Fe^0, and PSM/Fe^0 after the reaction with the targeted contaminant (Nitrate and phosphorus).

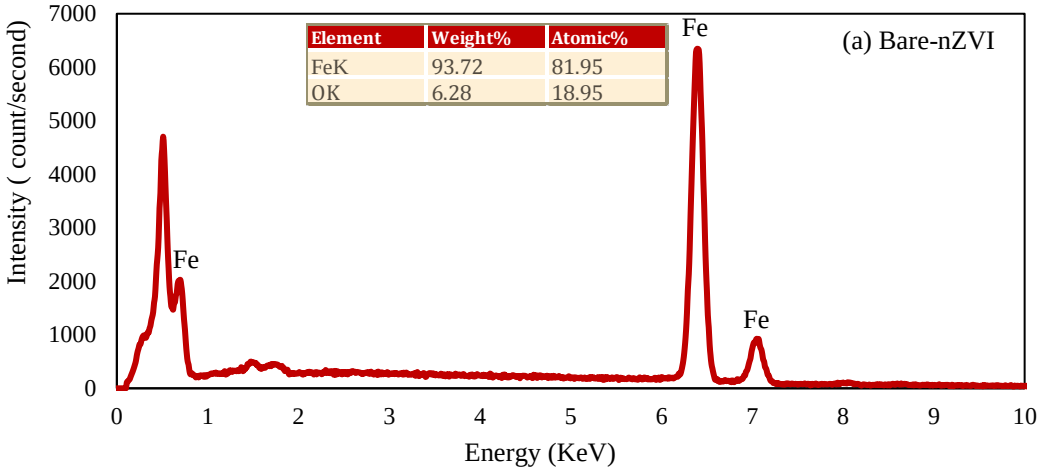
(a) Bare-nZVI
Intensity (count/second)
Energy (KeV)
Fe
Fe
Fe
Element | Weight% | Atomic%
FeK | 93.72 | 81.95
OK | 6.28 | 18.95

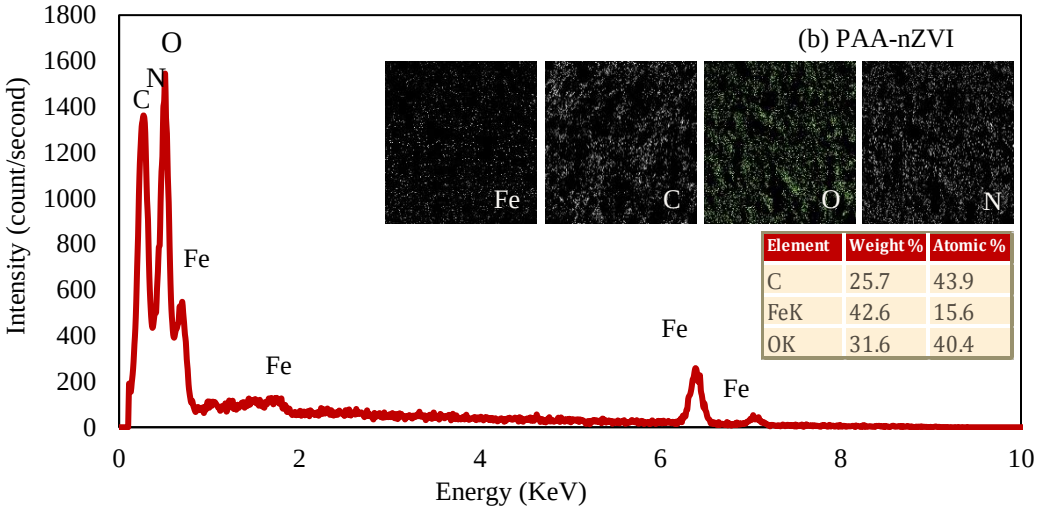
(b) PAA-nZVI
Intensity (count/second)
Energy (KeV)
O
N
C
Fe
Fe
Fe
Fe
Fe
C
O
N
Element | Weight % | Atomic %
C | 25.7 | 43.9
FeK | 42.6 | 15.6
OK | 31.6 | 40.4

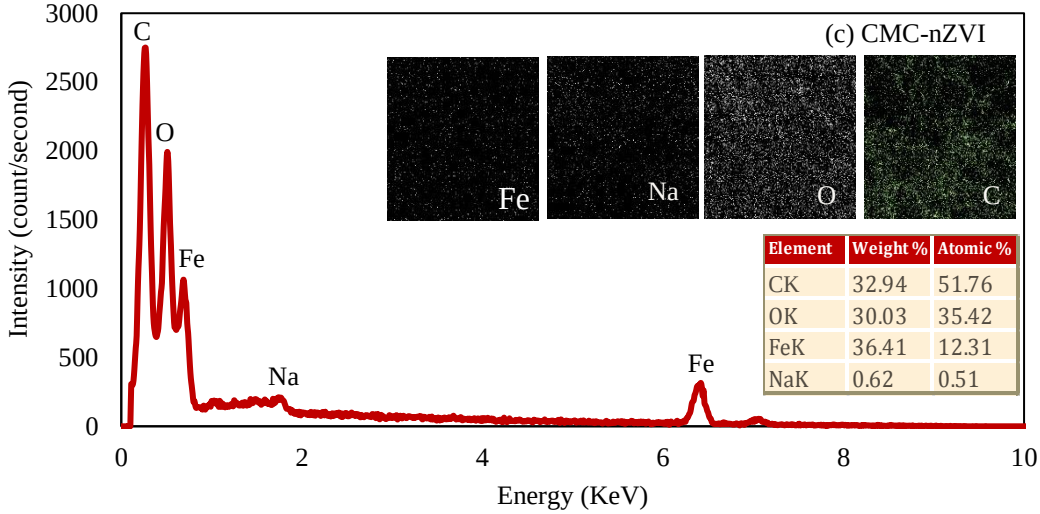
(c) CMC-nZVI
Intensity (count/second)
Energy (KeV)
C
O
Fe
Na
Fe
Fe
Na
O
C
Element | Weight % | Atomic %
CK | 32.94 | 51.76
OK | 30.03 | 35.42
FeK | 36.41 | 12.31
NaK | 0.62 | 0.51

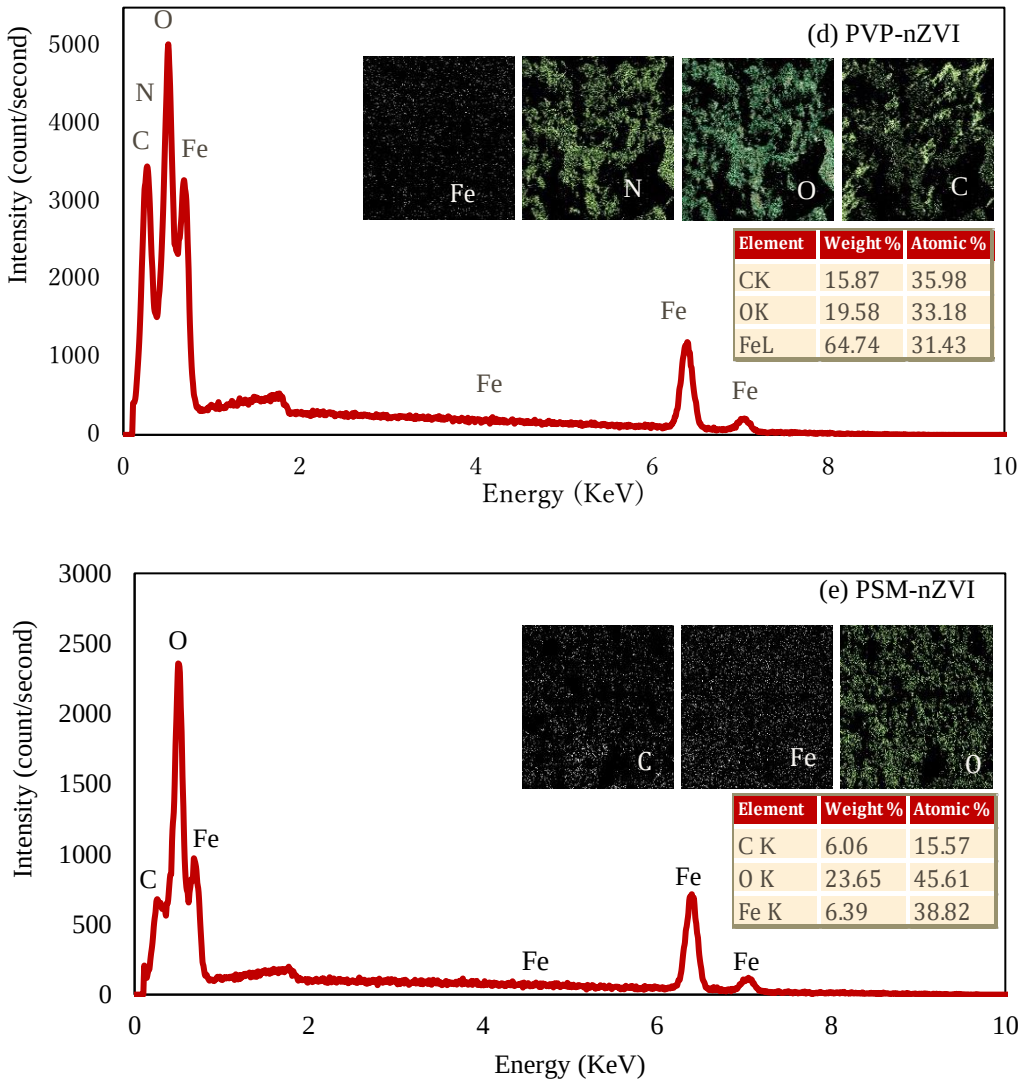

Fig. 3-4. EDX results of Fe^0 particles; a) bare/Fe^0; b) PAA/Fe^0; c) CMC/Fe^0; d) PVP/Fe^0; and e) PSM/Fe^0.

Regarding FT-IR patterns, Fig. 3-5 presents characteristic bands of observable functional groups; 3390 cm^{-1} (-OH stretching in hydroxyl groups) and 1750, 2360 cm^{-1} (COO- stretching in Carbonyl groups). These bands (the band at 3390 cm^{-1} from stretching vibrations of O-H and the band at 1750 cm^{-1} from stretching vibrations of C=O) were clearly appeared in FTIR patterns after the stabilization process of Fe^0 particles. Based on these bands, the used polymers of CMC, PVP, PSM, and PAA were adsorbed on the surface of Fe^0 particles through carbonyl and hydroxyl groups.

This was further illustrated in Fig. 3-6 by showing how polymers were attached with Fe^0 nanoparticles. These findings were also confirmed by XRD and EDX analyses. Both XRD and SEM confirmed the presence of carbon on the surface of Fe^0 as a results of stabilization process. EDX confirmed the presence of carbon on the surface of Fe^0 as a weight percentage, XRD confirmed the combination of carbon with Fe^0 through chemical bonds. And FTIR showed the functional groups of carbon on the surface of Fe^0, clarifying how the polymers were bound to the Fe^0 surface. Liang et al. [51], used PVP to improve the mobility of Fe^0 particles in porous media. They also discovered the adsorption mechanism of PVP on the surface of Fe^0 through carbonyl groups.

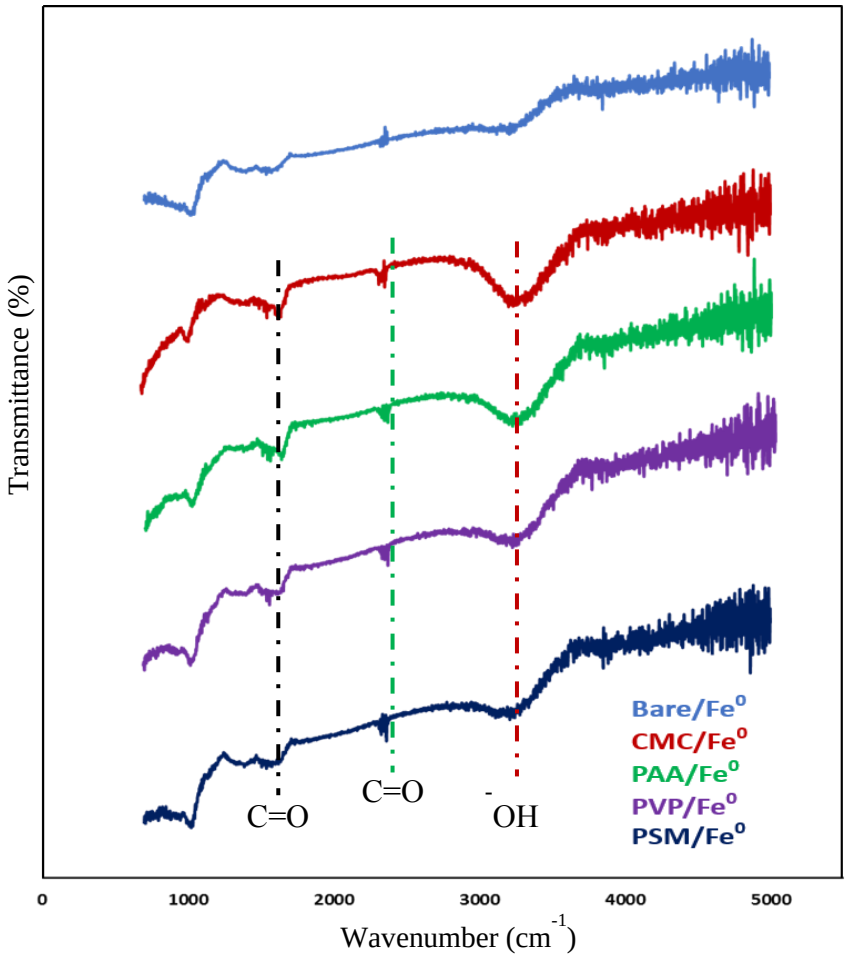

Fig.3-5. FTIR analysis of Fe^0 particles before and after the stabilization process with CMC, PAA, PVP, and PSM.

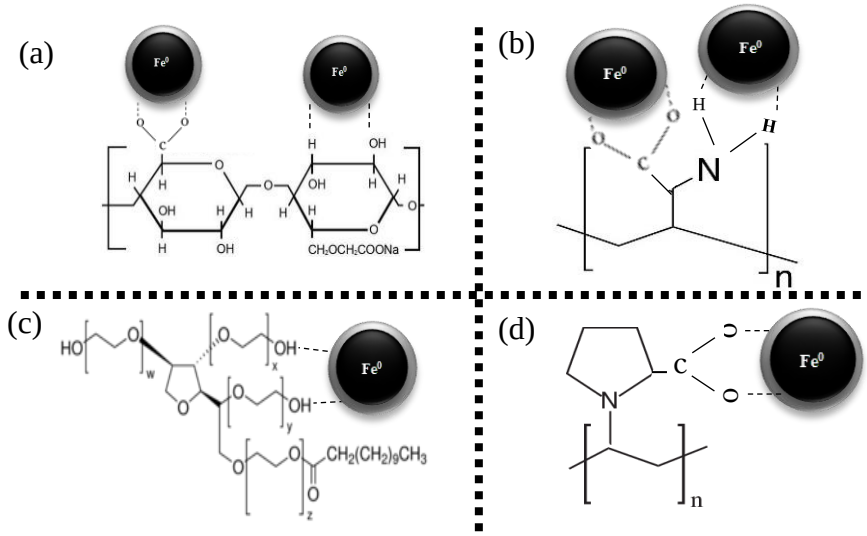

Fig.3-6. Boundation mechanisms between polymers and Fe^0 particles; a) CMC/Fe^0, b) PAA/Fe^0, c)PSM/Fe^0, and d) PVP/Fe^0.

3.4. Nitrate and phosphorus removal mechanism

The removal pathways of nitrate by Fe^0 particles were illustrated in our previous research [9]. Monitoring the formed products during the removal of nitrate by Fe^0 could illustrate the removal mechanism. During the removal of nitrate by Fe^0, three main products were generated. Nitrite was found as the first formed product with a high concentration at the beginning of the reaction. After that, in a side reaction, nitrite was converted to ammonia and nitrogen gas as a final products of nitrate removal. Tracing nitrite proved the reduction mechanism of nitrate by the released electrons from the core of Fe^0 particles. The removal pathways of nitrate by Fe^0 were illustrated in the following chemical reactions.

$$4Fe^0 + NO_3^- + 10H^+ \rightarrow 4Fe^{2+} + NH_4^+ + 3H_2O \quad (1)$$

$$Fe^0 + NO_3^- + 2H^+ \rightarrow Fe^{2+} + H_2O + NO_2^- \quad (2)$$

$$3Fe^0 + NO_2^- + 8H^+ \rightarrow 3Fe^{2+} + 2H_2O + NH_4^+ \quad (3)$$

$$3Fe^0 + 2NO_2^- + 8H^+ \rightarrow 3Fe^{2+} + 4H_2O + N_2 \quad (4)$$

On the other hand, phosphorus removal pathways were also illustrated in the current and previous research works [44, 52]. The removal pathways of phosphorus include two different mechanisms. First, the direct adsorption of phosphorus on the oxy/hydroxide shell. The formation of the hydroxide layer increases after the corrosion of Fe^0 to Fe^{2+} and Fe^{3+}. The oxy/hydroxide layer offers a huge adsorption capacity for aqueous phosphate species.

Second, with the released iron ions (Fe^{2+} & Fe^{3+}) by the corrosion of Fe^0 particles, phosphate species bind with Fe^{2+} and Fe^{3+} and precipitate on the surface of Fe^0 particles, implying that Co-precipitation mechanism was included during the removal of phosphorus from aqueous solutions by Fe^0 particles as shown in Fig. 3-7.

Polymers contribute to improve the above mechanisms by shifting isoelectric point to acidic medium to maintain positive surface charge of the Fe^0 particles which induces the electrostatic attraction between Fe^0 particles and phosphate species. Polymers also contribute to decrease the agglomeration of Fe^0 particles through steric and electrostatic stabilization to increase the particle's surface for further removal of contaminants from water.

However, despite decreasing the particle aggregation using the polymeric stabilization process, there is a possibility for blocking the reactive sites of Fe^0 particles using the polymers, which affects the absorbability of the targeted contaminants. Therefore, the target of the current research was to search on how to improve all mechanisms including adsorption, reduction, and co-precipitation using polymeric stabilization process

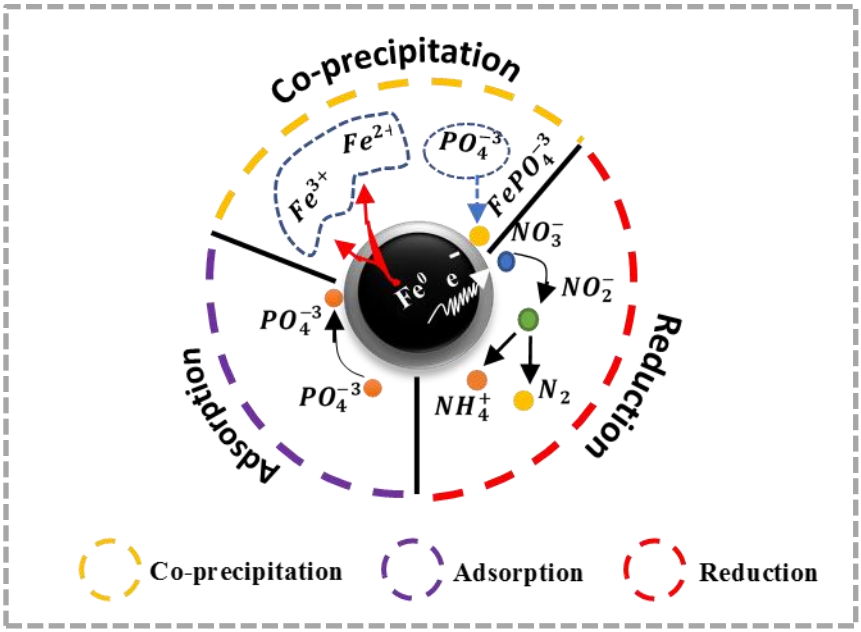

Fig.3-7. Shows the removal pathways of nitrate and phosphorus by Fe^0 particle

3.5. Reactivity of bare and stabilized Fe^0 particles

3.5.1. Evaluating the reactivity of Fe^0 stabilized by PAA

The performance of PAA in improving the removal efficiency of nitrate and phosphorus byFe^0 was assessed. The synthesis of Fe^0 was implemented using various mass ratios (0.04–0.40 % g/L) of PAA to Fe^0. Results showed that when PAA was added from 0.04 to 0.12%, the reactivity of Fe^0 particles towards both nitrate and phosphorus removal was improved. However, anymore concentrations of PAA higher than 0.12% did not improve the reactivity, which implies that the mass ratio of 0.12% was considered as the optimal mass concentration of PAA for the stabilization of Fe^0.

Fig. 3-8 a presents nitrate reduction efficiency by Fe^0 in the presence of different concentrations of PAA. Nitrate reduction reached 99% by Fe^0 at the optimum concentration of PAA with an uptake capacity of 237.6 mg/g. whereas, the reduction of nitrate was only 55.6% using the bare/Fe^0 with an uptake capacity of 133 mg/g. Obviously, PAA greatly improved the reduction mechanism of nitrate by Fe^0 particles.

Interestingly, PAA had the ability to improve phosphorus adsorption mechanism by Fe^0 particles as shown in Fig.3-8 b. The removal efficiency of phosphorus reached 97% by Fe^0 at the optimum concentration of PAA with an adsorption capacity of 133.6 mg/g. whilst, the efficiency of phosphorus removal was only 76.3% using the bare/Fe^0 with an adsorption capacity of 61.1 mg/g.

Evidently, PAA had the ability to improve both adsorption and reduction mechanisms of Fe^0 particles. To the best of the authors' knowledge, the performance of PAA/Fe^0 indicated nitrate uptake capacity higher than any other reported values in the literature using either bimetallic or stabilized/Fe^0 as shown in Table 1.

Besides, PAA/Fe^0 showed higher phosphorus adsorption capacity than many reported values in the literature as displayed in Table 2. It was reported that PAA increases the pore space of the powdered nanoparticles, leading to improve uptake capacity of the contaminants through the available pore volumes [53].

Moreover, the morphological structure of PAA/Fe^0 showed the particles dispersed with lesser aggregation compared to the bare/Fe^0. Therefore, the stabilization of Fe^0 with PAA increased the surface area of Fe^0 particles to increase the contact with any targeted pollutants.

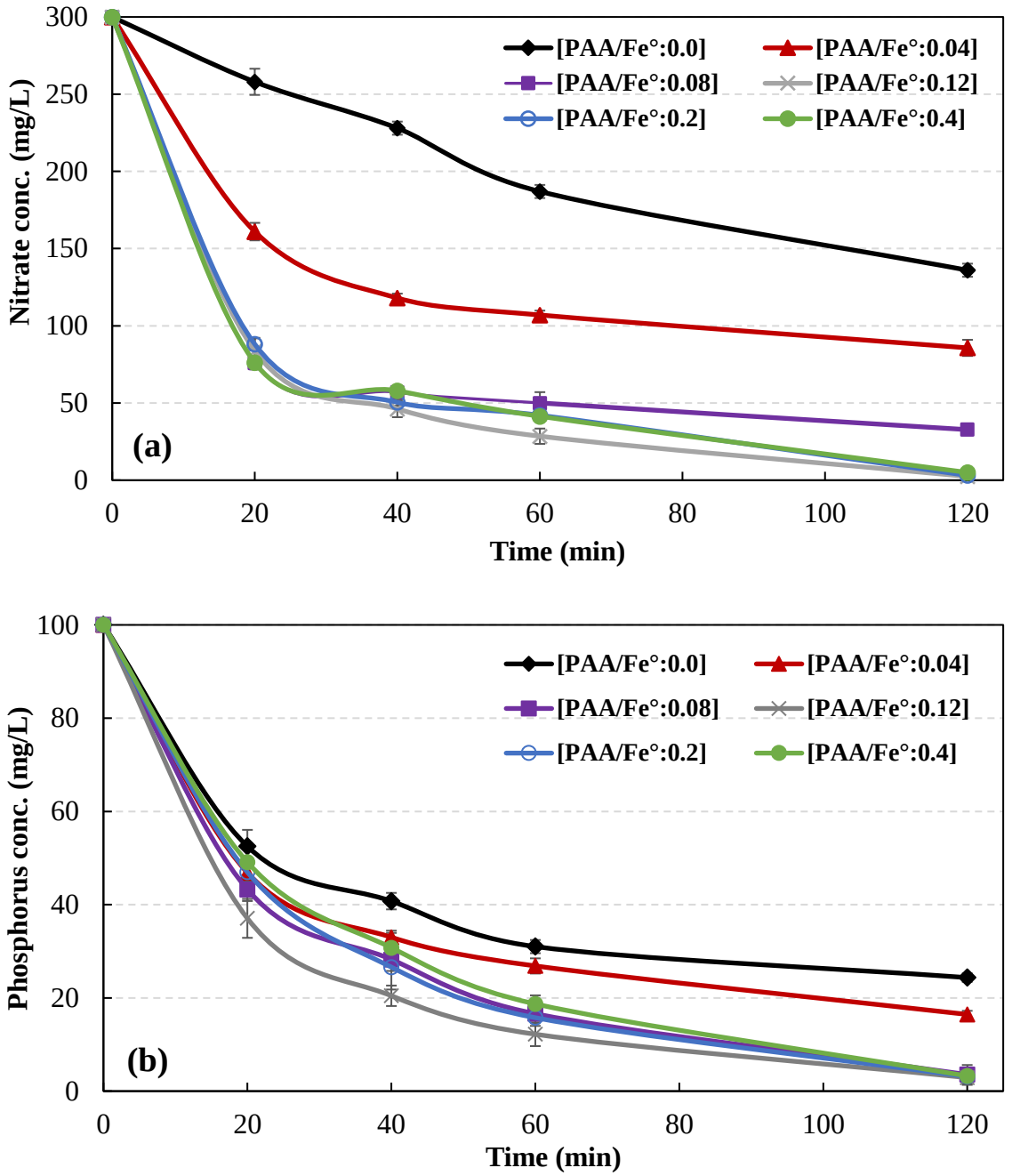

Fig.3-8. Effect of PAA mass ratio on the reactivity of Fe^0 towards: (a) nitrate reduction, (b) phosphorus adsorption. Reaction conditions; dosage: 1 g/L, pH: 7 ± 0.2, reaction time: 2 h, mixing speed: 1000 rpm and at 25 ± 1 °C.

Report #	Iron-based materials	Uptake capacity of NO_3^- mg/g	References
1	Ze/nZVI	10	[54]
2	Resains/nZVI	20	[55]
3	Cooper/nZVI	49	[9]
4	Activated C/ZVI	85	[22]
5	Clays/nZVI	100	[18]
6	Optimized nZVI	133	In this research
7	CMC/nZVI	216	In this research
8	PSM/nZVI	233	In this research
9	PAA/nZVI	237.6	In this research
10	PVP/nZVI	238.9	In this research

Table 3-1: Nitrate uptake capacity by iron-based material based on several reports

Report #	Iron-based materials	Adsorption capacity of P mg/g	References
1	Akaganeite	4	[56]
2	Synthetic goethite	7.9	[56]
3	Iron oxide tailing	6	[57]
4	Steel slag	5.3	[58]
6	NZVI	24.3	[59]
7	NZVI/$CuCl_2$	50	[44]
8	Optimized nZVI	61	In this research
9	PSM/nZVI	60	In this research
10	CMC/nZVI	56.8	In this research
11	PVP/nZVI	58.4	In this research
12	PAA/nZVI	78	In this research

Table 3-2: Phosphorus uptake capacity by iron-based material based on several reports.

3.5.2. Evaluating the reactivity of Fe^0 stabilized with CMC

In this research, CMC was used as one of the anionic polymers to assess its role in improving the reactivity of Fe^0 particles. Different mass ratios of CMC from the range of 0.04 to 0.40 % were applied during the synthesis process of Fe^0 particles. Fig. 3-9 a displays nitrate reduction by Fe^0 particles under different concentrations of CMC. The findings proved the effectiveness of CMC in improving the nitrate reduction process. Among different mass ratios of CMC, the percent of 0.12% was considered the best for achieving the highest nitrate reduction. Nitrate reduction reached 70% by CMC/Fe^0 at the optimum concentration of CMC with an uptake capacity of 216 mg/g. besides, nitrate reduction by the bare/Fe^0 was only 55.6% with an uptake capacity of 133 mg/g. However, it was noted that the use of high mass ratios of CMC to Fe^0 higher than 0.12% largely deteriorated the removal efficiency of nitrate. For instance, when using 20 and 40 % of CMC, the reactivity of nitrate removal dropped down to be less than the bare/Fe^0.

The removal rate of nitrate by CMC/Fe^0 was higher than several reported vales in the literature using similar nanoparticles as shown in Table1. On the other hand, the removal of phosphorus was not improved using CMC. Fig. 3-9 b shows phosphorus adsorption by Fe^0 particles at different concentrations of CMC. The bare/Fe^0 showed the highest adsorption rate of phosphorus compared to the stabilized Fe^0 with different concentrations of CMC. The maximum uptake capacity of phosphorus was 56.8 mg/g using CMC/Fe^0 at the best conditions, while it was 61 mg/g using the bare/Fe^0. As conclusion, CMC improved the reduction mechanism of Fe^0 without improving the adsorption mechanism.

The stabilization of Fe^0 particles using CMC decreases the size to less than 10 nm by preventing the particle aggregation through the electrostatic mechanism, which resulted in improving the surface area of Fe^0 for more nitrate reduction by the released electrons from the core of Fe^0. However, CMC adversely affects phosphorus adsorption, which could be attributed to blocked reactive sites of Fe0 by CMC molecules, preventing phosphorus adsorption. Additionally, the carboxylate groups of CMC bring a formal negative surface charge, then the adsorption of the negatively charged ions such as phosphorus ions could be obstructed [60]. Therefore, CMC/Fe^0 could be proposed only for the removal of the reducible contaminates such as nitrate

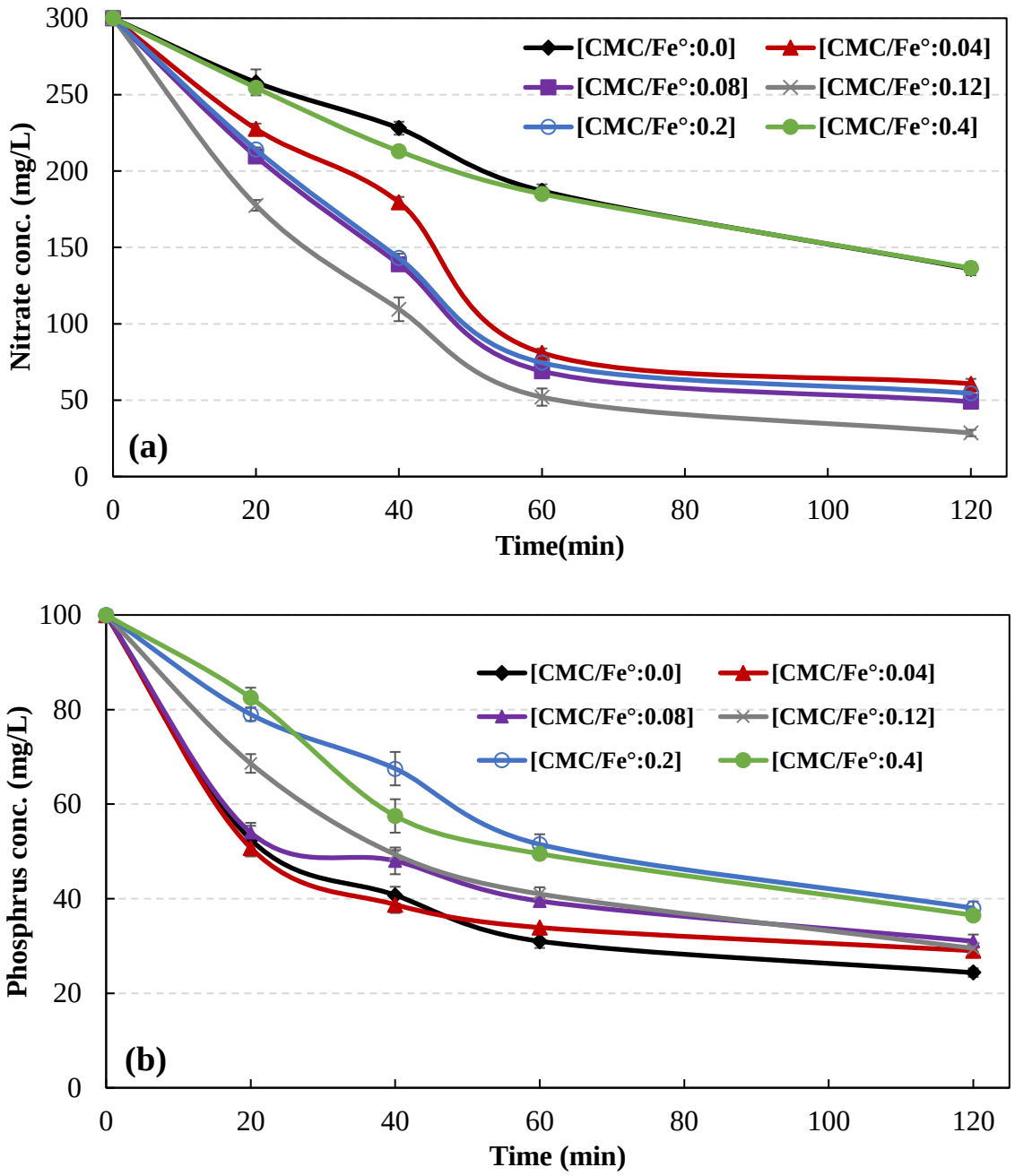

Fig.3-9. Effect of CMC mass ratio on the reactivity of Fe^0 towards: (a) nitrate reduction, (b) phosphorus adsorption. Reaction conditions; dosage: 1 g/L, pH: 7 ± 0.2, reaction time: 2 h, mixing speed: 1000 rpm and at 25 ± 1

3.5.3. Evaluating the reactivity of Fe^0 stabilized with PVP

The effect of PVP on the performance of Fe^0 particles was evaluated based on the removal efficiency of nitrate and phosphorus. Various mass ratios of PVP ranged from 0.04 to 0.40 % were used during the synthesis of Fe^0 to acquire the optimum concentration of PVP. Fig. 3-10 a presents the removal of nitrate by Fe^0 under different concentrations of PVP. The results showed that the reduction of nitrate considerably increased with increasing the mass ratio of PVP up to 40% (PVP/Fe^0: 40%). Therefore, the mass ratio of 40% of PVP was considered as the optimal mass ratio of PVP to Fe^0 to achieve the highest removal of nitrate. Nitrate reduction by PVP/Fe^0 indicated the outstanding performance of PVP in improving the reactivity of Fe^0 for nitrate reduction with an uptake capacity of nitrate above 238.9 mg/g.

Furthermore, PVP/Fe^0 displayed an uptake capacity of nitrate higher than any other reported values in the literature as presented in Table 1. According to the results above, we could conclude that the higher reactivity of PVP-Fe^0 was due to the role of PVP in preventing the particle aggregation of Fe^0, thus leading to offer a higher surface area for NO_3 reduction. Additionally, PVP serves as an electron conductor, which results in enhanced electron transfer from Fe^0 for further nitrate reduction. On the other hand, the removal of phosphorus was not improved using the stabilized Fe^0 with PVP. As presented in Fig. 3-10 b, the removal of phosphorus by the bare/Fe^0 remained higher than the stabilized PVP/Fe^0 even at different stabilizing ratios. This could be attributed to the effect of PVP coating layer on the reactive sites of Fe^0 particles, leading to prevent the contact with phosphorus.

The presence of stabilizers may reduce Fe^0 catalytic activity by blocking active sites. For example, polyvinylpyrrolidone (PVP) is commonly used to stabilize the Fe^0 nanoparticles. However, the carbonyl groups of PVP interact strongly with the Fe^0 surface, which could block a significant number of active sites. It can be concluded that the use of PVP was highly recommended for the removal of reducible contaminants such as nitrate. In contrast, PVP was not preferred for the absorbable contaminants such as phosphorus. Obviously, the stabilization of Fe^0 with PVP enhanced the selectivity of Fe^0 particles towards nitrate reduction. Therefore, PVP would be a proper choice for targeting one reducible contaminant.

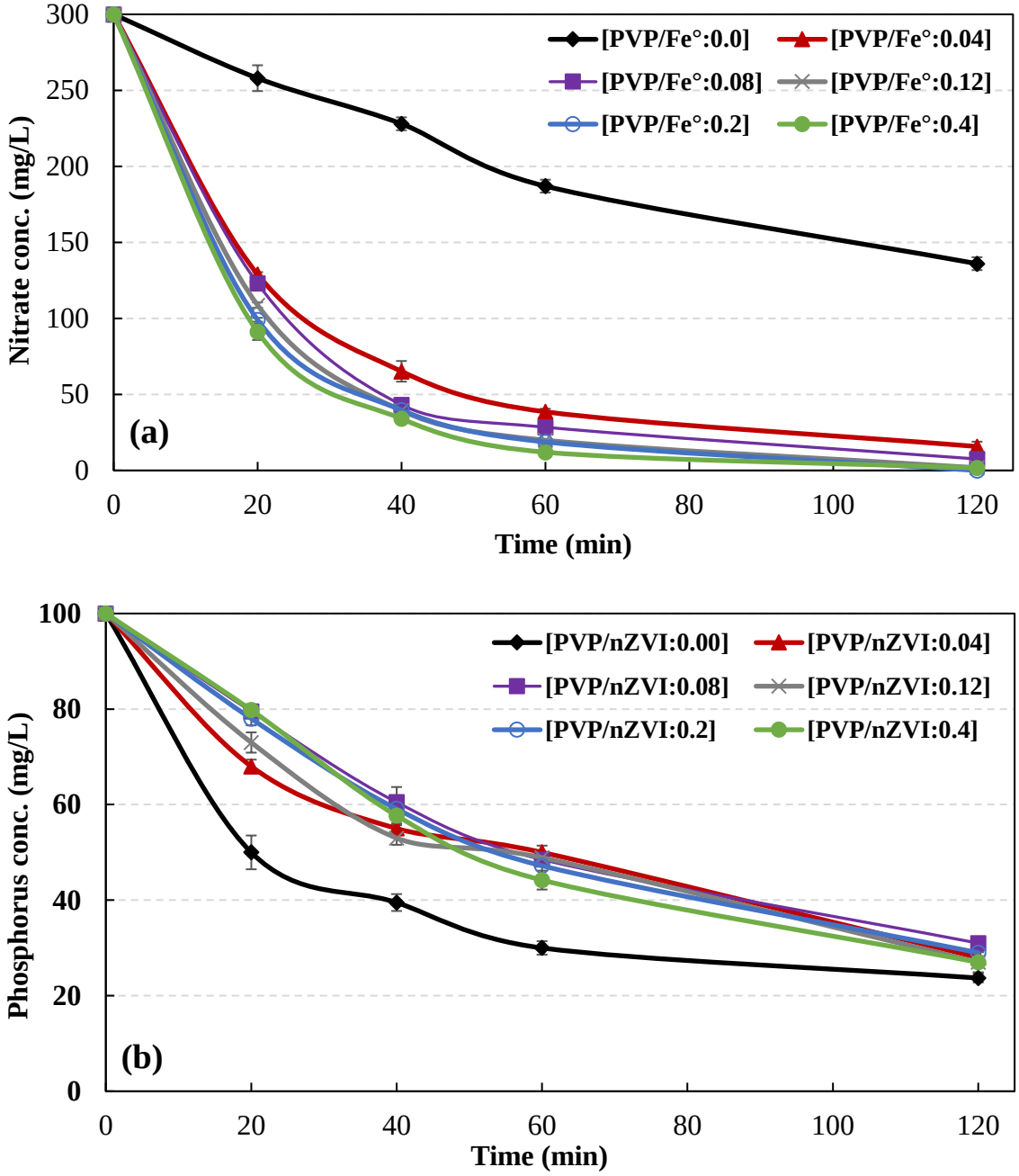

Fig.3-10. Effect of PVP mass ratio on the reactivity of Fe^0 towards: (a) nitrate reduction, (b) phosphorus adsorption. Reaction conditions; dosage: 1 g/L, pH: 7 ± 0.2, reaction time: 2 h, mixing speed: 1000 rpm and at 25 ± 1

3.5.4. Evaluating the reactivity of Fe^0 stabilized with PSM

In this research, PSM was used as an emulsifier to emulsify the Fe^0 particles and make them as an oil droplet. The performance of the emulsified Fe^0 was evaluated based on the removal efficiency of nitrate and phosphorus. Fig.3-11 a depicts the removal of nitrate by Fe^0 using different mass ratios of PSM. Among different ratios of PSM, 0.12% exhibited the highest reduction of nitrate. Therefore, 0.12% was determined as the optimal concentration of PSM for preparing Fe^0 with high reactivity. Nitrate reduction improved largely by increasing the PSM ratio up to 0.12%. However, high PSM concentrations more than the optimum percent negatively affected nitrate reduction. The maximum nitrate uptake capacity of nitrate using the bare/Fe^0 reached 133.6 mg NO_3/g Fe^0, whereas the maximum uptake capacity of nitrate using PSM/Fe^0 at the optimum concentration of PSM to Fe^0 reached 233.04 mg NO_3/g PSM/Fe^0.

The improvement of nitrate reduction could be attributed to the lower agglomeration of PSM/Fe^0 particles as it was observed from the obtained TEM images. The separated particles of Fe^0 after being emulsified with PSM resulted in increasing the reaction rate of nitrate reduction due to the increased number of the released electrons from the core of Fe^0. Therefore, the emulsifier of PSM is highly recommended to be used for synthesizing dispersed Fe^0 particles for efficient nitrate removal. on the other hand, the stabilization of Fe^0 with PSM was not improved the removal of phosphorus as shown in Fig. 3-11 b. the reactivity of bare/Fe^0 remained better for phosphorus removal than the emulsified Fe^0 at all stabilizing ratios. It could be attributed to the hydrophobic oil-water film formed by the emulsifier on the surface of Fe^0. This film prevents the absorbable contaminants such as phosphorus to be diffused through the film, decreasing the contact with the Fe^0 surface. To sum up, PAA was the best polymer among the others for the simultaneous removal of nitrate and phosphorus with an excellent removal efficiency for both.

In comparison, the reduction of nitrate by the used types of Fe^0 in this study follows the order of PVP/Fe^0 (238.9 mg/g) > PAA/Fe^0 (237.6 mg/g) > PSM/Fe^0 (233 mg/g) > CMC/Fe^0 (216 mg/g) > bare/Fe^0 (133 mg/g). For phosphorus removal, the effectiveness of the used polymers follows the following order: PAA/Fe^0 (78 mg/g) > bare/Fe^0 (61 mg/g) > PSM/Fe^0 (60 mg/g) > PVP/Fe^0 (58.4 mg/g) > CMC/Fe^0 (56.8 mg/g)

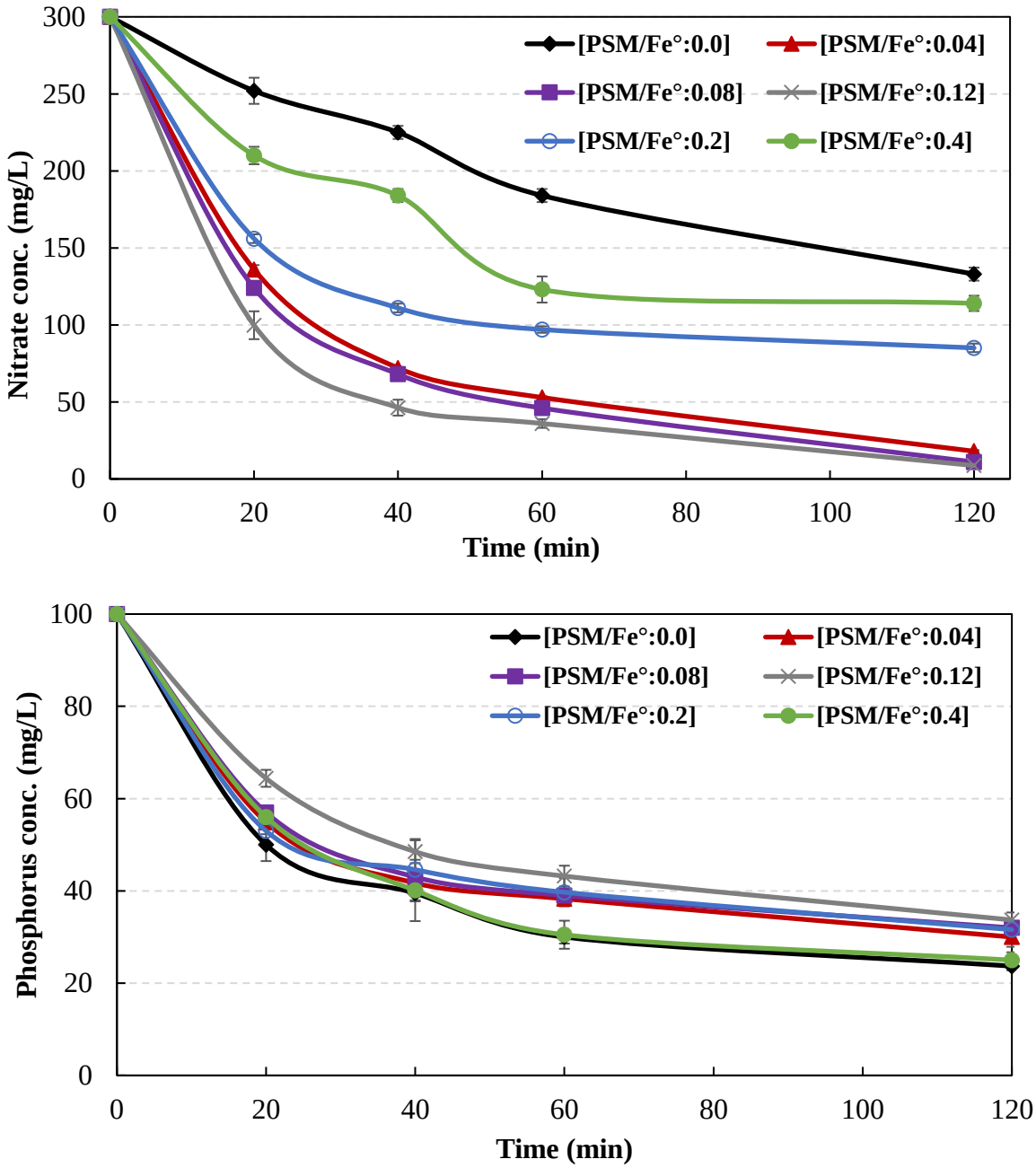

Fig.3-11. Effect of PSM mass ratio on the reactivity of Fe^0 towards: (a) nitrate reduction, (b) phosphorus adsorption. Reaction conditions; dosage: 1 g/L, pH: 7 ± 0.2, reaction time: 2 h, mixing speed: 1000 rpm and at 25 ± 1 °C

3.6. Effect of pH

The results of pH experiments using either bare or stabilized/Fe^0 confirmed the sensitivity of Fe0 performance to pH values. Fig. 3-12 shows the removal of nitrate using the bare and stabilized types of Fe^0 at different pH values with the time. In all cases, either using bare or stabilized Fe0, the nitrate reduction process favors acidic and neutral media. Therefore, compared to alkaline medium, acidic medium offers a greater nitrate reduction due to the following reasons; 1) it is commonly known that the oxide hydroxide shell layer of Fe^0 affects the reduction of nitrate by obstructing electrons motion from the core of Fe^0, therefore, low solution pH dissolves the oxide layer and clears the surface of Fe^0 which could allow to release further electrons for nitrate reduction. 2) at low pH value the concentration of proton in the medium is higher than at high pH, these protons participate in nitrate removal according to the following equations [61].

$$NO_3^- + Fe^0 + 2H^+ \rightarrow Fe^{2+} + NO_2^- + H_2O \quad (5)$$

$$NO_3^- + 4H^{2+}\ 2H^+ \rightarrow NH_4^- + 3H_2O \quad (6)$$

Interestingly, both PAA and PVP showed a high reduction of nitrate in the neutral and alkaline media as presented in Fig. 3-14 a. Therefore, PAA/Fe^0 and PVP/Fe^0 were suggested to treat nitrate, and all reducible contaminates from water at a wide range of pH (acidic, neutral, and alkaline). Similarly, the results illustrated the higher performance of phosphorus removal in the acidic medium compared to other media. Fig.3-13 shows the removal of phosphorus using the bare and stabilized types of Fe^0 with the time at different pH values. At all cases, either using bare or stabilized Fe^0, phosphorus removal favors the acidic pH. It should be mentioned that the improved reactivity towards phosphorus removal at acidic pH using all types of Fe^0 is attributed to the surface charge state of Fe^0. The pH value of point of zero charges (isoelectric point, IEP) of Fe^0 is determined around 8.1 [62]. Therefore, when pH is lower than the IEP, the particles will be positively charged, which enhances the electrostatic attraction with anionic contaminants such as PO_4^{3-}. In contrast, when the solution pH is higher than the IEP, both adsorbent and adsorbate become negatively charged, leading to cause an electric repulsion between them. Therefore, PAA was the best polymer among the other used polymers for stabilizing Fe^0 for phosphorus removal at a wide range of pH value

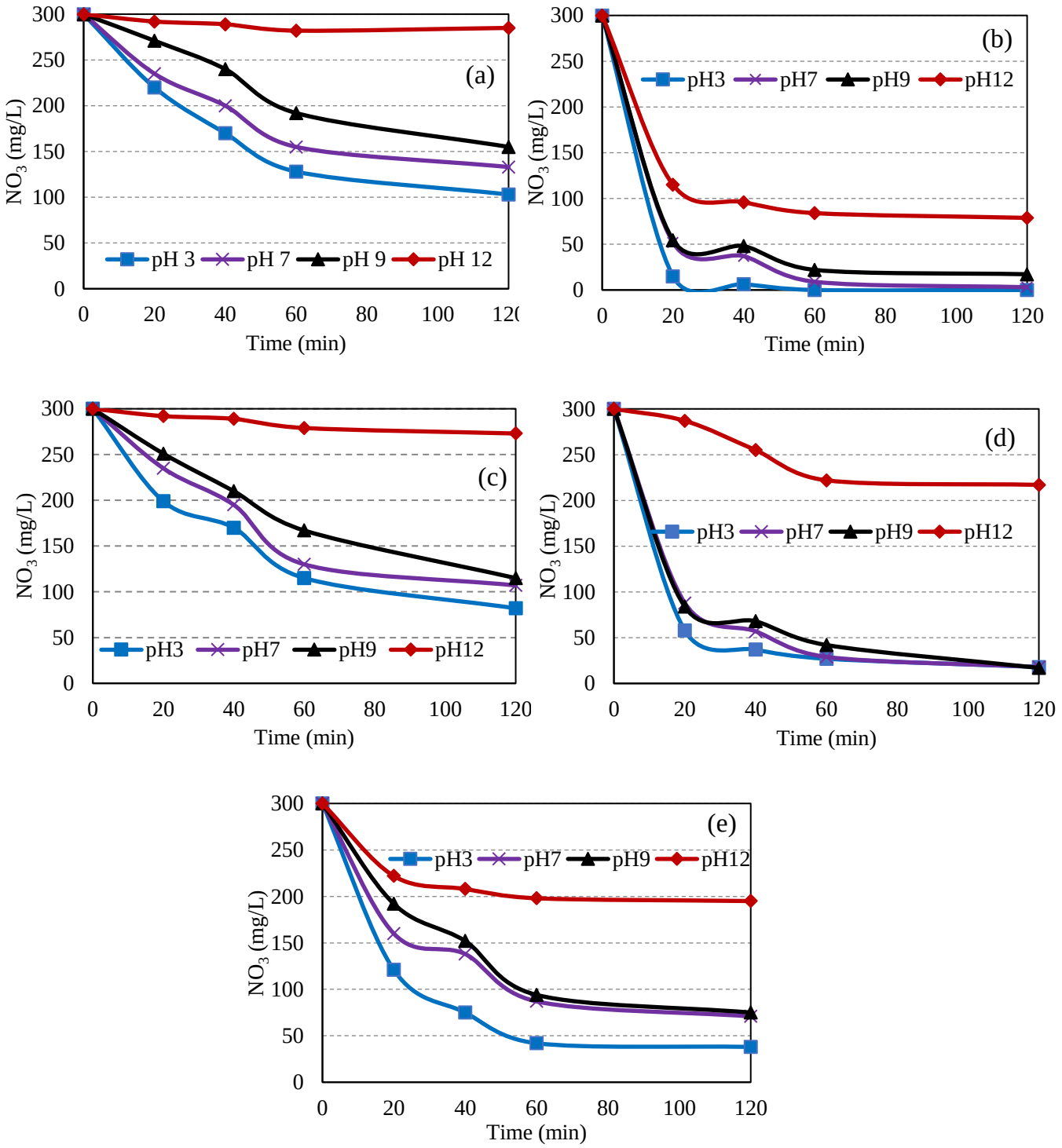

Fig.3-12. Nitrate removal under different pH using a) bare/Fe^0, b)PAA/Fe^0, c) CMC/Fe^0, d) PVP/Fe^0, and e) PSM/Fe^0. Reaction conditions; dosage: 1 g/L, pH: 7 ± 0.2, reaction time: 2 h, mixing speed: 1000 rpm and at 25 ± 1 °C.

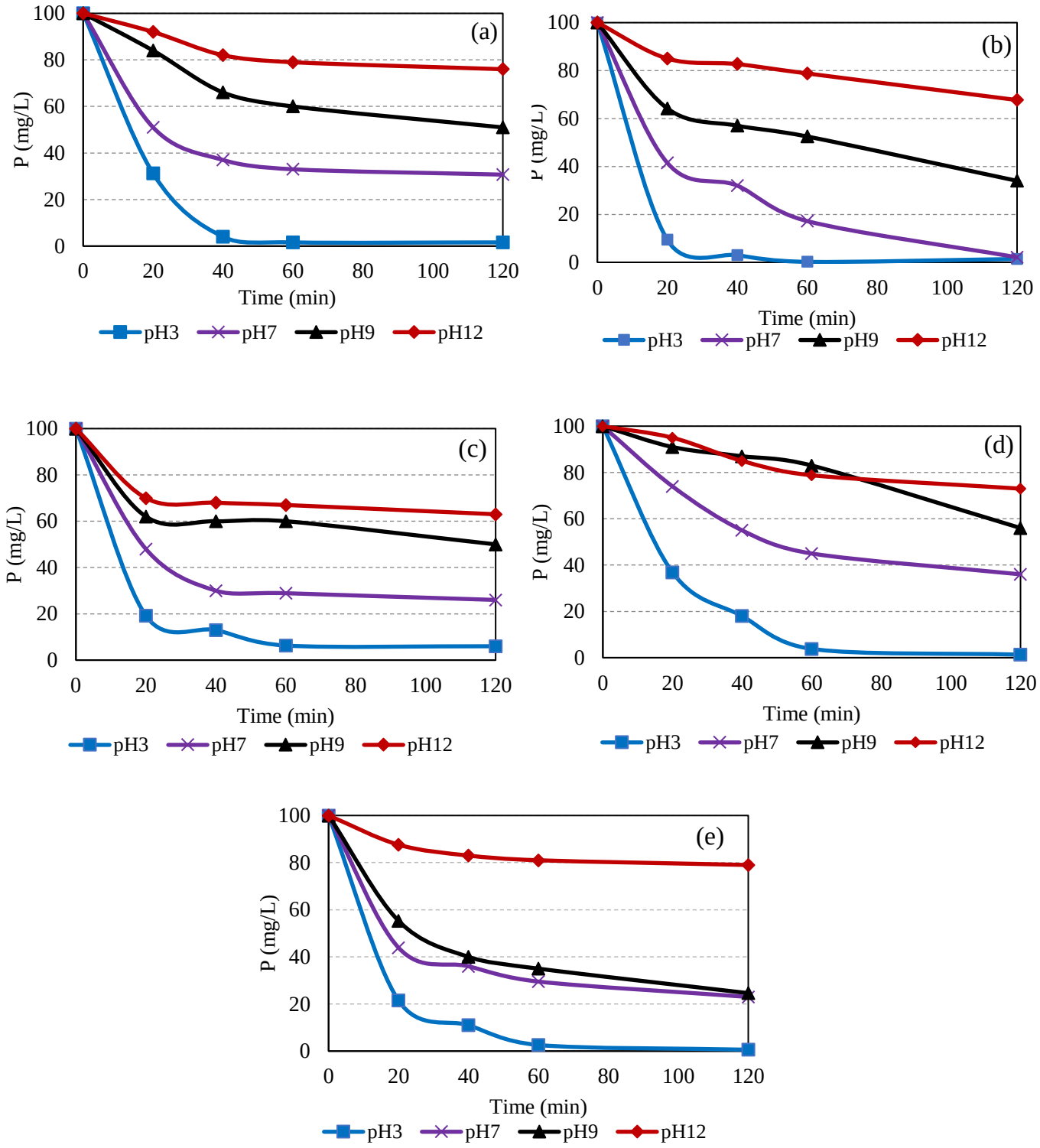

Fig.3-13. Phosphorus removal under different pH using a) bare/Fe^0, b)PAA/Fe^0, c) CMC/Fe^0, d) PVP/Fe^0, and e) PSM/Fe^0. Reaction conditions; dosage: 1 g/L, pH: 7 ± 0.2, reaction time: 2 h, mixing speed: 1000 rpm and at 25 ± 1 °C.

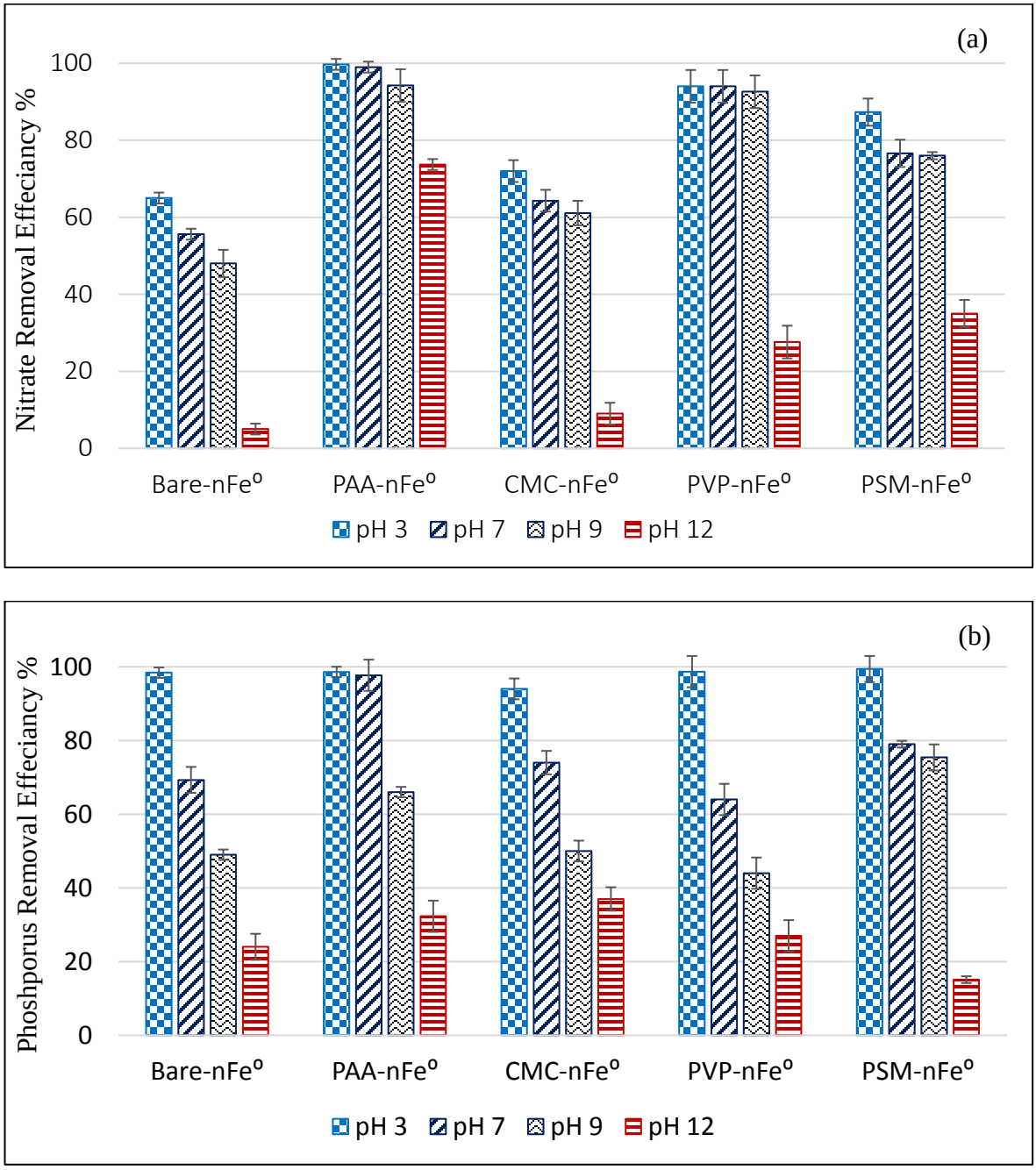

Fig.3-14. Shows the final removal efficiency of nitrate and phosphorus (after a reaction of 2 hr.) by the bare and stabilized types of Fe^0 particles under different pH

3.7. Effect of initial contaminants concentrations

Equilibrium studies were conducted to discover the effect of initial nitrate and phosphorus concentrations on the process of adsorption onto Fe^0 and the stabilized Fe^0. Fig. 3-15 and 3-16 show the removal of nitrate and phosphorus with time at different initial concentrations by the bare and the stabilized types of Fe^0. At all cases, the adsorption capacities increased by increasing the initial concentrations of nitrate and phosphorus.

Fig. 3-17 a shows the relationship between equilibrium adsorption capacities of Fe^0 and stabilized Fe^0 for nitrate and concentrations of nitrate in aqueous solutions at equilibrium. The results indicated further removal of nitrate at high concentrations. This could be attributed to the availability of nitrate at high concentration which could increase the interaction between the adsorbent and the adsorbate.

Interestingly, PAA/Fe^0 had the highest uptake capacity of nitrate at all initial concentrations. Also, PAA/Fe^0 showed the highest adsorption capacity of phosphorus at different initial concentrations. Therefore, and to elucidate more, two adsorption isotherm models Langmuir and Freundlich were used to understanded the uptake mechanism of nitrate and phosphorous. The calculated parameters of these models, including maximum adsorption capacities (qs), were obtained. As shown in Fig. 3-18 and 3-19, the results of nitrate and phosphorus removal were fit more with Langmuir model using the bare Fe^0, indicating that monolayer adsorption layer was the dominant removal mechanism of nitrate and phosphorus.

On the other hand, the results of nitrate and phosphorus removal were more fit to Freundlich model, indicating the heterogeneous surface of Fe^0 and multilayer adsorption occurred on its surface after being stabilized with PAA. This could illustrate how the stabilization of Fe^0 by PAA improved the uptake capacity of phosphorus and nitrate.

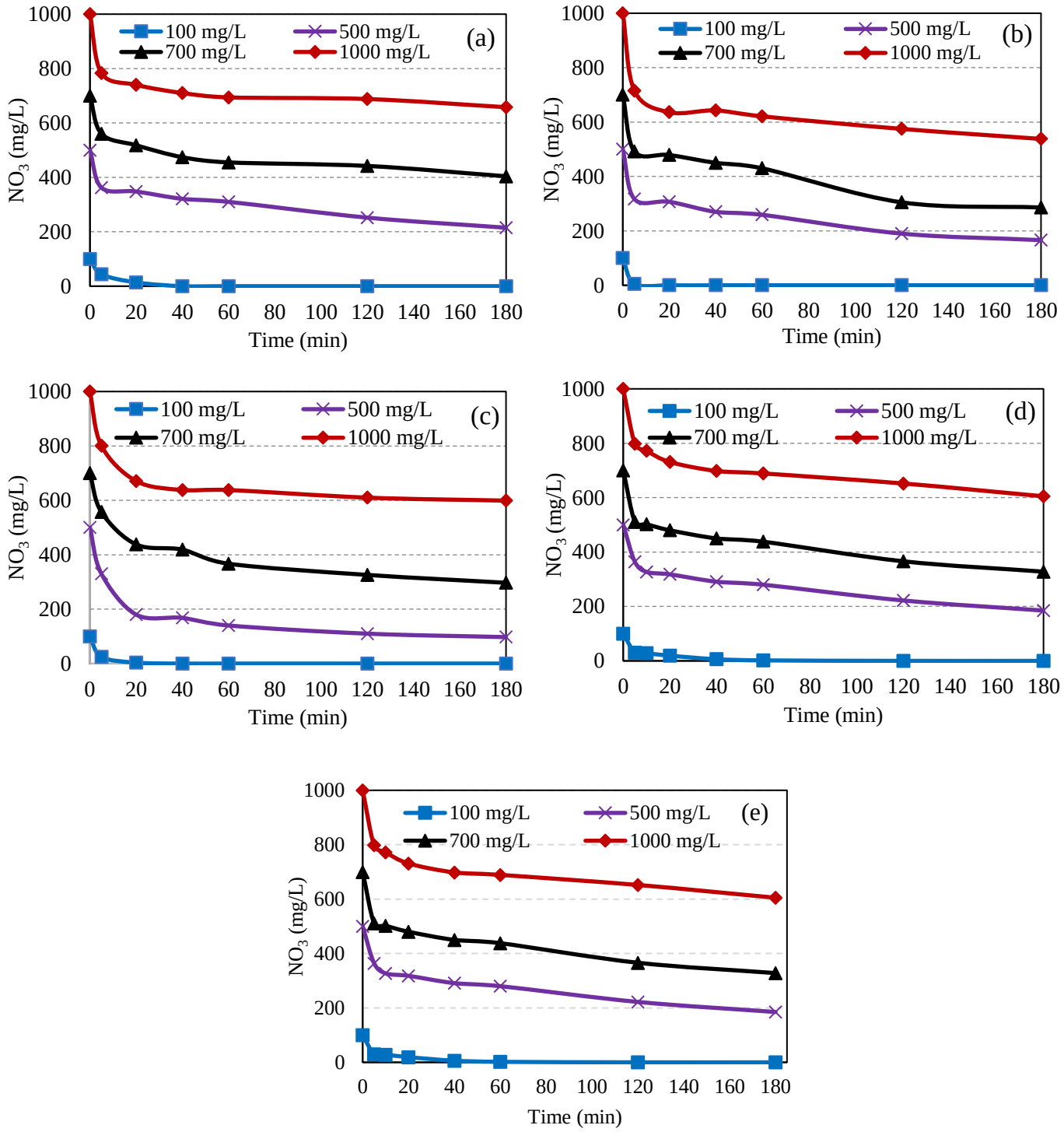

Fig.3-15. Nitrate removal at different initial concentrations using a) bare/Fe^0, b)PAA/Fe^0, c)PVP/Fe^0, d) CMC/Fe^0, and e) PSM/Fe^0. Reaction conditions; dosage: 1 g/L, pH: 7 ± 0.2, reaction time: 3 h, mixing speed: 1000 rpm and at 25 ± 1 °C.

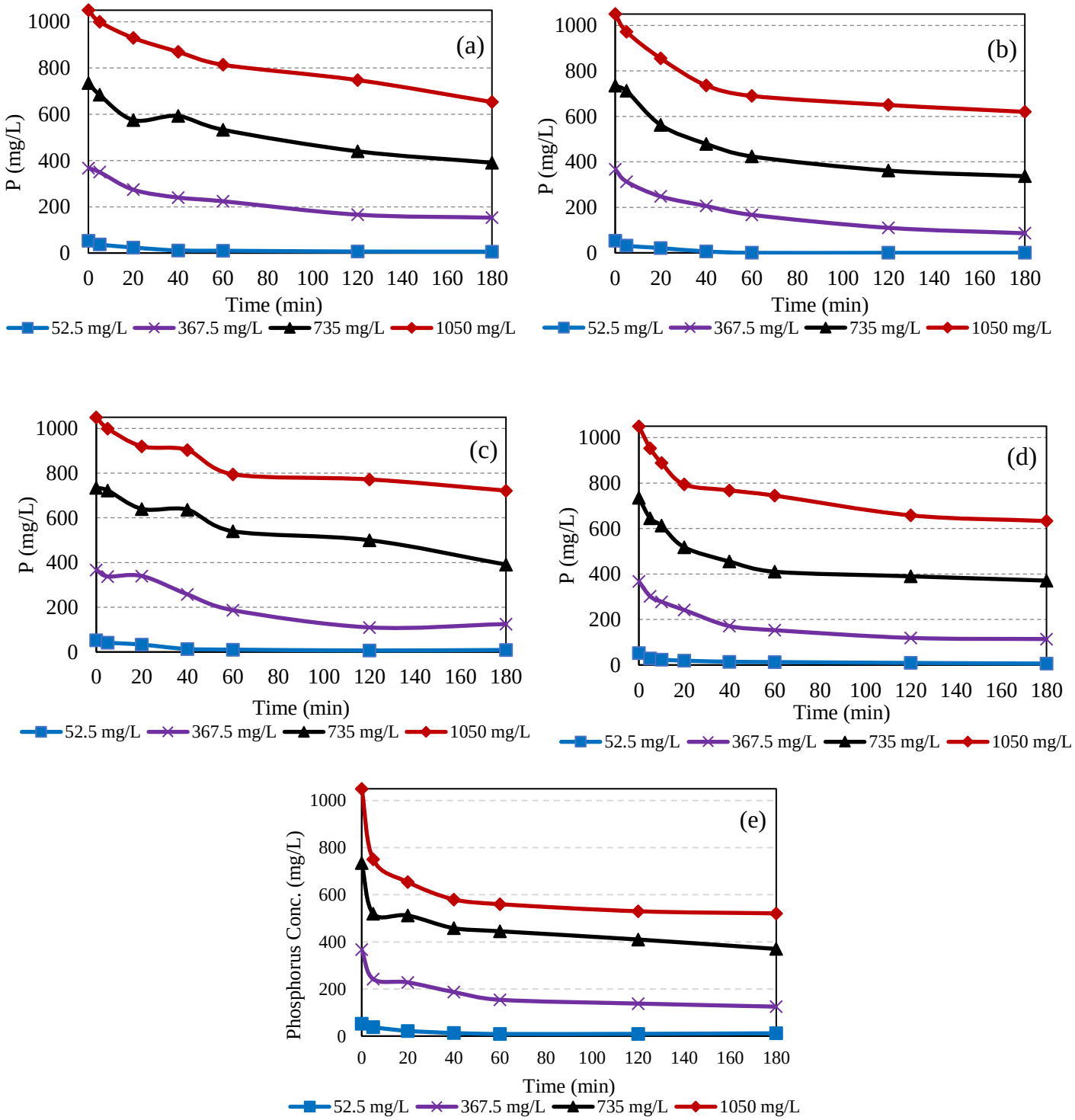

Fig.3-16. Phosphorus removal at different initial concentrations using a) bare/Fe^0, b)PAA/Fe^0, c)PVP/Fe^0, d) CMC/Fe^0, and e) PSM/Fe^0. Reaction conditions; dosage: 1 g/L, pH: 7 ± 0.2, reaction time: 3 h, mixing speed: 1000 rpm and at 25 ± 1 °C.

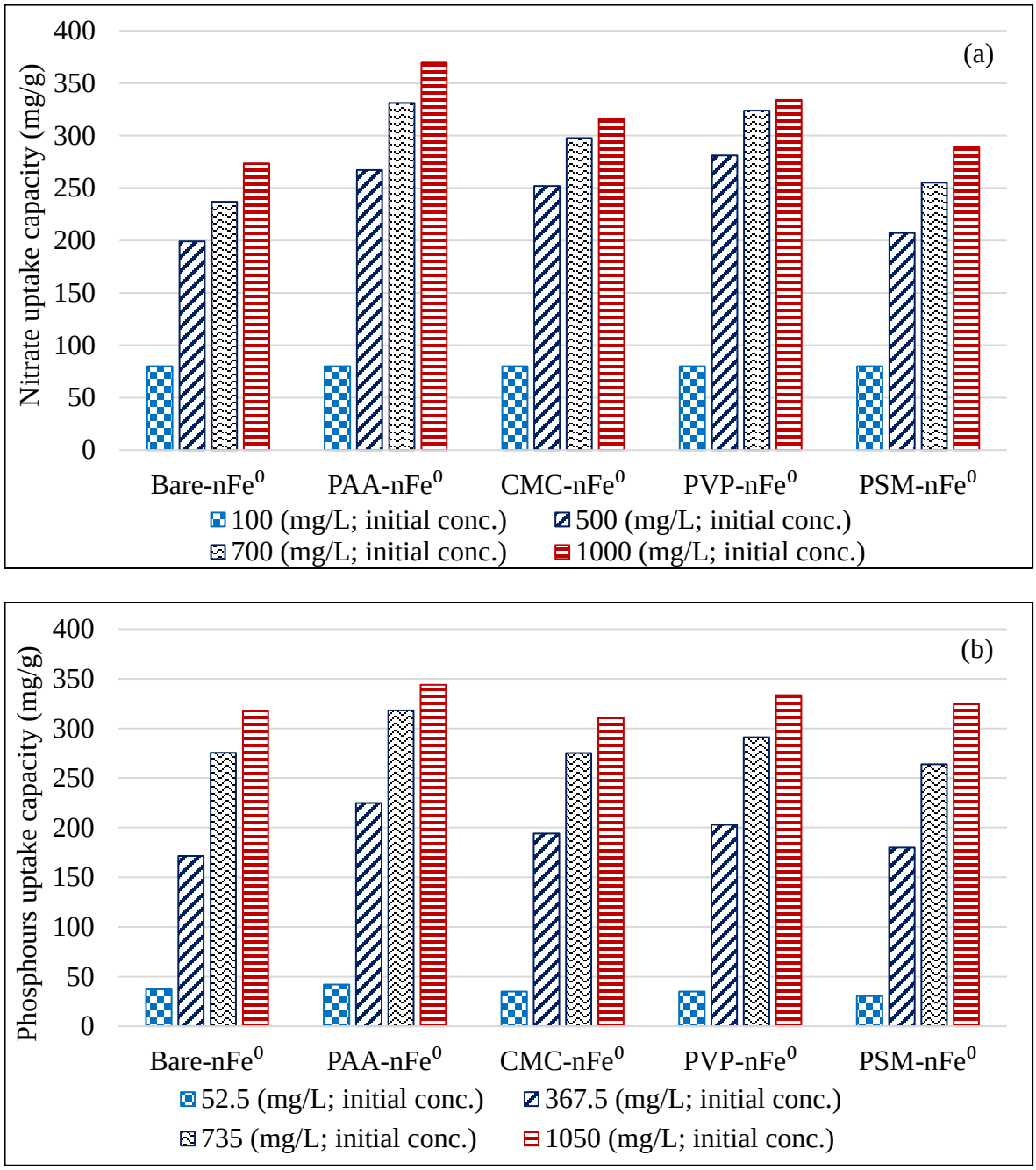

Fig.3-17. Shows the final uptake capacity of nitrate and phosphorus (after a reaction of 3 hr.) by the bare and stabilized types of Fe^0 particles at different initial concentrations of nitrate and phosphoru

3.8. Isotherm study

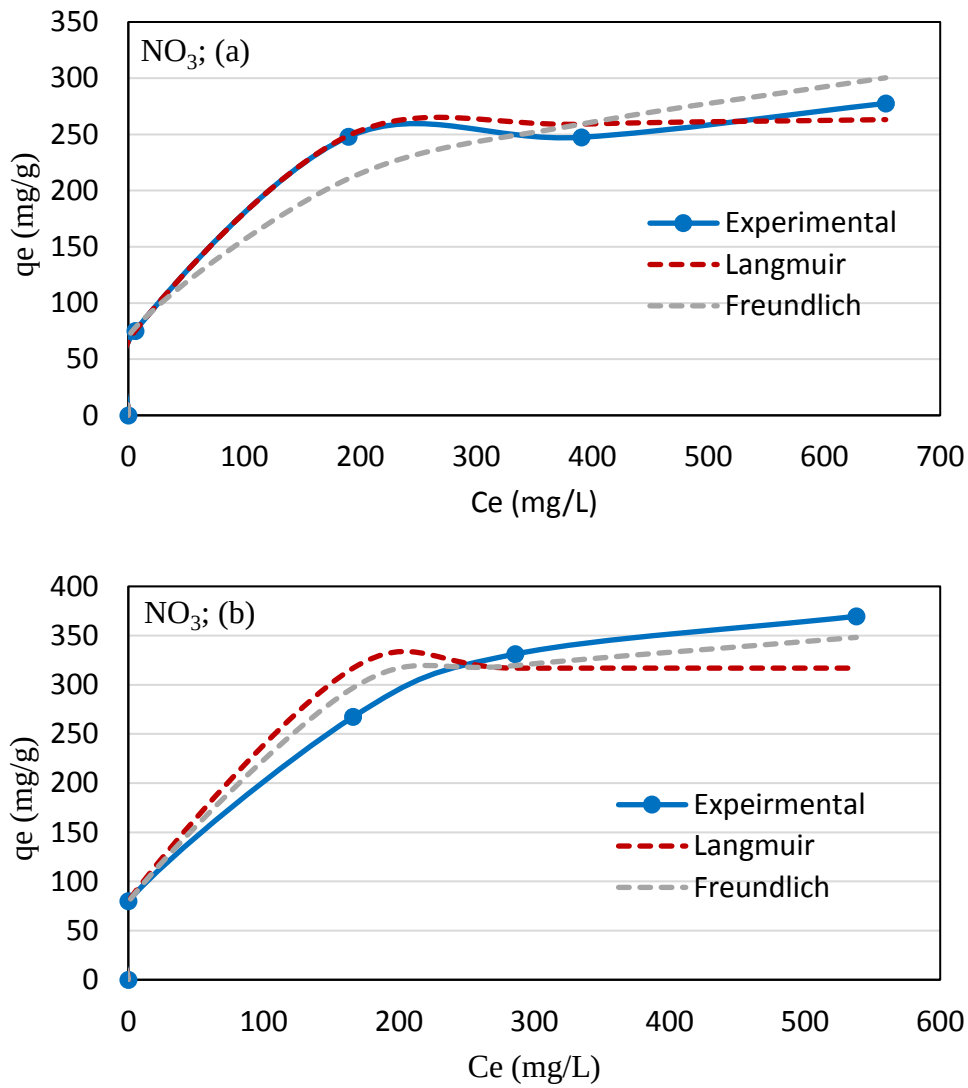

Fig.3-18. Shows the adsorption capacity of experimental data, Langmuir and Freundlich isotherm models for nitrate removal using a) bare/Fe^0, and b) PAA/Fe^0

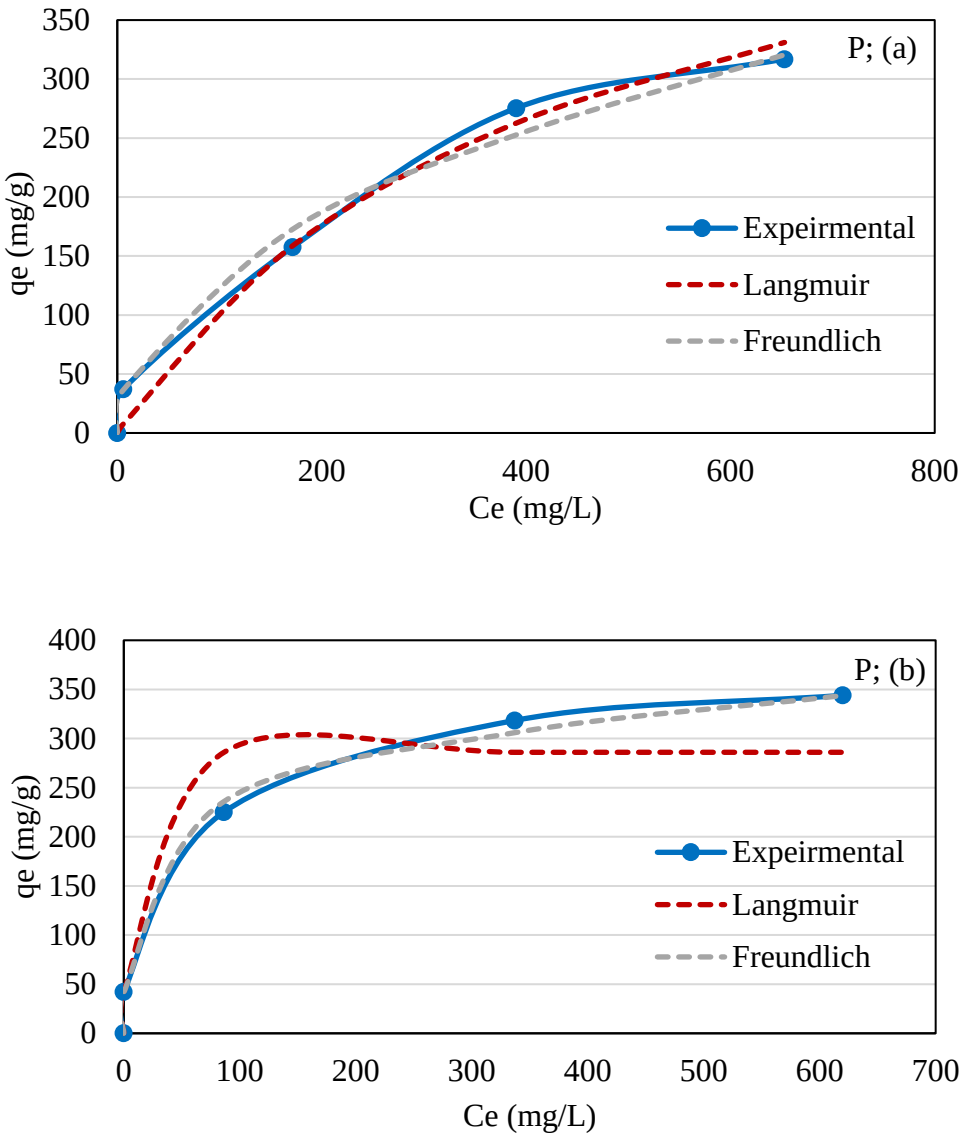

Fig.3-19. Shows the adsorption capacity of experimental data, Langmuir and Freundlich isotherm models for phosphorus removal using a) bare/Fe^0, and b) PAA/Fe^0

3.9. Reaction kinetics

In this study, four different models were used to find out the best applicable model and to describe the reaction kinetic rate of nitrate and phosphors removal using bare and PAA-nZVI. PAA-nZVI was selected among the other species of the stabilized nZVI for kinetic investigations due to its superior performance of nitrate and phosphorus removal. Four different models were applied including first-order, second-order, elovich and intra-particle diffusion. These models are usually used to describe the catalytic and non-catalytic reaction and the removal kinetics of nitrate and phosphorus from water [32, 33]. The applied model's equations were used as follows:

First-order equation: $\frac{\mathrm{dC}}{dt} = -KC,$ (7)

and its liner form: $C = C_i e^{-kt},$ (8)

second-order equation: $\frac{dC}{dt} = -K_1 C^2$ (9)

and its liner form: $\frac{1}{C} = k_2 t + \frac{1}{C},$ (10)

Elovich equation: $q_t = \ln(\propto \beta) + ln\frac{1}{\beta}$ (11)

Intera-particle eq: $q_t = K_{diff} t^{1/2} + C$ (12)

where C is the concentration of phosphorus or nitrate at time t, C_i is initial concentration of nitrate or phosphorus. K, K_1, K_2 are the reaction rate constant. q_t is the maximum uptake capacity of nitrate or phosphorus at time t, α is the initial sorption rate of elovich, β is the adsorption constant and K_{diff} represents the intera-particle diffusion rate.

Table 3 documents the results of the applied models on the experimentally investigated results of nitrate removal.

The results showed that the used model's equations were competing in describing the reduction kinetic of nitrate. However, if the average values of R^2 are higher than 0.9 means that the experiments profiles do match the rate equation.

When it comes to the loaded ratio of PAA, nitrate reduction followed elovich, first order and intera-particle diffusion as the average values of R^2 are 0.96, 0.94 and 0.93, respectively, implying elovich was the fittest model for nitrate reduction by nZVI in the presence of PAA.

Based on elovich and first-order models, the reaction kinetic of nitrate removal increased by increasing the loaded ratio of PAA which is in good agreement with experiment's profiles. However, these models were failed to describe nitrate removal at high initial concentrations and at high pH values and elovich remained the fittest rate equation among the others to describe the removal of nitrate at different conditions.
Table 4 documents the results of the applied models on the experimentally investigated results of phosphorus removal.

The average value of R^2 of first-order, second order, elovich and intera-particle diffusion models were 0.93, 0.89, 0.94 and 0.9, respectively, implying elovich was the fittest model of phosphorus removal at different conditions.
The kinetic results of first order and elovich models do match the experiment's profiles, confirming the higher reaction rates in the presence of PAA and at low p

Table 3-3: Implementation of first, second order, elovich and intera-particle diffusion kinetic rate equations on the investigated experiential data of nitrate removal under different conditions

Experiment NO.	PAA:Fe^0 (wt/wt)	Initial nitrate Conc.	Initial pH	First-order (R^2)	K 1/min	Second -order (R^2)	K 1/min^2	Elovich (R^2)	beta (g/mg)	alpha (mg/g/min)	Intera-particle (R^2)	K_{diff} 1/seqrt(min)
1	0	300	7	0.98	0.0068	0.99	4.00E-0	0.97	0.018354	8.247	0.98	15.05
2	0.008	300	7	0.9	0.0087	0.83	6.00E-0	0.93	0.033591	6.2071	0.84	7.469
3	0.016	300	7	0.91	0.0158	0.94	0.0002	0.99	0.05291	9.547	0.95	5.07
4	0.024	300	7	0.98	0.0387	0.81	0.0037	0.97	0.02629	1.2268	0.91	10.11
5	0.04	300	7	0.97	0.0367	0.8	0.003	0.98	0.027898	6.769	0.97	9.738
6	0.08	300	7	0.96	0.0537	0.81	0.0028	0.96	0.03183	4.817	0.99	8.753
7	0.024	300	3	0.9	0.0958	0.99	0.0038	0.85	0.14294	2.423	0.74	1.792
8	0.024	300	6.5	0.9	0.0363	0.92	0.0029	0.9	0.04254	1.2759	0.85	6.2514
9	0.024	300	9	0.71	0.0206	0.91	0.0005	0.85	0.0545	1.53721	0.82	4.9394
10	0.024	300	12	0.56	0.0089	0.69	7.00E-0	0.92	0.0605	1.11037	0.84	4.3124
11	0.024	100	7	0.75	0.18	0.99	0.0324	0.62	0.99458	6.7368	0.39	3.9828
12	0.024	500	7	0.65	0.0083	0.7	2.00E-0	0.92	0.028646	2.29389	0.84	17.065
13	0.024	700	7	0.58	0.0059	0.64	1.00E-0	0.9	0.020603	7.9206	0.88	21.936
14	0.024	1000	7	0.52	0.0057	0.56	8.00E-0	0.88	0.02763	3.33239	0.7	21.876

Table 3-4: Implementation of first, second order, elovich and intera-particle diffusion kinetic rate equations on the investigated experiential data of phosphorus removal under different conditions

Experiment NO.	PAA:Fe^0 (wt/wt)	Initial Phosphorus. conc.	Initial pH	First-order (R^2)	K 1/min	Second -order (R^2)	K $1/min^2$	Elovich (R^2)	beta (g/mg)	alpha (mg/g/min)	Intera-particle (R^2)	K_{diff} 1/seqrt(min)
1	0	300	7	0.8	0.0108	0.93	3.00E-0	0.97	0.08275	922.18	0.92	3.2231
2	0.008	300	7	0.86	0.0139	0.99	0.0004	0.99	0.07539	1226.08	0.94	3.5495
3	0.016	300	7	0.99	0.0313	0.85	0.004	0.99	0.05611	0.02926	0.96	4.8074
4	0.024	300	7	0.98	0.0322	0.87	0.0046	0.97	0.06879	473576.4	0.92	3.8609
5	0.04	300	7	0.99	0.0312	0.85	0.0038	0.97	0.05155	6.24293	0.91	5.135
6	0.08	300	7	0.99	0.0301	0.84	0.0033	0.99	0.05094	4.42888	0.96	5.2874
7	0.024	300	3	0.97	0.0989	0.65	0.076	0.7	0.2727	7.83759	0.56	0.9019
8	0.024	300	6.5	0.96	0.0277	0.83	0.004	0.97	0.05507	0.001797	0.97	4.9864
9	0.024	300	9	0.85	0.0103	0.97	0.0002	0.93	0.07541	2.60229	0.98	3.7335
10	0.024	300	12	0.86	0.0037	0.95	4.00E-0	0.89	0.12948	1.94039	0.96	2.2002
11	0.024	100	7	0.97	0.0502	0.9	0.0035	0.96	0.12629	778.37	0.8	3.0841
12	0.024	500	7	0.97	0.0124	0.99	5.00E-0	0.96	0.01919	3.9724	0.97	17.3
13	0.024	700	7	0.97	0.0095	0.98	2.00E-0	0.94	0.01161	2.57466	0.93	26.23
14	0.024	1000	7	0.96	0.007	0.97	8.00E-0	0.97	0.01217	7.59268	0.91	26.96

3.10. Conclusions

In this chapter, Fe^0 was synthesized to decontaminate nitrate and phosphorus from water. The Fe^0 particles were synthesized through chemical reduction of iron ions using sodium borohydride as strong reductant. Additionally, to overcome the particle aggregation, four different polymers were used to stabilized Fe^0 particles during the synthesis process. Via analysis and characterization, the obtained Fe^0 had a necklace-like structure with completely aggregated particles. The stabilization of Fe^0 with the used polymers broke down necklace-like structure and showed the particles smaller and dispersed. CMC was the most efficient polymer for producing small particle size lower than 10 nm. For example, CMC/Fe^0 exhibited the smaller size (10 nm), followed by bare/Fe^0 (65.4 nm), PAA/Fe^0 (106.4 nm) and PVP/Fe^0 (108.8 nm).

The synthesized Fe^0 particles were characterized before and after the stabilization process with the used polymers. TEM results confirmed that the aggregation of Fe^0 can be prevented by the used polymers through steric and electrostatic repulsion mechanisms. XRD and EDX confirmed the adsorption of the polymers on the surface of Fe^0. In addition, FTIR analysis confirmed the adsorption of polymers on the surface of Fe^0 through carbonyl and hydroxyl groups.

Concerning the effect on nitrate removal, all the used polymer in this research enhanced nitrate removal as follows in the following order; PVP/Fe^0 (238.9 mg/g) > PAA/Fe^0 (237.6 mg/g) > PSM/Fe^0 (233 mg/g) > CMC/Fe^0 (216 mg/g) > bare/Fe^0 (133 mg/g). Concerning phosphorus adsorption, the removal of phosphorus was improved only by using PAA/Fe^0, following the order of PAA/Fe^0 (78 mg/g) > bare/Fe^0 (61 mg/g) > PSM/Fe^0 (60 mg/g) > PVP/Fe^0 (58.4 mg/g) > CMC/Fe^0 (56.8 mg/g). The results of this research suggested PVP/Fe^0 as the best stabilized type of iron for efficient removal of nitrate, but at the same time it was not preferred for phosphorus removal. The stabilized PAA/Fe^0 was the most efficient stabilized iron type over the rest for simultaneous removal of nitrate and phosphorus with excellent removal rate at a wide range of pH

CHAPTER 4

APPLICATION OF COATED Fe^0 WITH $Mg(OH)_2$ IN ENERGY GENERATION

Chapter 4: Application of coated/Fe^0 for biogas and methane production

This chapter presents a literature survey on renewable energy generation, anaerobic digestion process, and the scenarios used to improve methane production. Also, presents a new technique used in this research to increase the production rate of methane gas. The new approach includes the use of Fe^0 coated with $Mg(OH)_2$ as an additive to improve the anaerobic digestion process of waste sludge. The experiments were performed in a batch mode and then scaled up to a semi-continuous system. The results of these experiments were explained, compared to that of Fe^0, and the previously reported in the literature.

4.1. Introduction

Anaerobic digestion (AD) of waste sludge has been widely used for methane production over the past decades. Although, the low conversion efficiency of organic matter to energy limits its further application as a renewable and dependable source of energy. Indeed, due to the exacerbation of environmental problems caused by the extensive use of unclean sources of non-renewable energy, the need has emerged to develop alternative and clean sources of energy.

Methane generation is considered as one of the clean sources of energy generated from the degradation of organic matter existed in the waste sludge. Due to its high production rate, high content of organic matter, and high disposal cost, the waste sludge is considered a suitable feedstock for the anaerobic digestion process.

The anaerobic digestion of waste sludge not only serves as a disposal and treatment method but also provides a considerable amount of methane [63]. For this reason, the concerns on how to improve the AD process have increased over the last two decades.

Therefore, numerous studies have been conducted to overcome the limitation of methane generation and increase its production rate. Generally, three main techniques have been applied in the literature to maximize methane production of waste sludge.

The pretreatment of waste sludge has proved as an efficient way to improve methane production rate. However, the high energy required for the pretreatment process is too high to be recompensed by the additional methane production making this approach unfeasible for the practical applications [64].

Co-digestion is another effective way to improve the production of methane. But, the increased rate of methane by applying this way comes from the co-digester, not from the efficient degradation of waste sludge [65]. For the above reasons, dosing external additives such as trace metal oxides and zero-valent metals have been used to increase methane production rate by increasing the degradation efficiency of organic matter of the waste sludge itself [66]. This option seems to be the most applicable for the AD process due to the availably and affordability of the trace additives and their crucial role in improving methane generation. Therefore, numerous studies have been conducted on the enhancement of methane generation using different additives.

It was previously reported that the metal oxides and zero-valent nanoparticles were the most used additives in AD [67]. Recently, CuO [11], ZnO [12], TiO_2, SiO_2, Al_2O_3 [13], and CeO_2 [14], and Fe_3O_4 [15] have been used in the AD. Results showed that the effect of metal oxides on the performance of AD has varied where CuO, ZnO harmed the AD in which methane production decreased by 15 % using 1.4 mg/L of CuO and 18 % using 120 mg/L of ZnO.

The reduction of methane production was attributed to the negative effect of CuO and ZnO on hydrogentrophic and acetoclastic methanogenesis.

On the other hand, methane production was not affected by the addition of TiO_2, SiO_2 and Al_2O_3 at varied dosages of 6, 30 and 150 mg/g TSS. In contrast to these results, Garcia et al. [68] studied the effect of TiO_2 and found 11 % increase in methane production compared to the control reactor. Also, Casals et al. [15], used iron oxides (Fe_3O_4, 7 nm) with a dose of 100 ppm to be slowly dissolved for supplying the living microorganism with the needed iron ions without causing any adverse effect.

The results showed that Fe_3O_4 greatly enhanced biogas and methane production by 180 % and 234 %, respectively. However, Strella et al. [69], investigated the effect of iron oxide (Fe_2O_3, 10-100 nm) with a dose of 1500 mg/L. The results showed the negative effect of Fe_2O_3 on the methanogens activities and this in disagreement with the results of Fe_3O_4 obtained by Casals.

Considering the above results of iron oxides (Fe_2O_3 and Fe_3O_4), iron oxide should be added with low dosages or with the optimal dosage to avoid any negative effect on anaerobes. Generally, most of metal oxides were not preferred or had no significant effect in enhancing methane production. Besides the metal oxides, zero valent nanoparticles such as Fe^0, Cu^0 and Ag^0 have been widely applied in the AD [67]. Obviously, zero valent iron was one of the most used zero valent nanoparticles in the AD [70].

The extensive application of zero-valent iron is ascribed to the following reasons:

First, the reduction/oxidation cycle of Fe^{2+} and Fe^{3+} could speed up the electron flow generated from the oxidation of acetate to hydrogenotrophic methanogenesis, proving its role in improving the methane production mechanism.

Second, the ability of Fe^0 to act as an electron donor makes it a suitable additive for the AD process [71, 72]. Along with the immediate release of electrons from the core of zero-valent iron, zero-valent iron oxidizes in the anoxic conditions, leading to produce H_2 to serve as an electron source to accelerate the conversion of CO_2 to CH_4 as presented in the following equations.

$$Fe^0 + 2H^+ \dashrightarrow Fe^{2+} + H_2 \quad (1)$$

$$CO_2 + 4H_2 \dashrightarrow CH_4 + 2H_2O \quad (2)$$

Third, it has been proved that the addition of Fe^0 in the AD reactors plays as a buffering substance for maintaining the pH value within the optimal range thereby, increasing the alkalinity to improve the AD process as described in the following equations [67, 73].

$$4Fe^0 + 8H^+ + CO_2 \dashrightarrow 4Fe^{2+} + CH_4 + 2H_2O \quad (3)$$

$$Fe^0 + 2H_2O \dashrightarrow Fe^{2+} + H_2 + 2OH^- \quad (4)$$

Fourth, iron is well known as an essential nutrient that stimulates the microbial activates and supports their metabolisms during the AD process [66]. For the above reasons, Fe^0 is a more attractive candidate for the AD process.

Several studies investigated the influence of micro and nano Fe^0 on the AD process. Su et al. [74], used 0.1 wt % of Fe^0 during the AD of waste activated sludge which lasted for 17 days. Their results showed the positive effect of Fe^0 on the AD process, where biogas and methane improved by 30.4 % and 40.4%, respectively. However, several studies have shown that the use of Fe^0 in the AD reactors harmed methanogens and methane production. Yang et al. [75], investigated the effect of Fe^0 (55±11 nm) on methanogens and their results have shown a decrease of 20 % and more in methane production at a dose of 1 mM and above. It was attributed to the fast hydrogen production and released iron ions due to the rapid corrosion of Fe^0. For this reason, several studies have used a second metal to be doped on the surface of Fe^0 to reduce the dissolution rate of Fe^0 and slowly supply the microorganism with the required iron ions.

For instance, Amen et al. [76], investigated the effect of Cu/Fe^0 nanoparticles on biogas and methane production. Their results showed that Cu doping on the surface of Fe^0 greatly improved biogas and methane production. Despite the extensive application of nanomaterials in AD, the use of Mg/Fe^0 nanoparticles have not been reported yet, highlighting the novelty of the present study. Therefore, the objective of the present study was to investigate the effect of Fe^0 coated with $Mg(OH)_2$ shell (Mg/Fe^0 coating ratios: 0.05, 0.5, and 1) on biogas and methane production.

4.2. Batch experiments

Batch experiments were conducted to investigate the effect of Fe^0 and Fe^0 coated with $Mg(OH)_2$ on methane production through an anaerobic digestion process of waste sludge. All factors that affect the operation process of anaerobic digestion, including the coating ratio of $Mg(OH)_2$ to Fe^0, Mg/Fe^0 dosage, Mg/Fe^0 dosing time, pH, and bacterial growth, were investigated using batch experiment mode.

The detailed operation conditions of the batch experiments were presented in chapter 2, section 2.6.2. After that, a semi-continuous system was operated for long-term investigation and to simulate the real application of the anaerobic digesters in the presence of Mg/Fe^0 nanoparticles. The detailed operation conditions of the semi-continuous system were presented in chapter 2, section 2.6.3.

4.3. Characterization of bare and coated Fe^0

4.3.1. Morphological structure of bare and coated/Fe^0 nanoparticles

The surface structure of Fe^0 before and after coating with $Mg(OH)_2$ shell was illustrated in Fig. 4-1. It was clear that the bare Fe^0 nanoparticles appeared aggregated with a chain-like structure of the spherical particles as shown in Fig. 4-1a. Correspondingly, the coated Fe^0 particles with a coating ration of 0.05 appeared with less aggregation than the bare Fe^0 particles. The $Mg(OH)_2$ shell appeared around the particles. But still, the coating ratio of 0.05 was not enough to produce completely separated particles with covering the whole surface of Fe^0 to control and preserve the reactivity.

Additionally, the $Mg(OH)_2$ coating ratio of 0.5 showed the particles separated with a remarkable coating layer on the surface of Fe^0 as shown in Fig. 4-1c. The image confirmed that the coating ratio of 0.5 was enough to coat the particles to organize and slow the corrosion reaction of Fe^0. Increasing the coating ratio of $Mg(OH)_2$ up to 1 resulted in forming a thick layer around the Fe^0 particles as shown in Fig. 4-1d. Therefore, among different coating ratios of $Mg(OH)_2$ shell to Fe^0, the ratio of 0.5 was considered the best coating ratio to produce separated and coated particles with a reasonable coating layer. Moreover, the ratio of 0.5 was the best in terms of showing a high performance of Mg Fe nanoparticles in the anaerobic digestion reactors for high methane production rate.

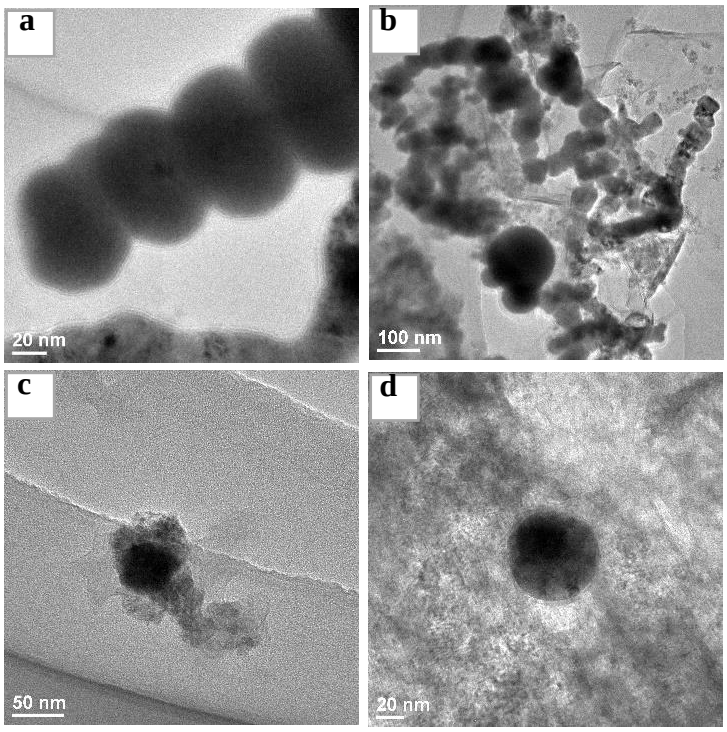

Fig. 4-1. TEM images of a) bare-Fe^0, b), c) and d) coated Fe^0 with Mg $(OH)_2$ shell with different coating ratios $[Mg/Fe^0]^{0.05}$, $[Mg/Fe^0]^{0.5}$, $[Mg/Fe^0]^1$, respectively.

4.3.2. Surface composition of bare and coated Fe^0 nanoparticles

XRD analysis was conducted to examine the crystallinity and surface composition of the prepared Fe^0 and Mg/Fe^0 nanoparticles. X-ray diffractogram of Fe^0 showed the formation of Fe^0 with its major peaks at 2θ of 35.5˚, 44.8˚(sharp), and 82.16˚. Also, X-ray diffractogram of $Mg(OH)_2$ (which synthesized to coat the Fe^0 particles) confirmed the formation of $Mg(OH)_2$ with its major peck at 2θ of 38˚. Three different coating ratios of $Mg(OH)_2$ were used to coat the Fe^0 particles and their X-ray diffractograms are shown in Fig. 4-2 as well. At a coating ratio of 0.05 %, the XRD pattern was identical to the bare/Fe^0 pattern with a slight decrease in the main peck of Fe^0 at 2θ of 44.8˚.

Moreover, $Mg(OH)_2$ or MgO peaks were not observed at a coating ratio of 0.05 % implied that the coating ratio of 0.05 % of $Mg(OH)_2$ was not enough to cover the surface of Fe^0 particles.

Correspondingly, the XRD pattern at a coating ratio of 0.5 % showed many peaks refer to the presence of $Mg(OH)_2$ and MgO, and $Mg(Fe^{3+})_2O_4$, confirming the formation of $Mg(OH)_2$ shell on the surface of Fe^0 particles as observed by the TEM image. Increasing the coating ratio to 1% resulted in increasing the peaks of Mg and $Mg(OH)_2$ with obtaining a pattern like the $Mg(OH)_2$ pattern.

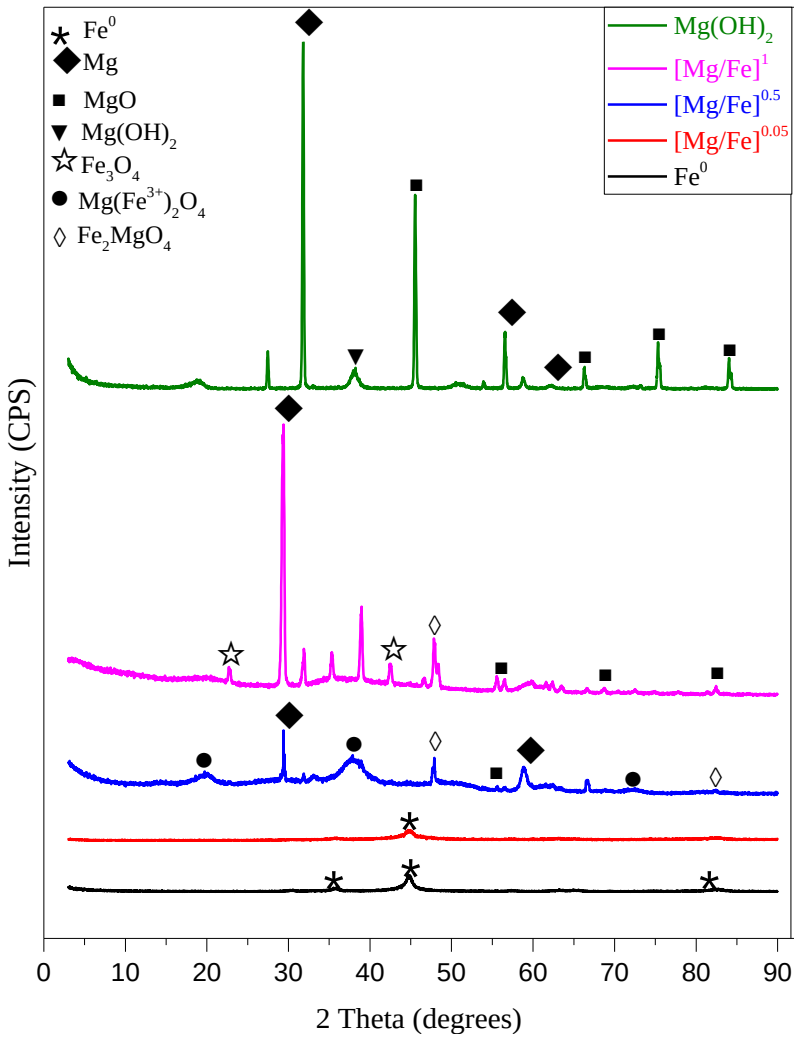

Fig. 4-2. XRD patterns of Fe^0, $Mg(OH)_2$, and coated-Fe^0 $[Mg/Fe^0]^{0.05}$; $[Mg/Fe^0]^{0.5}$; $[Mg/Fe^0]$

The surface composition of Fe^0 and the coated/Fe^0 was also examined by energy dispersive X-ray analysis (EDX) coupled with TEM. The EDX spectrum of bare-Fe^0 showed the presence of iron as the main component on the particle's surface. Also, the elemental mapping analysis of the bare/Fe^0 showed an extreme distribution of the metallic iron in the transmission electron micrograph image.

Besides, EDX of the coated-Fe^0 with magnesium at different coating ratios of 0.05, 0.5 and 1% was investigated. The EDX spectrum of the coated-Fe^0 at a coating ratio of 0.05 (Mg/Fe^0:0.05) did not show Mg in the EDX spectrum nor mapping analysis, indicating that the ratio of 0.05 was not enough to accomplish the coating process of Fe^0. In contrast, the EDX spectrum at a coating ratio of 0.5 (Mg/Fe^0:0.5) showed a broad peak of Mg at approximately 2.2 keV, confirming the adsorption of Mg nanoparticles on the surface of Fe^0. Moreover, the Elemental mapping analysis of the coated-Fe^0 (Mg/Fe^0:0.5) showed the distribution of Mg nanoparticles in the transmission electron micrograph image as shown in Fig. 4-3b.

The EDX spectrum of the coated-Fe^0 at a coating ratio of 1 (Mg/Fe^0:1) exhibited a higher Mg peck compared to other low coating ratios and the elemental mapping analysis showed an extreme distribution of Mg nanoparticles on the surface of Fe^0 particles. Hence, the EDX was quantitatively representative, and the results showed a good correlation with the variation in three different coating ratios.

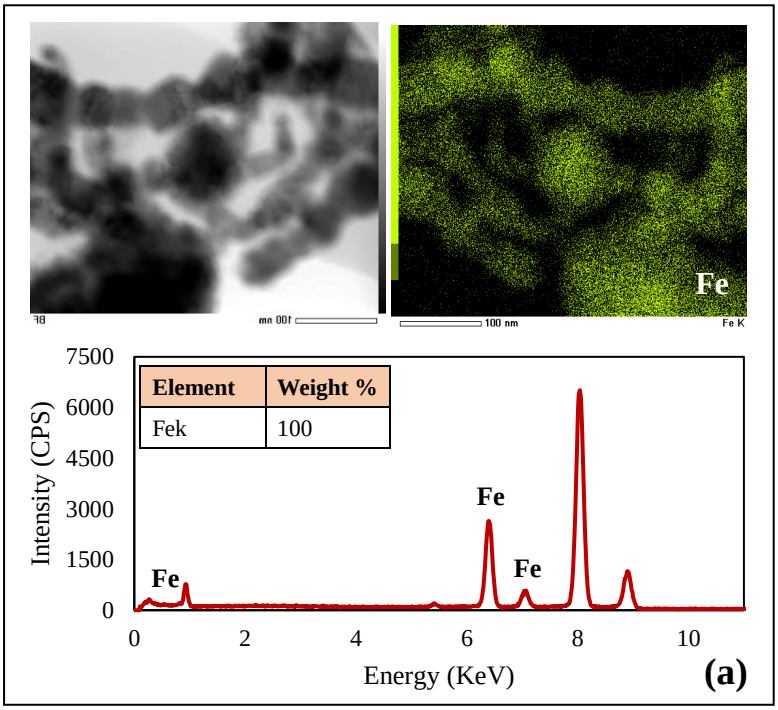
Fe
100 nm
Fe K
Element
Weight %
Fek
100
Intensity (CPS)
7500
6000
4500
3000
1500
0
Fe
Fe
Fe
0
2
4
6
8
10
Energy (KeV)
(a)

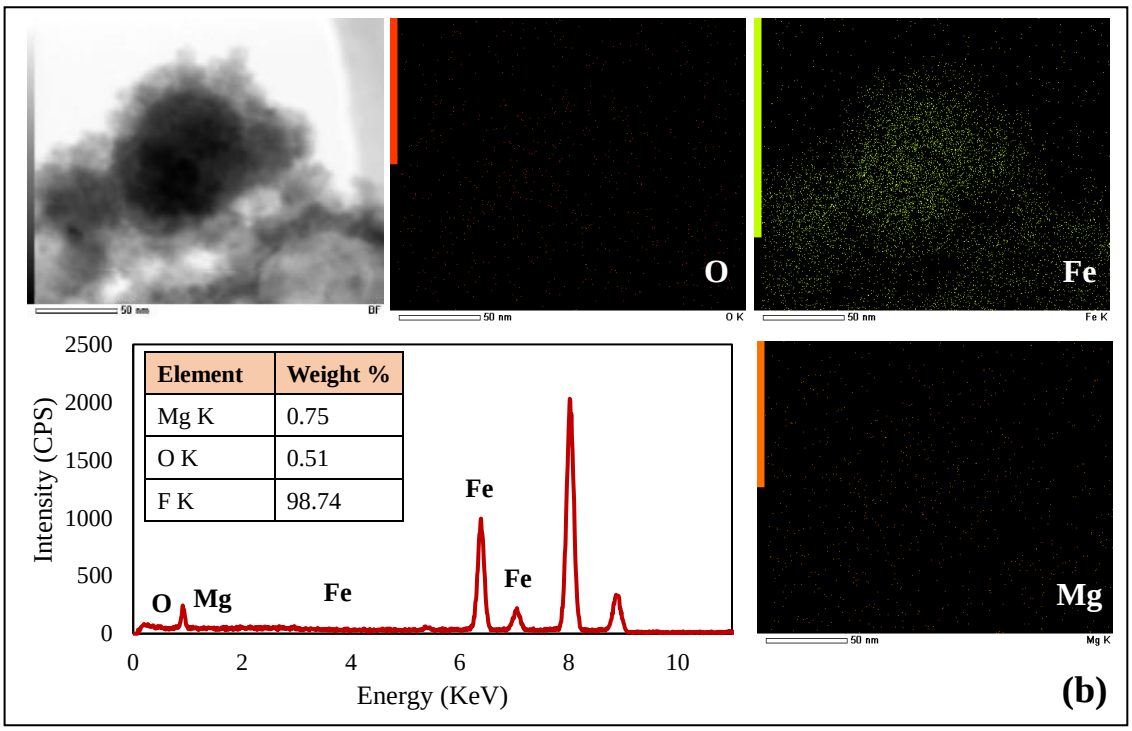

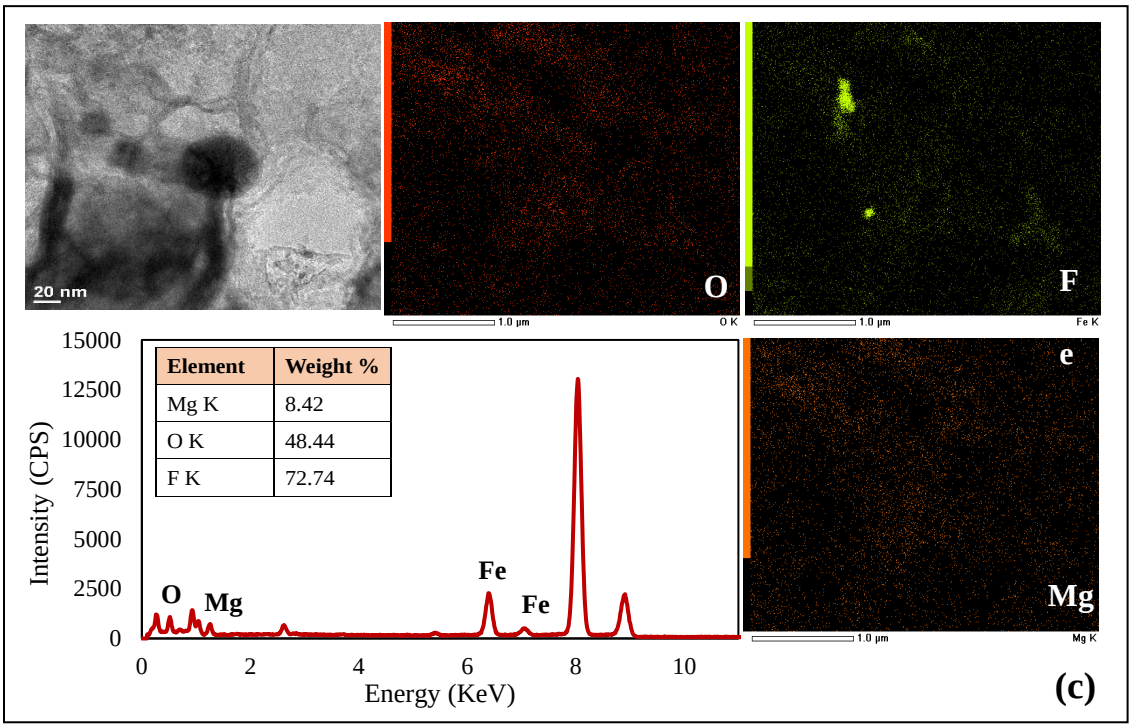

Fig. 4-3. TEM-EDX analysis of (a) bare-Fe^0; (b) coated-Fe^0 $[Mg/Fe^0]^{0.5}$; (c) coated-Fe^0 $[Mg/Fe^0]^1$.

4.4. Effect of Fe^0 on biogas and methane generation

To investigate the effect of Fe^0 nanoparticles on biogas and methane production, experiments were conducted using different dosages of Fe^0 varied between 3 to 139 mg/g VS. The results shown in Fig.4-4 showed the slight effect of Fe^0 nanoparticles on both biogas and methane production. According to the findings shown in Fig.4-4 b, methane generation was slightly increased from 255.4 to 257.5 mL/gVS when the dosage of Fe^0 raised from 3 to 14 mg/g VS. But, when the dosage of Fe^0 increased from 14 to 139 mg/g VS, methane production was adversely affected. These results were based on experiments performed three times to detect the effect of Fe^0 nanoparticles on methane generation. However, all tests confirmed the weak-positive effect of Fe^0 nanoparticles at low concentrations and the negative effect at high concentrations.

In the literature, trace elements including iron, nickel, and cobalt were used as an additive to improve the performance of anaerobic reactors. As discussed in the introduction section, Fe^0 is one of the most efficient elements that can serve as a nutrient and electron donor to enhance the efficiency of the anaerobic reactors. However, Fe^0 nanoparticles used in this study had no effect or negative effect (at dosages higher than 14 mg/g VS) on methane production. It was reported that, with high dosages, Fe^0 nanoparticles inactivate bacterial growth rate, especially during the log and lag phases [77]. Several inactivation mechanisms have been proposed, including cell membrane/wall disruption, cell structure damage, and cell function interference [78].

Bacterial inactivation by Fe^0 nanoparticles is higher under anaerobic or semi-anaerobic conditions compared to aerobic conditions, which could increase the adverse effect of Fe^0 on the anaerobic digestion process [79]. Besides that, Fe^0 with small particle size is highly reactive and releases H_2 within a short time, which could cause a significant H_2 shock to AD as described in eq. 4. [80]. In addition, the accumulation of iron ions (Fe^{2+} and Fe^{3+}) released by the rapid corrosion reaction of Fe^0 may affect methanogens activities.

Therefore, the modification of Fe^0 nanoparticles has become necessary to slowly provide the microorganisms with the needed iron ions and utilize the tremendous benefits of Fe^0 in improving the AD process, which synthesized based on the optimized synthesis conditions in our previous research [30]. To do that, Fe^0 particles were coated using $Mg(OH)_2$ following the thermal deposition method. $Mg(OH)_2$ was deposited on the surface of Fe^0 particles to overcome the drawbacks of Fe^0 particles and make them suitable for stimulating the anaerobic digestion process.

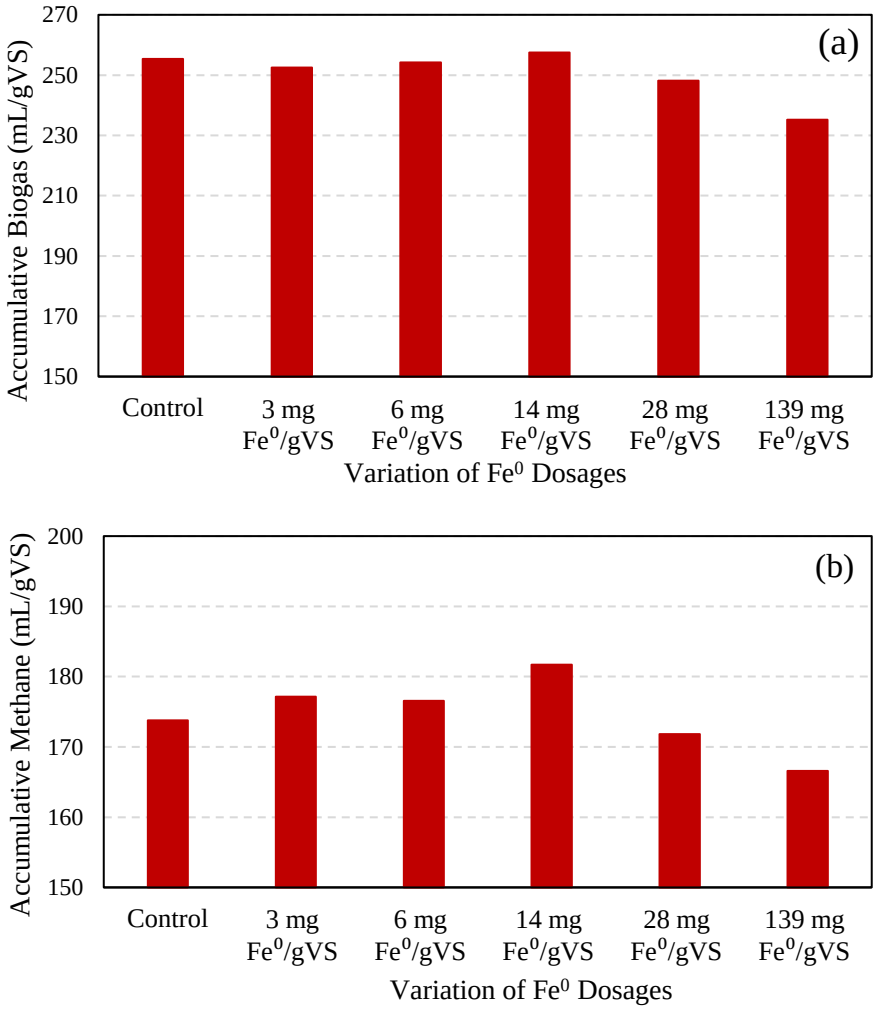

Fig.4-4. Effect of Fe^0 dosages on biogas and methane production after 45 days of fermentation

4.5. Effect of $Mg(OH)_2$ on biogas and methane generation

$Mg(OH)_2$, which was used for Fe^0 coating, was also applied in the anerobic digesters to figure out its role in accelerating methane production. $Mg(OH)_2$ nanoparticles were added into anaerobic digesters with various dosages ranged between 3 to 140 mg/gVS. Results showed that the addition of $Mg(OH)_2$ nanoparticles did not contribute in improving biogas production as displayed in Fig. 4-5.

For methane gas production the addition of $Mg(OH)_2$ nanoparticles
contributed a little in enhancing methane production. As shown in Fig. 4-5 b, methane production was enhanced by 13 % with respect to control at a dose of 140 mg of $Mg(OH)_2$/gVS.

Noticeably, the addition of Fe^0 and $Mg(OH)_2$ separately in the anaerobic digesters did not contribute significantly to improve methane production. However, when the Fe^0 nanoparticles were coated with $Mg(OH)_2$ and added into anaerobic digesters, a considerable increase in biogas and methane production was noticed as shown in section 4.6.
The reason behind this increment was due to the synergistic effect of $Mg(OH)_2$ shell and Fe^0 as discussed in section 4.6.

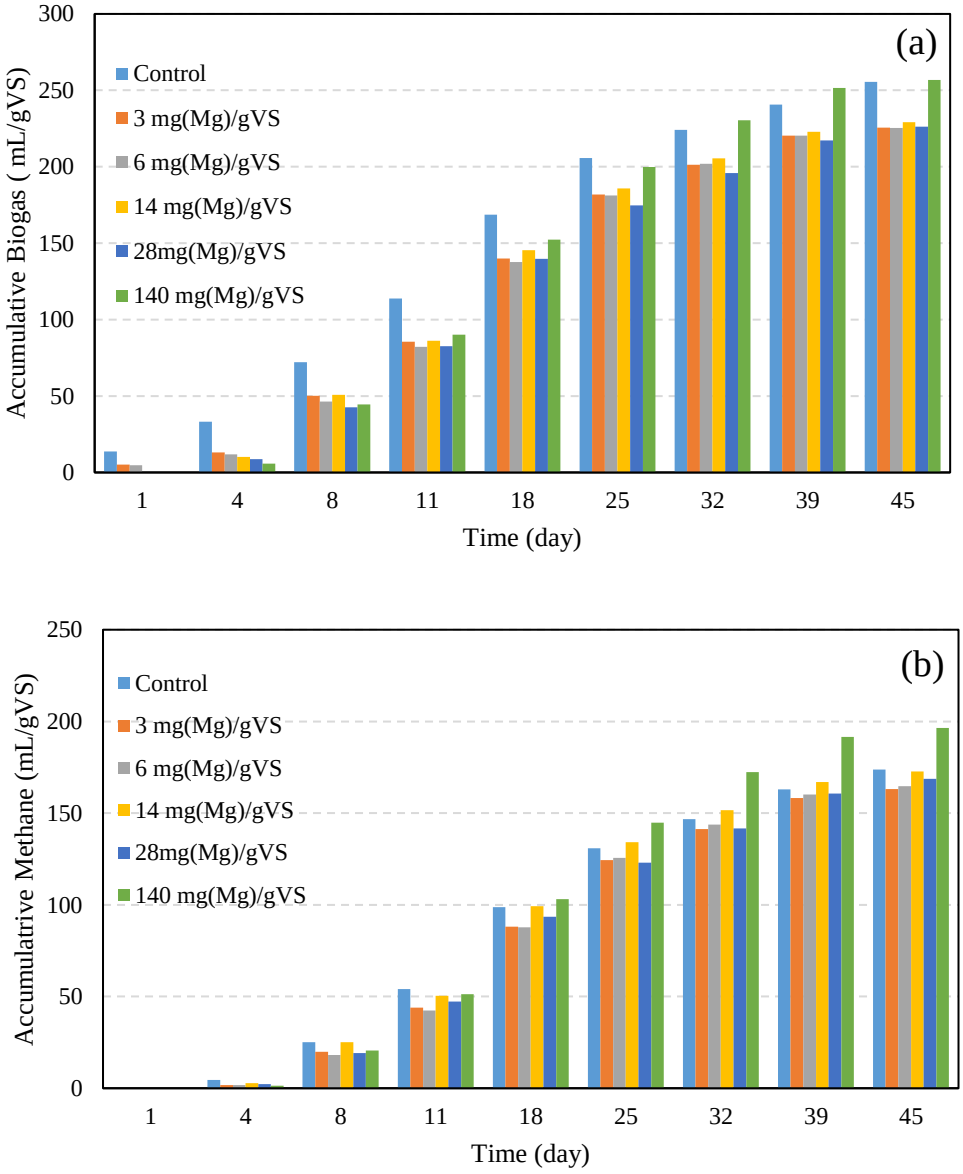

Fig.4-5. Effect of Mg^{2+} dosages on biogas and methane production over 45 days of fermentation

4.6. Effect of coated/Fe^0 on methane production; coating ratios and dosages

The Fe^0 nanoparticles were coated with $Mg(OH)_2$ shell to overcome the limitations of applying Fe^0 in the anaerobic digesters. In this regard, the particles coated with three different coating ratios (0.05, 0.5, and 100), and each investigated at various dosages (5 - 250 mg/g VS) to demonstrate the optimum coating ratio of Fe to Mg and acquiring the optimum dosage to be added in bioreactors. Fig.4-6a and Fig.4-7a show cumulative biogas and methane production over 55 days of fermentation, respectively, with adding various dosages of Mg/Fe^0 nanoparticles synthesized at a low coating ratio of 5% (Mg/Fe^0:0.05). The effect of Mg/Fe^0:0.05 nanoparticles on biogas and methane production was similar to that effect obtained by bare-Fe^0, indicating that the low coating ratio of 5% of $Mg(OH)_2$ was not enough to control and slow the reaction kinetic of Fe^0 in the anaerobic digesters. On the other hand, Mg/Fe^0:0.5 nanoparticles synthesized at a coating ratio of 50 % showed a great performance in improving the production rate of biogas and methane as shown in Fig.4-6 b and Fig.4-7 b, respectively.

Concerning dosage effect, when Mg/Fe^0:0.5 nanoparticles were dosed from 5 to 25 mg/gVS, biogas production gradually increased, and any more dosages more than 25 mg/gVS did not improve biogas/methane production. These results indicated that 25 mg/gVS of Mg/Fe:0.5 was the optimal dosage for increasing biogas and methane production. The cumulative biogas yield enhanced by 6.3, 11.1, and 25.5 % at 5, 10 and 25 mg/gVS of Mg/Fe^0:0.5 nanoparticles, respectively. Also, the cumulative methane yield enhanced by 10.9, 19.2, and 46.6% at 5, 10, and 25 mg/gVS of Mg/Fe^0:0.5 nanoparticles, respectively. It should be noted that at a dose of 5 mg/gVS, methane improvement began from the first days of the experiment, while at 10 and 25 mg/gVS, a noticeable lag period of around 10 and 18 days was observed, respectively. Despite the observed lag phase at a dose of 25 mg/gVS, methane production reached the highest level at the end of the AD compared to all other cases. To avoid any lag phases and increase the kinetic rate of methane production from the first days of AD, particle dosing time factor was well studied and addressed in the next section. Besides that, Mg/Fe^0:1 nanoparticles with a high coating ratio of 100% were investigated and exhibited less performance in improving biogas and methane production

compared to the coating ratio of 50%. The results indicated that biogas and methane production enhanced by 9 and 17.9 with adding 28 mg/gVS of Mg/Fe^0:1 as presented in Fig.4-6c and Fig.4-7c, respectively. Anymore doses higher than 28 mg/gVS of Mg/Fe^0:1 resulted in deteriorating biogas and methane generation. Overall, Mg/Fe^0 prepared at a coating ratio of 50 % had the highest methane content, up to 46.6%, compared to other coating ratios of 5% and 100%.

The improvement of methane production was attributed to the role of $Mg(OH)_2$ coating layer in controlling and slowing the corrosion reaction of Fe^0. The reasons behind this improvement can be summarized in the following points:

First, H_2 is necessary for CO_2 conversion during methanogens process as shown in eq. 2. [81], and the released H_2 from iron corrosion reaction might promote hydrogenotrophic methanogenesis and homoacetogenesis bacteria [82].

However, the rapid corrosion of Fe^0 could affect the accumulation of H_2, which will adversely affect the AD process [80]. Therefore, Coating of Fe^0 slowed the evolution rate of H_2 as described in eq. 4. Doing so, H_2 was slowly supplied in the bioreactors and methanogenesis activities were promoted. Second, the released electrons by the corrosion reaction of Fe^0 are necessary for methanogens to generate methane and reduce the protons to H_2 (Eq. 1), which is subsequently utilized for CO_2 conversion (Eq. 2).

However, a moderate release of electrons is necessary to avoid the reductive decomposition of the cell membrane [80]. Additionally, during the AD, the high iron's corrosion leads to the high electron's accumulation, which will further affect the electron's flow resulting from the oxidation of acetate. Therefore, the coating process of Fe^0 nanoparticles leads to mitigate their reductive force by slowing the transfer rate of electrons, leading to improve the AD mechanism and methane generation rate.

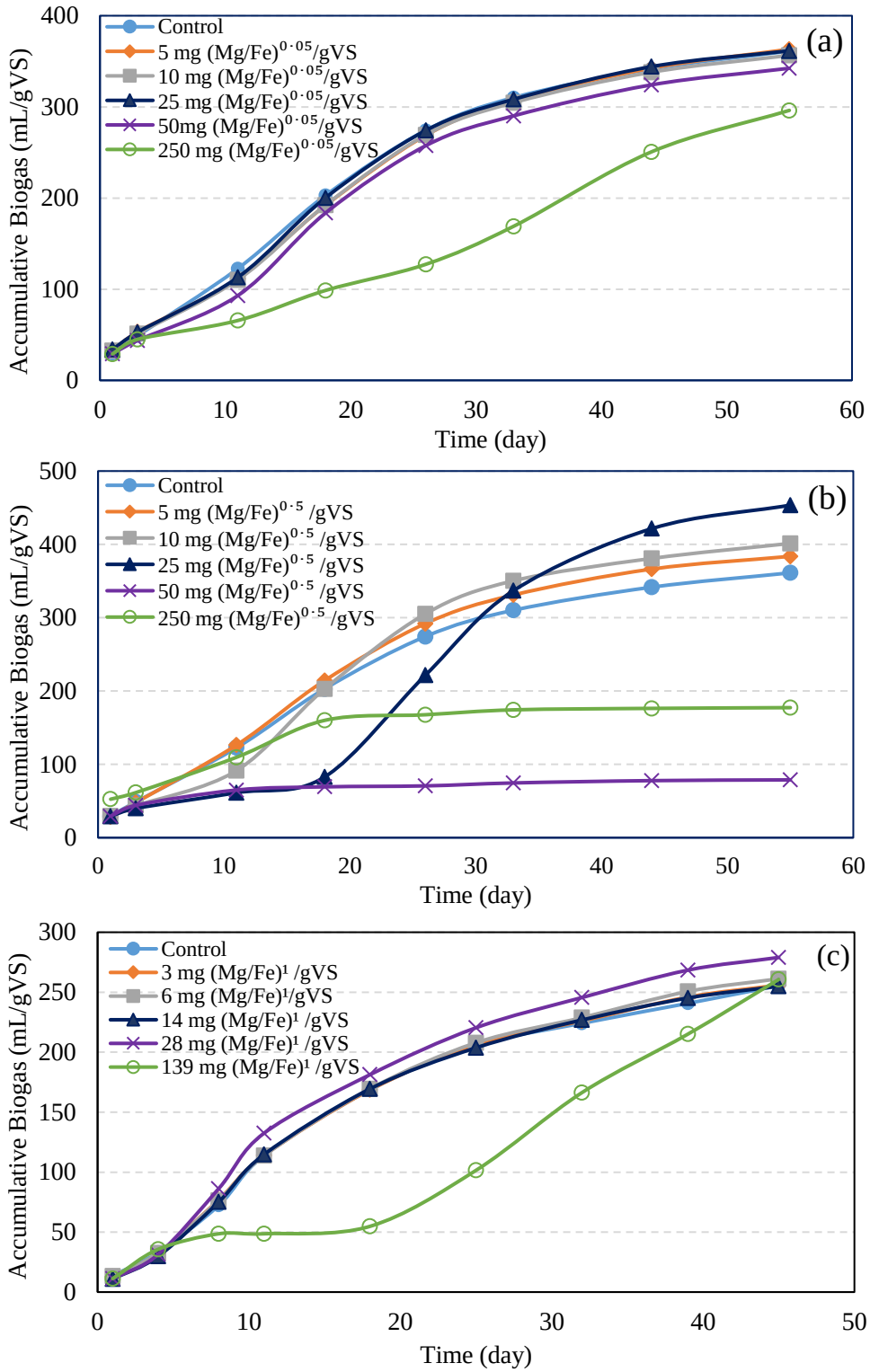

Fig.4-6. Effect of coated-Fe^0 with Mg nanoparticles on biogas production a) coating ratio of 5%, b) coating ratio of 50% and c) coating ratio of 100%.

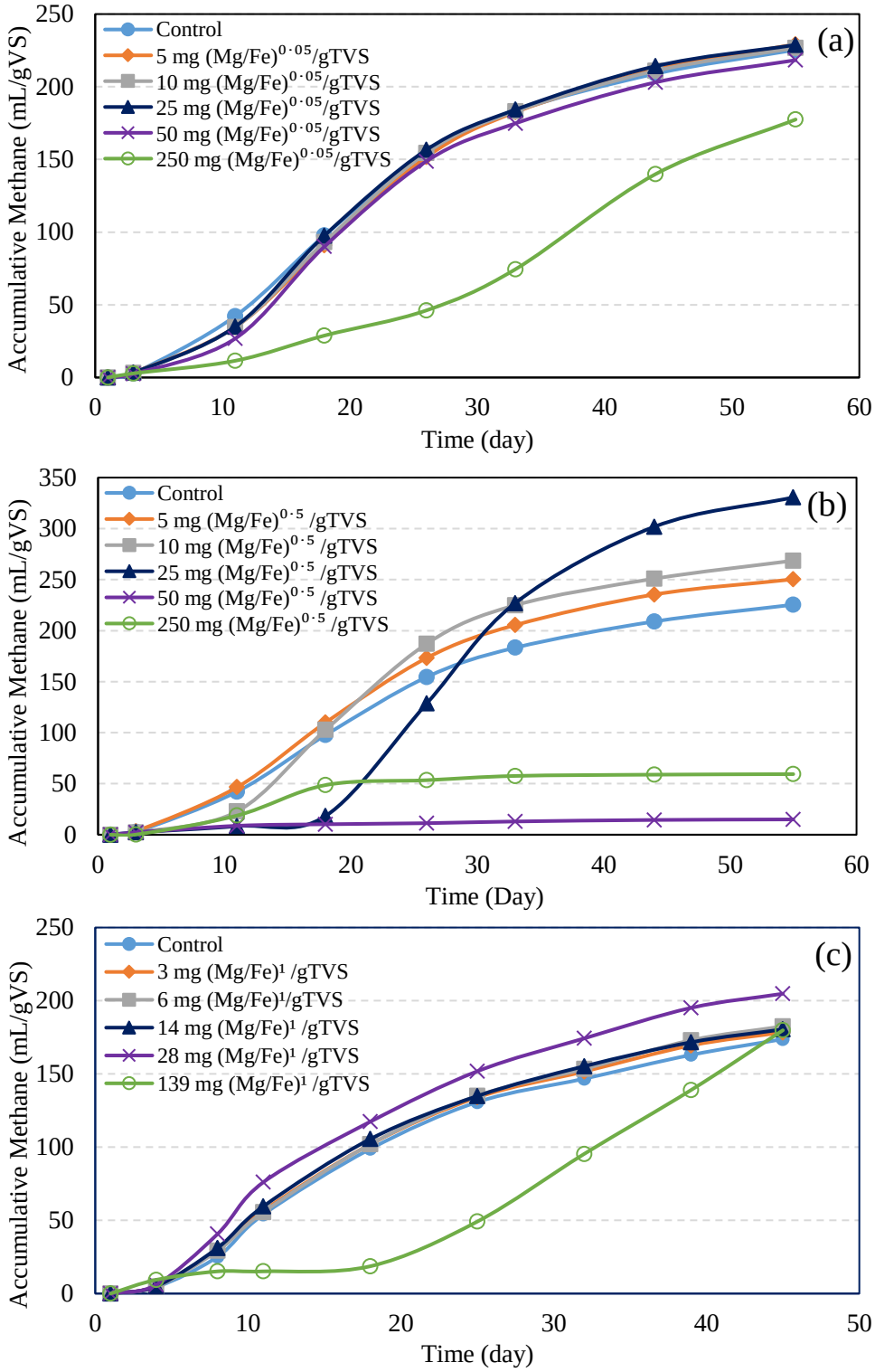

Fig.4-7. Effect of coated-Fe^0 on methane production a) coating ratio of 5%, b) coating ratio of 50% and c) coating ratio of 100%.

4.7. Effect of dosing time of Mg/Fe^0:0.5 nanoparticles

As shown in Fig.4-7b, the highest accumulative methane was observed in the reactor with 25 mg Mg/Fe^0:0.5 per gVS. However, a long lag period of around 18 days was observed. To speed up the digestion rate along with eradicating the possibility of having any lag phases, Mg/Fe^0:0.5 nanoparticles were added to the bioreactors at different times. A fixed dosage of 50 mg Mg/Fe^0:0.5 per gVS, which was higher than the optimum dose of Mg/Fe^0:0.5 obtained in Fig. 4-7b, was used to discover the best addition time of Mg/Fe^0:0.5 on the AD process. Fig.4-8 a and b show the accumulative biogas and methane generated after 55 days of fermentation, respectively.

The results indicated that the addition of Mg/Fe^0:0.5 immediately at the beginning of the AD resulted in inhibiting biogas and methane production with a lag period lasted for 55 days with very low, and in some cases, no biogas and methane production. On the contrary, the addition of Mg/Fe^0:0.5 nanoparticles after 1, 3, 4, 5, 7, 10 and 15 days led to improve biogas production by 16.5%, 10.8%, 15.2%, 16.6%, 23.2%, 25.4%, and 16.1% compared to the control, respectively.

Also, methane further improved by delaying the addition time of Mg/Fe^0:0.5 nanoparticles. Methane improved by 21.5%, 18.3%, 24.7%, 26.1%, 38.0%, 38.7% and 27.3% compared to the control when Mg/Fe^0:0.5 were added after day 1, 3, 4, 5, 7, 10, and 15, respectively. These results have proved the importance of the dosing time of Mg/Fe^0:0.5 nanoparticles on biogas and methane generation. It was reported that the addition of iron and iron-based nanoparticles at the beginning of the AD could affect the acidifying bacteria. Thereby, methanogens phase stars with a low concentration of VFAs. Therefore, methane generation will be lower when the nanoparticles are added immediately at the beginning of AD [82]. Moreover, these results are consistent with the obtained results by Chaithawiwat et al. [77], which proved that the effect of nanoparticles on bacteria was growth phase dependent.

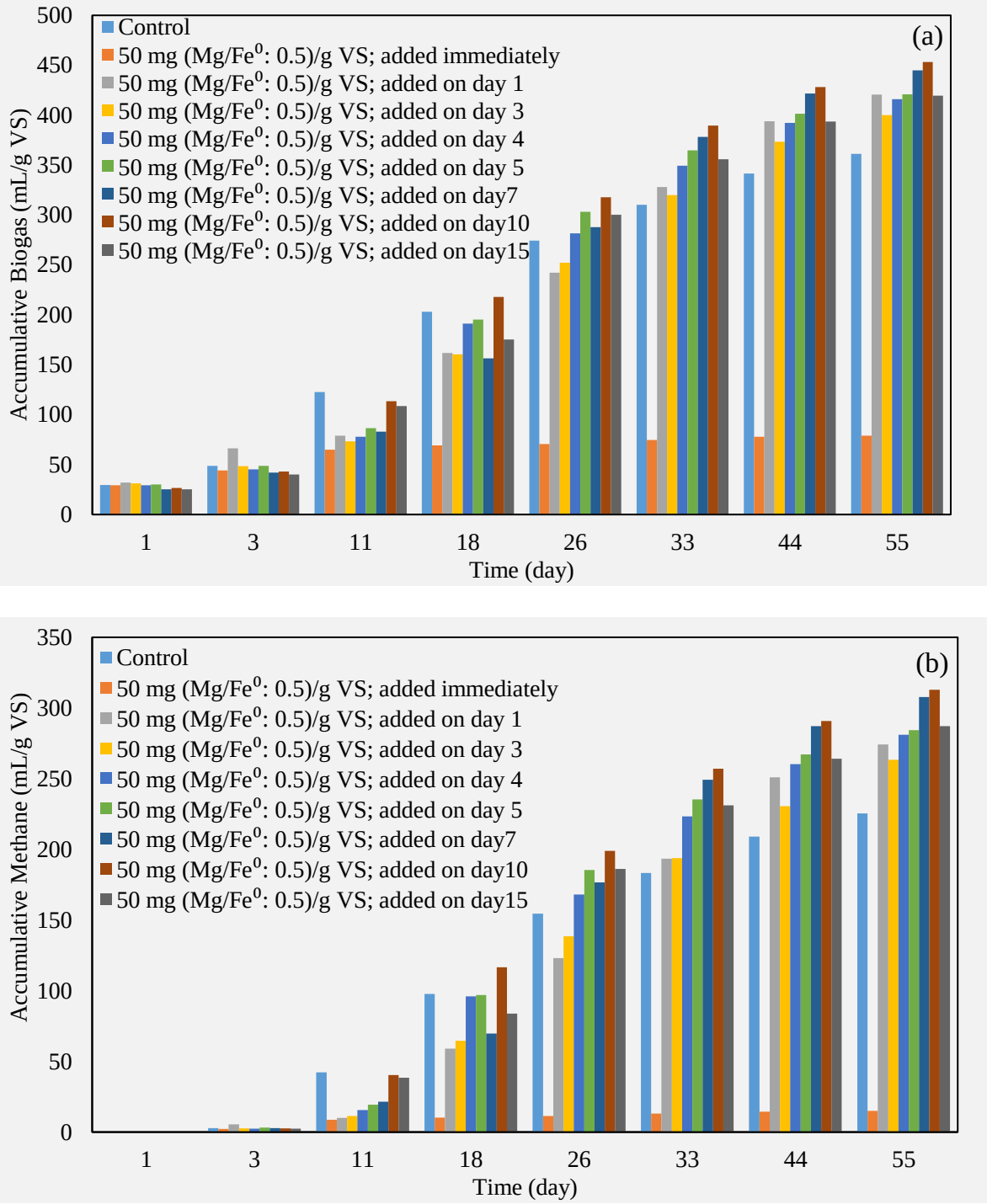

Fig. 4-8. Effect of dosing time of coated-Fe^0 (Mg/Fe^0:0.5) on a) biogas and b) methane production.

4.8. Effect of pH

The digester pH is a crucial parameter that influences the microbial activity and the stability of the anaerobic digesters [83]. The optimum pH value for methanogenic activity has been proved in the range of 6.6 to 7.8 [84]. Under the optimum pH value, anaerobes exhibit their highest growth rate, which leads to achieving the highest degradation rate of organic matter. During the AD, the pH value decreases at the early stage of AD due to the accumulation of VFA. Moreover, several feedstocks have pH values lower than the optimum range (e.g., food waste pH is lower than 4.5), which leads to slow the AD process using such feedstocks [85, 86].

It was reported that when methanogens were exposed to acidic pH (pH = 5.1) in a batch experiment, their specific decay rate was increased ten times compared to that at pH 7.0 [87]. Therefore, the pH value must be maintained within the optimum range during the AD. In this study, batch experiments were conducted by adjusting the initial pH of the used waste sludge to four different values (3, 7, 9, and 12), to investigate the performance of the anaerobic digesters under different pH values and to find out the role of the used nanoparticles (Fe^0 and Mg/Fe^0:0.5) in maintaining the pH value within the optimum range during the AD process. During the AD, the changes in pH values were monitored over 55 days in all reactors set at different initial pH values, and the corresponding cumulative biogas/methane production was measured. Fig4-9 a shows the changes in pH in three digesters, where the initial pH of each was set at 3. The results showed that the addition of Fe^0 and Mg/Fe^0 to the digesters, at a dose of 18 mg/gVS, was brought the pH to be within the optimum range, whereas the control pH remained less than three over the whole period.

This observation could be the main reason behind the inhibited biogas and methane production in the control reactor when the initial pH was adjusted at 3 as shown in Fig 4-10. On the other hand, the addition of Fe^0 or Mg/Fe^0 to the other digesters has neutralized the pH, which resulted in stimulating methanogens for further biogas/methane production. Fig. 4-10 b, c, and d display the changes in pH of the reactors whose initial pH values were set at 7, 9, and 12, respectively. The results showed that while the initial pH was above 7, the pH of the digesters was in the desired range and the reactors which Mg/Fe^0 was added had the highest pH at all initial pH values.

Moreover, as shown in Fig 4-10, the addition of $MgFe^0$ in the reactors resulted in increasing the biogas and methane production rate at all initial pH values (3, 7, 9 and 12) compared to that of Fe^0 and control reactors. These results illustrate one of the reasons behind the improved methane production with the addition of Mg/Fe^0. Evidently, both Fe^0 and $MgFe^0$ served as buffering substances during the AD for neutralizing the pH value to be within the optimum range by dissolution of Fe^0 as described in the following equations [67, 73].

$$4Fe^0 + CO_2 + 8H^+ \rightarrow = 4Fe^{2+} + CH_4 + 2H_2O \quad (5)$$

$$Fe^0 + 2H_2O \rightarrow Fe^{2+} + H_2 + 2OH^- \quad (6)$$

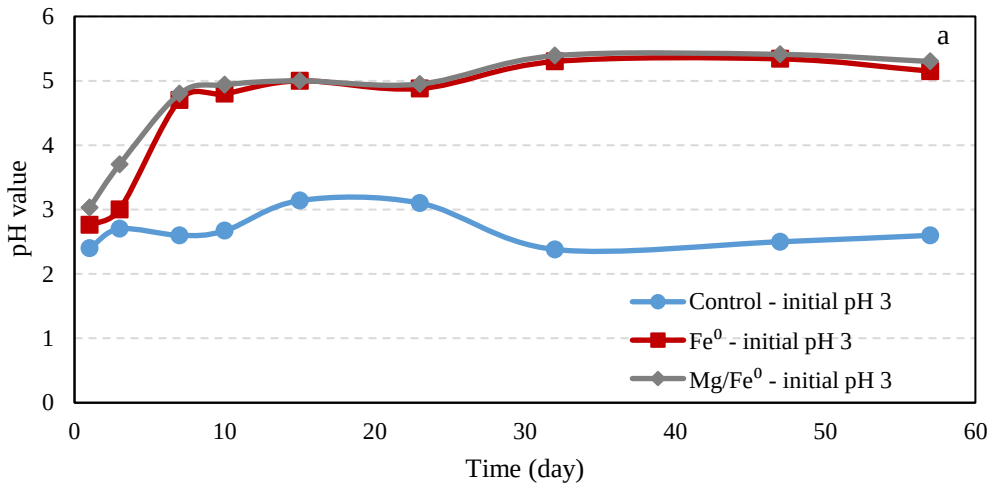

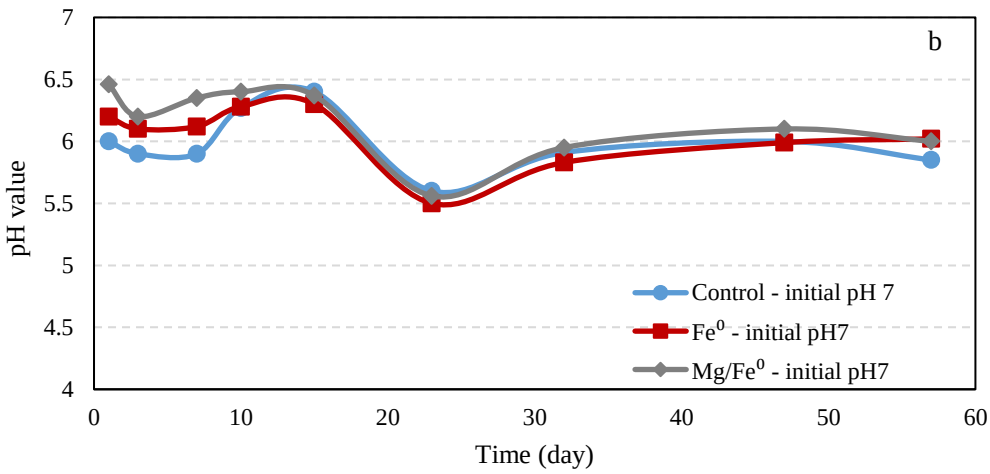

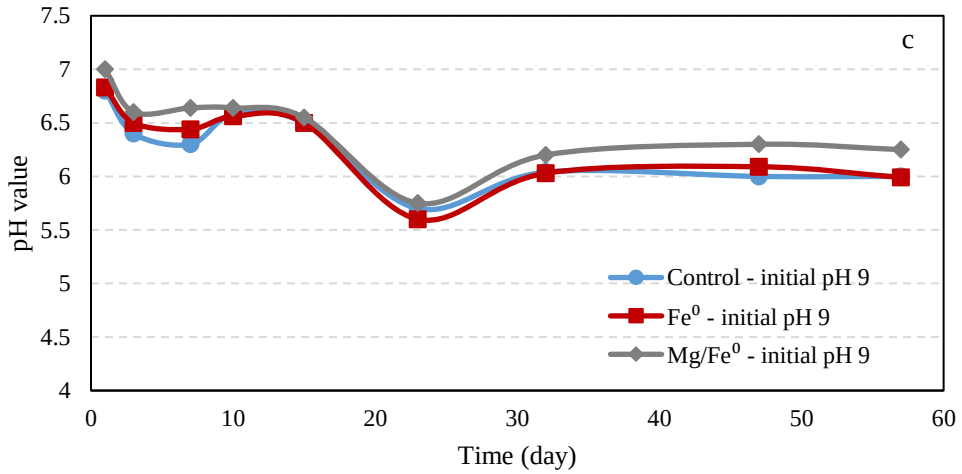

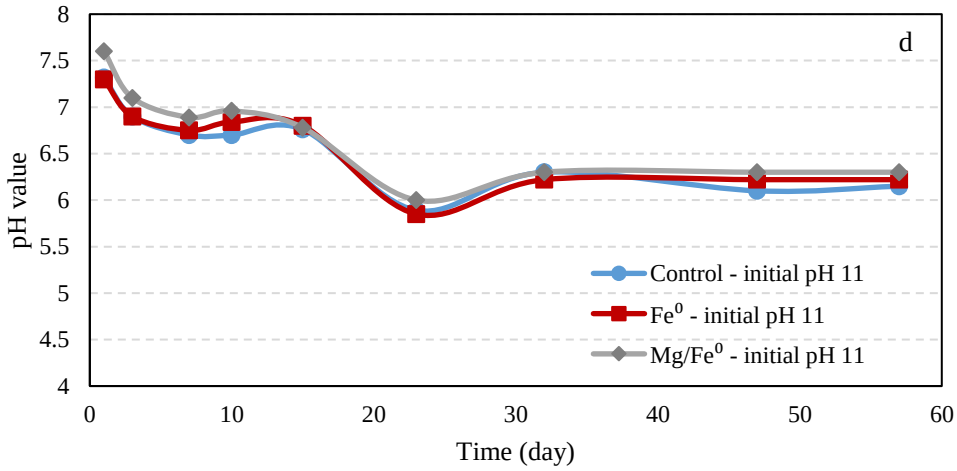

Fig.4-9. Changes of pH values during the AD process of waste sludge at different initial pH values; a) initial pH3, b) initial pH7, c) initial pH9, d) initial pH12

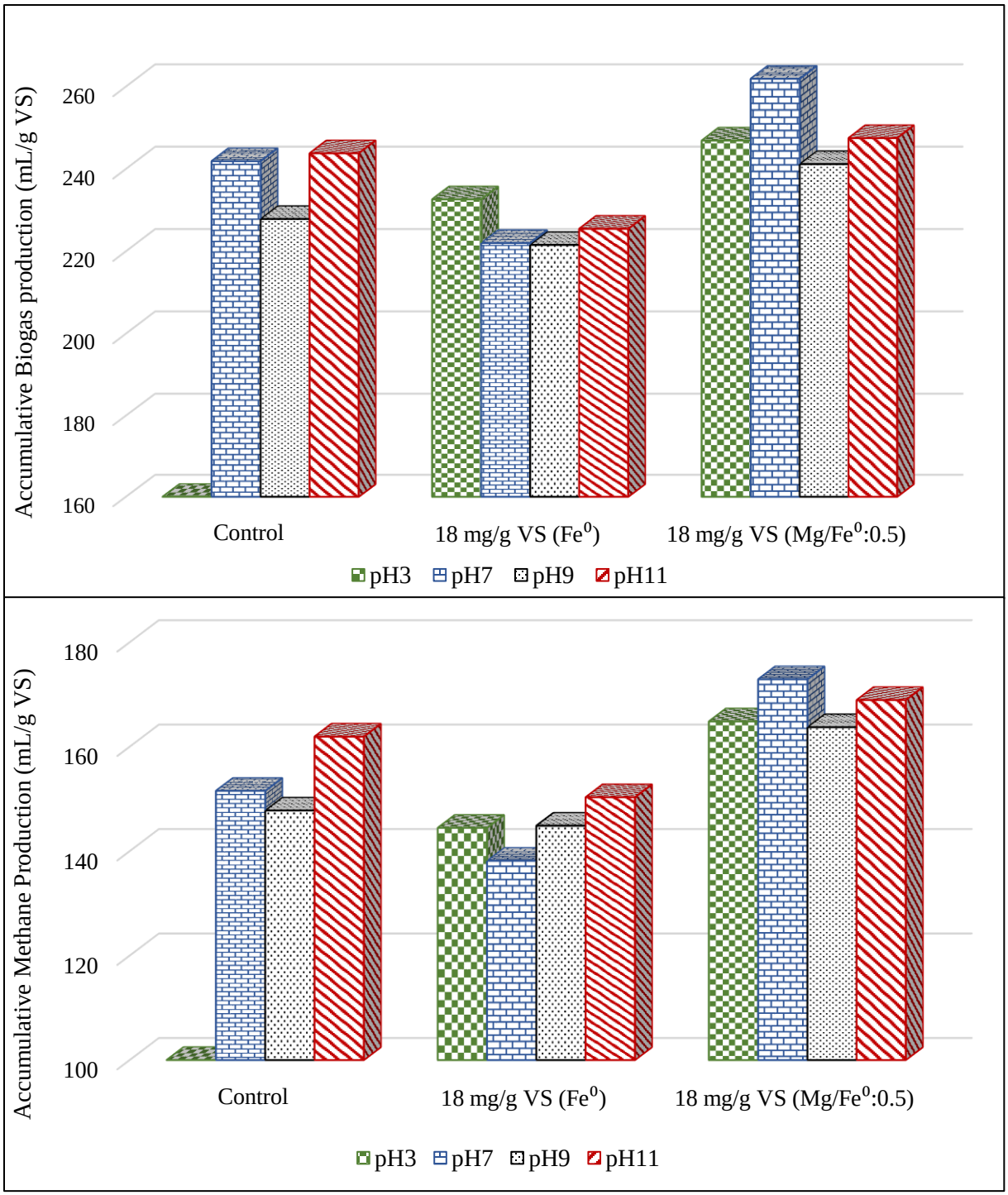

Fig. 4-10. Effect of initial pH values of waste sludge on biogas and methane production with demonstrating the role of Fe^0 and coated-Fe^0 (Mg/Fe^0:0.5) in improving biogas and methane generation under different initial pH values.

4.9. Effect of coating process on the corrosion reaction of Fe^0

The accumulation of iron ions during the AD process could negatively affect methanogen's activities, especially at the beginning of AD. The addition of bare/Fe^0 particles largely contributed in accumulating iron ions (Fe^{3+} and Fe^{2+}) in the anaerobic digesters due to its high corrosion reaction. As shown in Fig. 4-11 a, b and c, ferrous, ferric, and total iron were regularly analyzed in the reactors during the AD.

Results indicated that the addition of bare/Fe^0 considerably increased iron ions concentration in the reactors compared to the control reactor. On the other hand, the addition of coated/Fe^0 particles did not increase iron ions concentration in the reactors which was like that concentrations in the control reactor. Tracing iron ions concentration indicates the crucial role of the coating process in controlling and reducing corrosion reaction of Fe^0 particles.

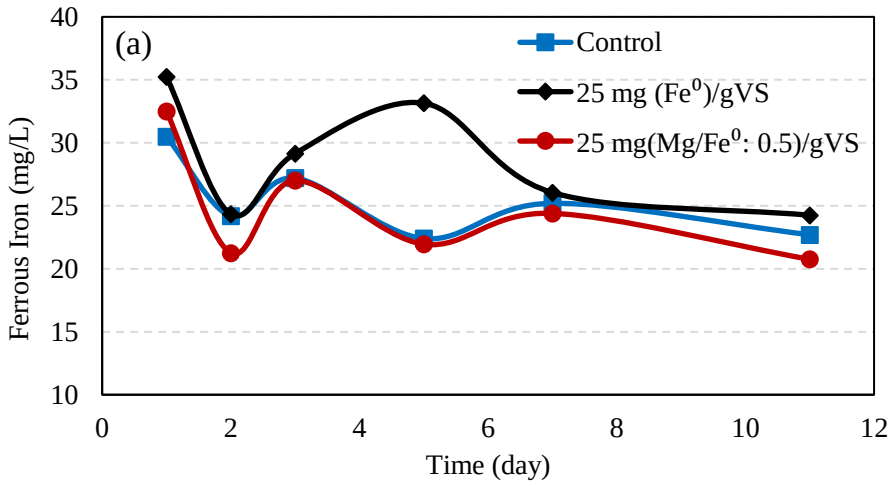

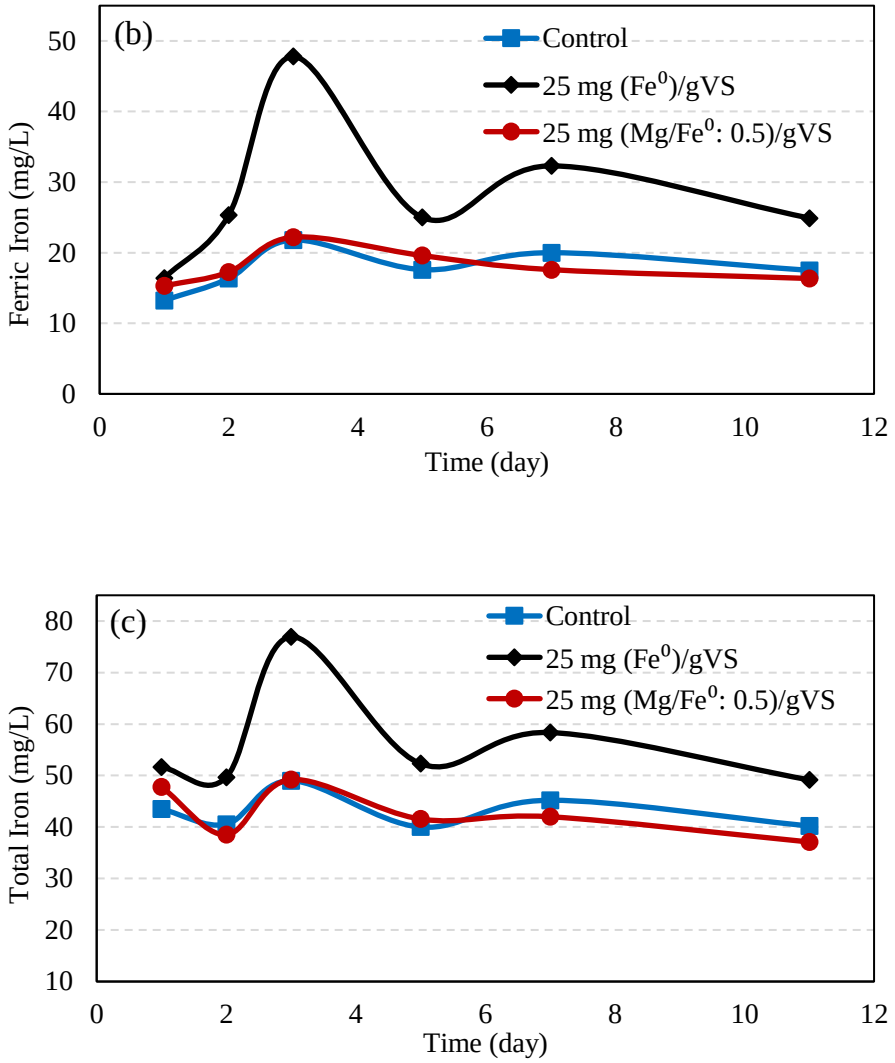

Fig. 4-11. Effect of $Mg(OH)_2$ coating shell on the released iron ions form the corrosion reaction of Fe^0 a) Ferrous iron, b) Ferric iron, c) Total iron

4.10. Semi-continuous system for biogas and methane generation

Fig.4-12 a and b show the daily and accumulative biogas measurements over 70 days in the semi-continuous system. During the operation process, the system in the first 24 days was operated as a batch mode without feeding or withdrawing the waste sludge. This period was given before starting the semi-continuous operation to effectively establish the anaerobic digestion process and stimulate methanogens bacteria.

The operation conditions of the semi-continuous reactors were well explained in chapter 2, section 2.6.3. In the first ten days, biogas production in R1 (control reactor) was quite like R2 (25 mg of Mg/Fe/gVS were added). On day 15, the difference in biogas production in R1 and R2 was clear, where the production curves began to diverge from each other. The semi-continues operation started on day 24th by feeding of 0.1425 gVS/L.d and discharging the very same amount every day.

The addition of Mg/Fe^0 particles into R2 improved biogas production two times with respect to the control. Fig. 4-13 a and b displays the daily and accumulative methane measurements in the semi-continuous system. The addition of Mg/Fe^0 particles into R2 greatly enhanced methane production rate in the system. This could be ascribed to role of Mg/Fe^0 particles in enhancing the bacterial growth rate as described in Fig.4-14. Bacterial growth was measured three times during the operation of the semi-continuous system on day 20, 40, and 52. Results showed that the addition of Mg/Fe^0 particles significantly increased the bacterial growth by 672.7%, 279.999%, and 318.5% on day 20, 40, and 52, respectively.

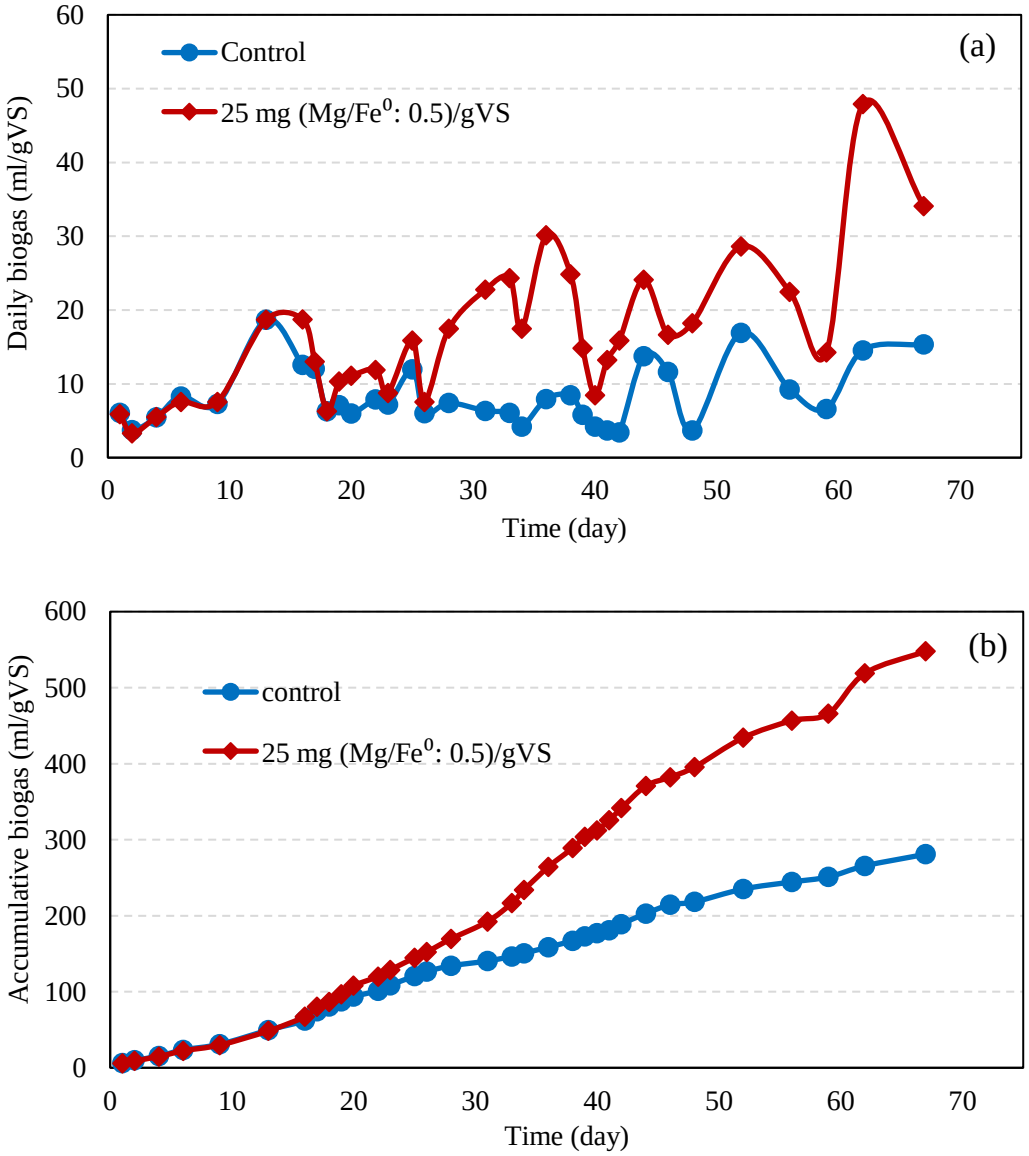

Fig. 4-12. Daily and cumulative biogas measurements in the semi-continuous reactors, showing the effect of Mg/Fe^0 nanoparticles on biogas production in the semi-continuous system.

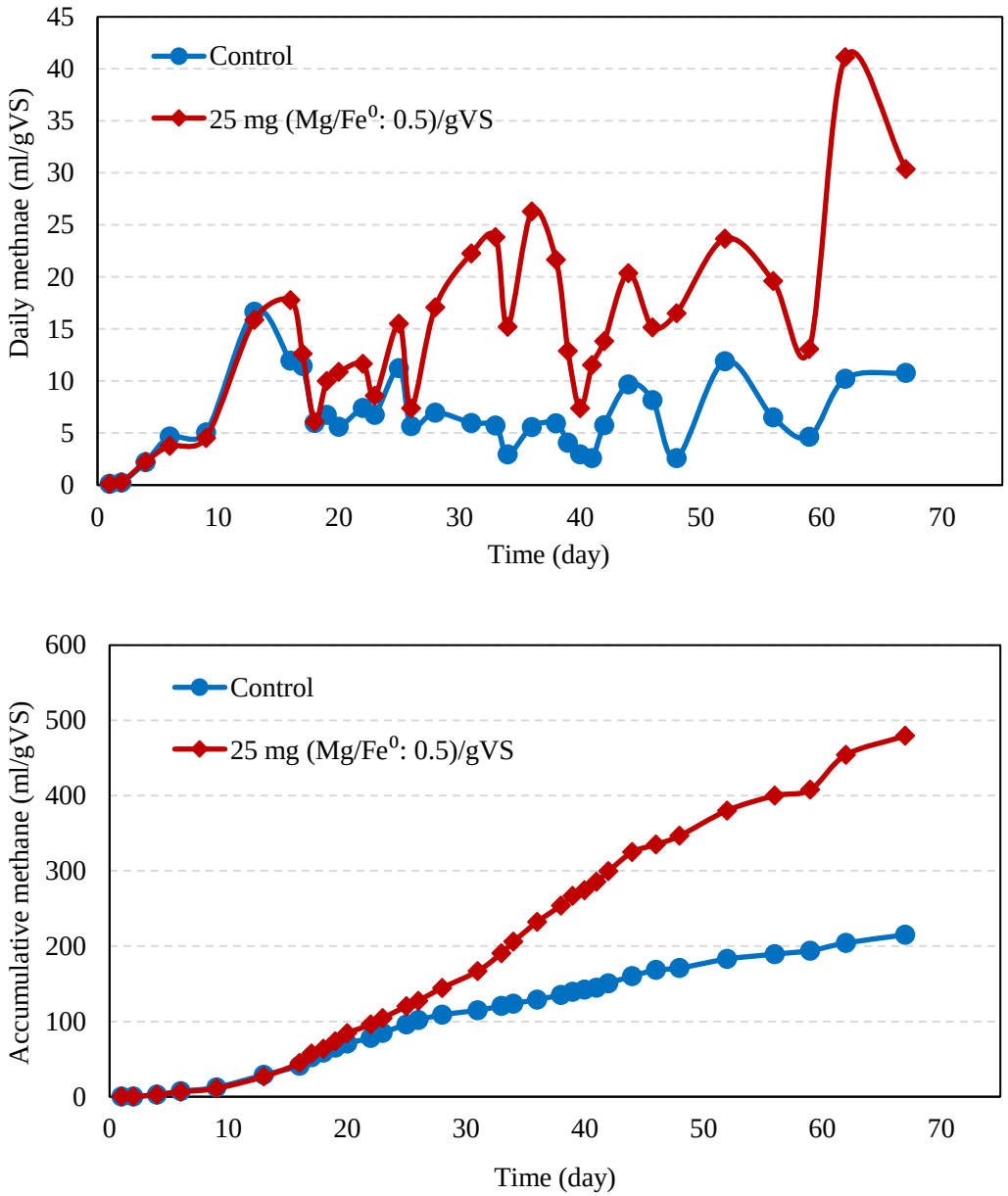

Fig. 4-13. Daily and cumulative methane measurements in the semi-continuous reactors, showing the effect of Mg/Fe^0 nanoparticles on methane production in the semi-continuous system

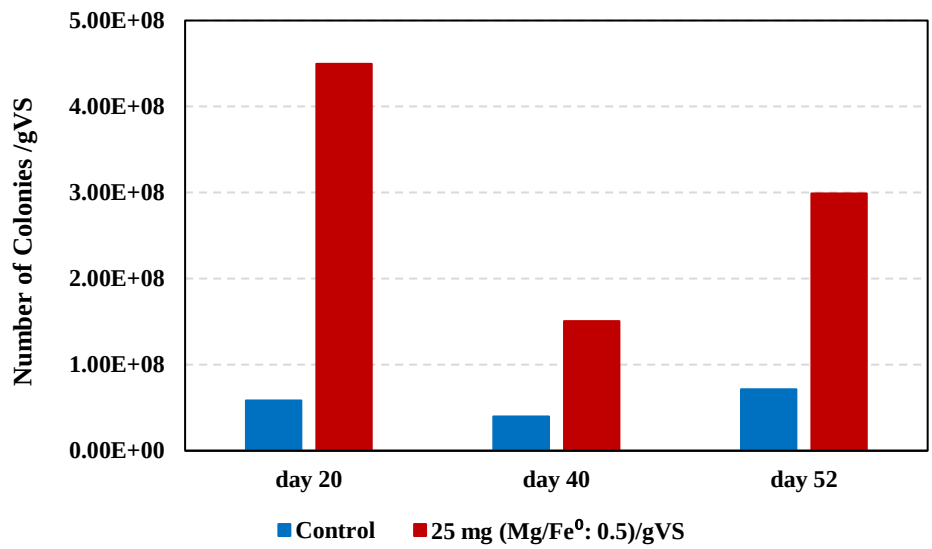

Fig. 4-14. Effect Mg/Fe^0 nanoparticles on the bacterial growth in the semi-continuous system for biogas and methane generation.

4.11. Kinetic analysis and prediction of biomethane production

Modified Gompertz equation (Eq. 4-1) was used to model methane production profiles obtained from the experimental measurements. The model was used mainly to determine methane production potential, maximum methane production rate and lag phase for each operating condition.

$$Y = Aexp\left\{-\exp\left[\left(\mu_m \frac{e}{A}\right)(\lambda - t) + 1\right]\right\} \quad (4\text{-}1)$$

Where Y is the accumulative methane production at time t (ml/gVS), A is methane production potential (ml/gVS), μ_m is the maximum methane production (ml/gVS/d), λ is the lag phase (day), e is equal to exp (1), and t is the digestion period (day) [88]. Gompertz's parameters were estimated by solving the nonlinear forms and best fitting with experimental measurements using SPSS.

All kinetic parameters obtained concerning the effect of coating ratios and dosages of coated/Fe^0 on methane production are presented in Table 4-1. The results suggested that the AD of waste sludge at the optimum conditions (optimum dosage: 25 mg/gVS ; optimum coating ratio: Mg/Fe^0:0.5) experienced higher methane production. At these optimum conditions, methane production potential was 335.3 ml/gVS, whereas it was only 227.02 ml/gVS in the control reactor. Also, the daily maximum methane production was 16 ml/gVS/d, which was two times higher than the control.

In addition, the dosing time of coated/Fe^0 was investigated using high dosage (50 mg/gVS) higher than the optimum dosage (25mg/gVS) to clearly demonstrate the effect of dosing time on the AD process.

The modeled results in Table 4-2 showed that the late addition of coated/Fe^0 gave higher methane production rate. The methane production potential was 283.6 ml/gVS when the coated/Fe^0 nanoparticles were added in the digesters on day 4 (methanogenic stage), while it was only 14 ml/gVS when they added immediately at the beginning of AD (acidogenic stage). The results suggested methanogenic stage, which is the fourth stage of AD, as the best stage of dosing the coated/Fe^0 in the digesters.

The addition of coated/Fe^0 on day 4 increased the daily maximum methane production to 11.07 ml/gVS/d compared to 0.66, and 9.73 ml/gVS/d when the particles were added immediately on day 0 and day 1, respectively.

In the semi-continuous system, as shown in Table 4-3, all parameters from modified Gompertz model including biogas/methane production potential and biogas/methane daily maximum production were almost two times higher than the control reactor by the addition of 25 mg/gVS of coated/Fe^0. Additionally, the predicted biogas and methane yields were well-fitted with the experimental profiles.

Therefore, the results were in excellent agreement with the obtained experimental data with a low difference range between the predicted and expediential values from (0.00-0.04%), suggesting that the modified Gompertz model could be used to predict methane values accurately.

Table 4-1 Kinetic parameters from the modified Gompertz model obtained based on the experimental data after 45-day of digestion at different concentrations of Mg/Fe^0 nanoparticles.

Coated Fe^0 with $Mg(OH)_2$		Parameters from modified Gompertz model			R^2	Y_{pre} (ml/gVS)	Y_{exp} (ml/gVS)	%Δ
Coating ratio	Dosage (mg/gVS)	A (ml/gVS)	μ_m (ml/gVS/d)	λ (d)				
Mg/Fe^0: 5 %	0	227.0	8.11	6.1	0.999	221.7	225.4	0.01%
	5	232.2	8.20	7.0	0.999	226.0	229.2	0.01%
	10	228.3	8.44	7.1	0.999	223.3	226.7	0.01%
	25	230.3	8.53	6.9	0.999	225.4	228.2	0.01%
	50	218.0	8.48	7.8	0.998	214.0	218.3	0.02%
	250	298.6	4.77	16.3	0.995	177.7	177.4	0.00%
Mg/Fe^0: 50 %	0	227.02	8.11	6.1	0.999	221.7	225.4	0.01%
	5	253.9	9.19	6.2	0.999	247.4	250.3	0.01%
	10	265.6	12.11	9.7	0.999	262.9	268.6	0.02%
	25	335.3	16	18	0.999	327.8	330.6	0.00%
	50	14.04	0.66	0.0	0.964	14.0	15	0.07%
	250	58.01	5.27	7.3	0.997	58.0	59.38	0.02%
Mg/Fe^0:100 %	0	172.2	7.24	4.4	0.995	167.7	173.7	0.03%
	3	178.5	7.27	4	0.996	173.4	178.4	0.02%
	6	183.4	7.29	4.2	0.996	177.4	182.4	0.02%
	14	180.0	7.46	3.9	0.995	175.3	180.4	0.02%
	28	204.9	8.07	3.1	0.991	198.1	204.7	0.03%
	140	621.0	7.89	22	0.993	181.9	179.9	0.01%

A: methane production potential, μ_m: maximum methane production, λ: lag phase, Y_{pre}: predicted methane values, Y_{exp}: experimental methane values, %Δ: difference between predicted and experimental values.

Table 4-2 Kinetic parameters from the modified Gompertz model obtained based on the experimental data after 45-day of digestion at different dosing time of Mg/Fe^0 nanoparticles.

Coated Fe^0 with $Mg(OH)_2$ nanoparticles			Parameters from modified Gompertz model			R^2	Y_{pre} (ml/gVS)	Y_{exp} (ml/gVS)	%Δ
Coating ratio	Dosage	Dosing time (d)	A (ml/gVS)	μ_m (ml/gVS/d)	λ (d)				
Mg/Fe^0: 50 %	50 (mg/gVS)	Control	227.0	8.11	6.1	0999	221.7	225.4	0.01%
		0	14	0.66	0.04	0.964	14.01	15.00	0.07%
		1	292.6	9.73	12.6	0.999	275.8	274.2	0.00%
		3	268.34	9.58	11.5	0.998	257.8	263.3	0.02%
		4	283.9	11.07	10.0	0.998	277.5	280.9	0.01%
		5	284.8	12.37	10.3	1	280.9	284.2	0.01%
		7	312.9	13.32	12.4	0.999	306.8	307.7	0.00%
		10	318.4	11.7	8.1	1	310.4	312.9	0.00%
		15	291.9	10.98	9.2	0.997	284.6	287.0	0.00%

A: methane production potential, μ_m: maximum methane production, λ: lag phase, Y_{pre}: predicted methane values, Y_{exp}: experimental methane values, %Δ: difference between predicted and experimental values.

Table 4-3 kinetic parameters from the modified Gompertz model obtained based on the experimental data after 67-day of digestion using the semi-continuous system

Coated Fe^0 with $Mg(OH)_2$		Parameters from modified Gompertz model			R^2	Y_{pre} (ml/gVS)	Y_{exp} (ml/gVS)	%Δ	
Coating ratio	Dosage (mg/gVS)	A (ml/gVS)	μ_m (ml/gVS/d)	λ (d)					
Mg/Fe^0: 5 %	0	328.4	5.1	3.4	0.993	273.2	280.9	0.02%	Biogas
	25	693.8	11.2	12.3	0.997	543.1	547.9	0.00%	
	0	224.9	4.6	6.1	0.991	205.2	215.0	0.04%	CH_4
	25	564.7	10.5	14	0.998	470.3	479.4	0.01%	

A: methane production potential, μ_m: maximum methane production, λ: lag phase, Y_{pre}: predicted methane values, Y_{exp}: experimental methane values, %Δ: difference between predicted and experimental values.

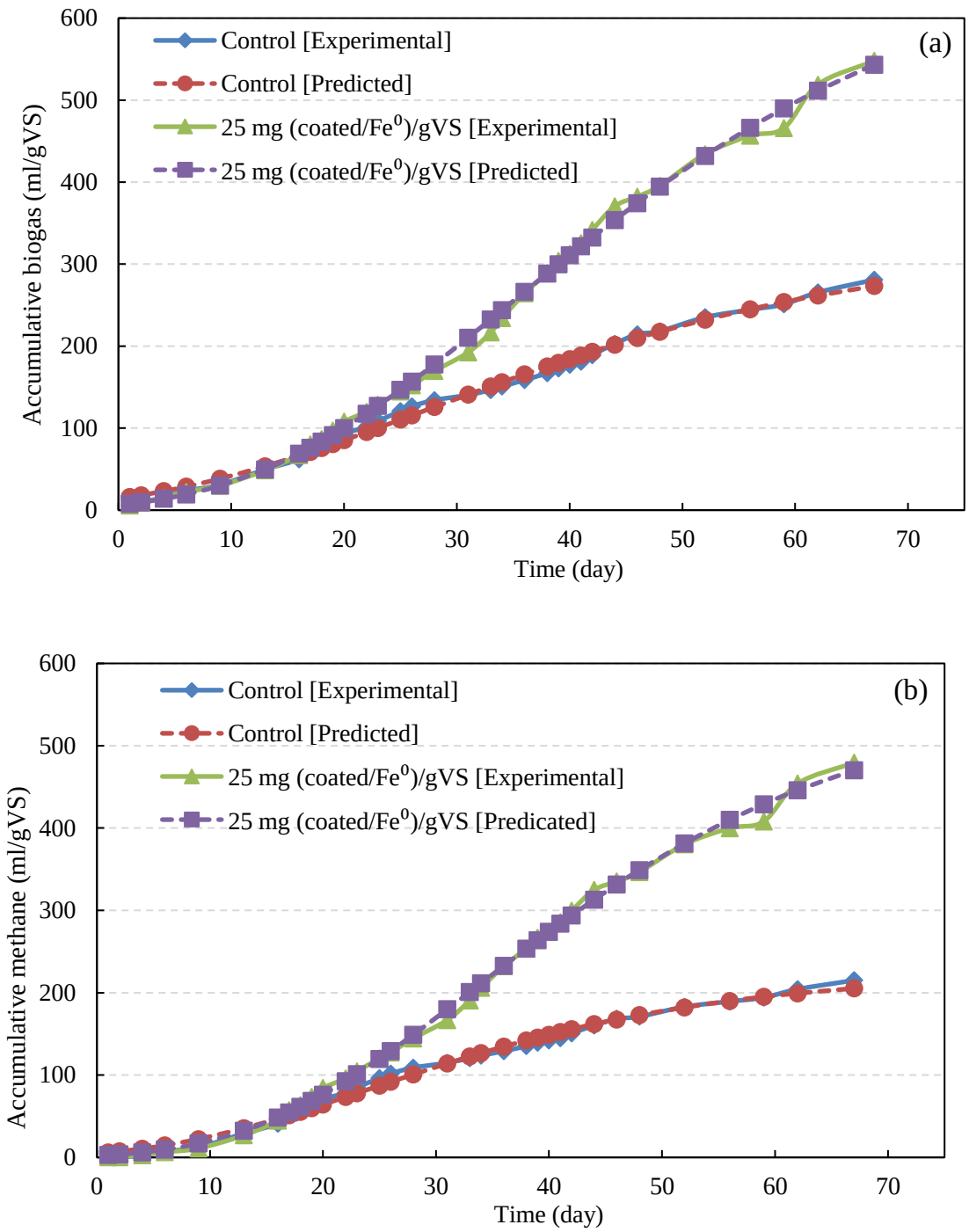

Fig. 4-15 Modified Gompertz model prediction well-fitted with the accumulative experimental values in semi-continuous bioreactors a) biogas, and b) methane.

4.12. Conclusions

- The bare/Fe^0 particles were successfully coated using $Mg(OH)_2$ as a coating layer by following thermal deposition method.
- The bare and coated Fe^0 particles fully characterized using different techniques and the results confirmed the coating process of Fe^0 particles.
- The coated Fe^0 particles with $Mg(OH)_2$, synthesized at different coating ratios 5, 50, and 100% of Mg to Fe^0) were applied in the anaerobic digesters to increase methane generation from waste sludge.
- In the batch test experiments, the coated/Fe^0 improved biogas and methane production by 25% and 46.6%, respectively at the optimum coating ratio of Mg/Fe^0:0.5 and at the optimum dosage of 25 mg/gVS.
- Due to its high reactivity, which could be indicated by the high corrosion reaction, the addition of bare/Fe^0 particles in anaerobic digesters did not improve biogas/methane generation.
- $Mg(OH)_2$ nanoparticles contributed a little in improving methane production (13 %), confirming that the increased methane production by Mg/Fe^0 was mainly due to synergistic effect of $Mg(OH)_2$ shell in controlling the reactivity of Fe^0.
- The coating of bare/Fe^0 particles with $Mg(OH)_2$ slowed down their corrosion reaction in aqueous conditions, which was indicated by the sharp decrease of the released iron ions (Fe^{2+} and Fe^{3+}), making the coated/Fe^0 particles excellent additives for enhancing methane production during the anaerobic digestion process.
- The investigations from this project proved that the coated/Fe^0 enhanced the production of biogas and methane by increasing bacterial growth rate and serving as a buffering agent in the reactors.
- Long-term investigation of methane generation was implemented using lab-scale semi-continuous system and the results showed the great performance of Mg/Fe^0 nanoparticles in improving biogas and methane generation

- In the semi-continuous system, the maximum methane production was 10.5 ml/gVS/d by the addition of 25 mg/gVS of Mg/Fe^0:0.5, whereas it was only 4.6 ml/gVS/d in the control reactor.
- The values of Methane production potential (A) and maximum methane production rate (μ_m) were two times higher by the addition of Mg/Fe^0 nanoparticles at the optimum dosage (25mg/gVS) with an excellent regression of R^2=0.999).
- The range of differences of in predicted and experimental yields were 0.00%-0.007%, suggesting that the modified Gompertz model could be used to predict the BMP profile accurately.

CHAPTER 5

APPLICATION OF Fe^0 IN AEROBIC GRANULAR TECHNOLOGY

Chapter 5:Application of Fe^0 particles for wastewater treatment and formation of aerobic granules

Waste sludge considerably discharged to the local wastewater treatment plants. It was reported that the cost of sludge management, which includes both treatment and disposal, could be as high as 60% of overall wastewater treatment costs [89]. Therefore, the reduction in sludge production reduces the cost of wastewater treatment. [90-92]. Aerobic granulation technology is a new approach that can be used to convert the waste sludge to aerobic granules, which will further be used to treat the contaminated water. However, the long time needed for full granulation is the main limitation of this technology, making it not applicable for wastewater treatment applications [93, 94]. Therefore, this research aimed to investigate the role of Fe^0 particles in accelerating the formation of aerobic granules and contaminants removal from wastewater using a sequencing batch reactor system (SBRS).

5.1. Introduction

Microbial granulation which is based on either aerobic or anaerobic technologies represents a pragmatic opportunity in biological wastewater treatment. Conventional anaerobic techniques such as Upward Sludge Blanket (USB) and Expanded Granular Sludge Bed (EGSB) have been increasingly employed in wastewater treatment for almost three decades [95-99]. However, most of the anaerobic sludge systems are insufficient for complete decomposition of organic compounds or inefficient at removing nutrients in addition to the formation of secondary pollution.

Hence, the need has emerged to develop alternative biodegradation technologies. Aerobic granulation is one of the most promising technologies in the biological treatment of wastewater which focused the attention of many researchers over the last 10 years [100]. Because of the elevated microbial concentration as well as the superior settling ability, aerobic granules have promising potential in various applications in municipal and industrial wastewater treatment [101, 102].

Aerobic granulation technique has superior performance compared to conventional activated sludge (CAS) in which COD completely could be removed by the formed aerobic granules. More importantly, the formation of aerobic granules decreases the production of seed sludge due to the formation of denser and heavier granules. It was reported that the cost of sludge management, which includes both treatment and disposal, could be as high as 60% of overall wastewater treatment costs [89]. Therefore, the reduction in sludge production reduces the cost of wastewater treatment. [90-92].Whilst aerobic sludge is widely adopted for organic compounds degradation and nutrients removal from a range of wastewater. However, it still has some drawbacks such as poor mobility and the long time needed for full granulation, which is not feasible for wastewater treatment applications [93, 94].

Granulation process within the aerobic sludge is mostly achieved through two main stages; starting with the formation of the grown bacterial aggregates via the bio-seed of the sludge, followed by the adhesion of such aggregates by the microbial extracellular polymeric substances (EPSs) to form an initial granular structure [103, 104]. Meanwhile, several factors are known to influence the start-up of the granulation process such as the loading rate of chemical oxygen demand (COD) as an indicator of wastewater microbial strength (high-strength: 1000-1500 mg/L-COD, low-strength:150-300 mg/L-COD) [105, 106]. Additionally, the presence of the divalent cations such as Ca^{2+}, Mg^{2+} and Mn^{2+} has a dual effect on the aerobic granulation: 1) functional cohesion by connecting EPSs cells into the three-dimensional structure of the granules and 2) neutralization effect by the cations charge resulting in accelerated granulation [107-109].

It has previously been reported that granulation time was reduced by almost 44% in the presence of divalent cations to form aerobic granules with more compact and dense structure [110]. Iron ions were also studied as possible accelerators of aerobic granular sludge (AGS). Yilmaz et al. investigated the effect of 1 and 10 mg/L ferrous ions concentration on the formation of AGS [94]. Additionally, it was reported that low Fe^{2+} (2 mg/L) concentration was favorable for the granulation process and the bacterial growth in aerobic activated sludge [111, 112]. Meanwhile, iron is an abundant metal low cost material and an essential trace element (< 1 mg/L) for the growth of almost all microbial organisms [94, 113].

Owing to its high redox potential and the significant catalytic effect, zero-valent iron (Fe^0) increasingly employed for treating contaminants [30, 44, 114, 115]. Moreover, Fe^0 can serve as an electron donor for better reductive degradation of pollutants by microorganisms [116]. Fe^0 has great advantages when it comes to the improvement in the settling ability of the granules within the aerobic sludge [104]. Comparing with other divalent ions, the addition of Fe^0 into aerobic reactors is beneficial in terms of operation and maintenance costs [104, 108]. In a previous study, the time needed for full granulation was reduced by nearly 33% when Fe^0 was added to the aerobic sludge reactor [104]. Moreover, a stable microbial structure was formed via Fe^0 addition into anaerobic sludge which resulted in accelerative nitrobenzene (NB) degradation [117]. However, these studies were used micro scale zero valent iron (mFe^0) which is less effective than nano scale zero valent iron. Fe^0 has several advantages such as the smaller particle size and higher specific surface area than that of mFe^0. Thereby, Fe^0 could offer a great performance in terms of contaminates removal and microbial growth rate. Nevertheless, no work has been reported demonstrating the use of Fe^0 in the aerobic sludge reactors.

Therefore, the objective of this study was to investigate the effect of Fe^0 on the formation of aerobic granules in terms of the settling rate as well as the microbial community growth. Sludge volume index was considered as an indicator of the start-up of the granulation process within the aerobic reactors. Moreover, this study amid to evaluate the removal efficiency of the total organic matter, ammonia, nitrate, nitrite, and phosphorus by the formed aerobic granules and demonstrate the role of Fe^0 in these process. Extraction and analysis of extracellular polymeric substances (EPSs) was undertaken to evaluate the growth of bacteria. Furthermore, the bacterial community structure was explored based on new generation sequencing (NGS) technology. For morphology investigation of the formed granules, bright field microscopy (BFM) analysis was employed. The present work could have a significant contribution in terms of improving understanding of biological treatment of wastewater based on integrating Fe^0 in aerobic granulation reactors

5.2. Operation conditions of sequencing batch reactor system (SBRs)

Experiments were conducted using two symmetrical lab-scale Sequencing Batch Reactors (SBRs) as shown in Fig.5-1. The reactors had an internal diameter of 12 cm and a length of 60 cm, giving a working volume of 5 L. Both reactors were operated in successive cycles (4 cycles per day) and each cycle lasted for 6 h. Each cycle consisted five successive phases: (1) 60 min static feeding, (2) 283 min aerobic reaction, (3) 2 min settling, (4) 15 min decanting the treated water.

The third phase of settling was 1 h at the first day of experiment and gradually reduced to two minutes to promote the formation of aerobic granules. Decreasing the settling time was slowly performed within 23 days to avoid wash-out of biomass from the reactors. The remaining cycle time was conveyed to the aeration phase. Air was introduced via a diffuser tube aerator at the bottom of the reactor during the aeration phase.

The reactors were operated automatically using three digital timers. These digital timers were used to run the devices of the rectors at specific times. During the operation time pH was monitored without adjusting. The reactors were operated at room temperature 25 ± 3 ^{0}C. The Fe^0 particles were added to the influent wastewater tank with at 10 mg/L as shown in Fig.5-1.

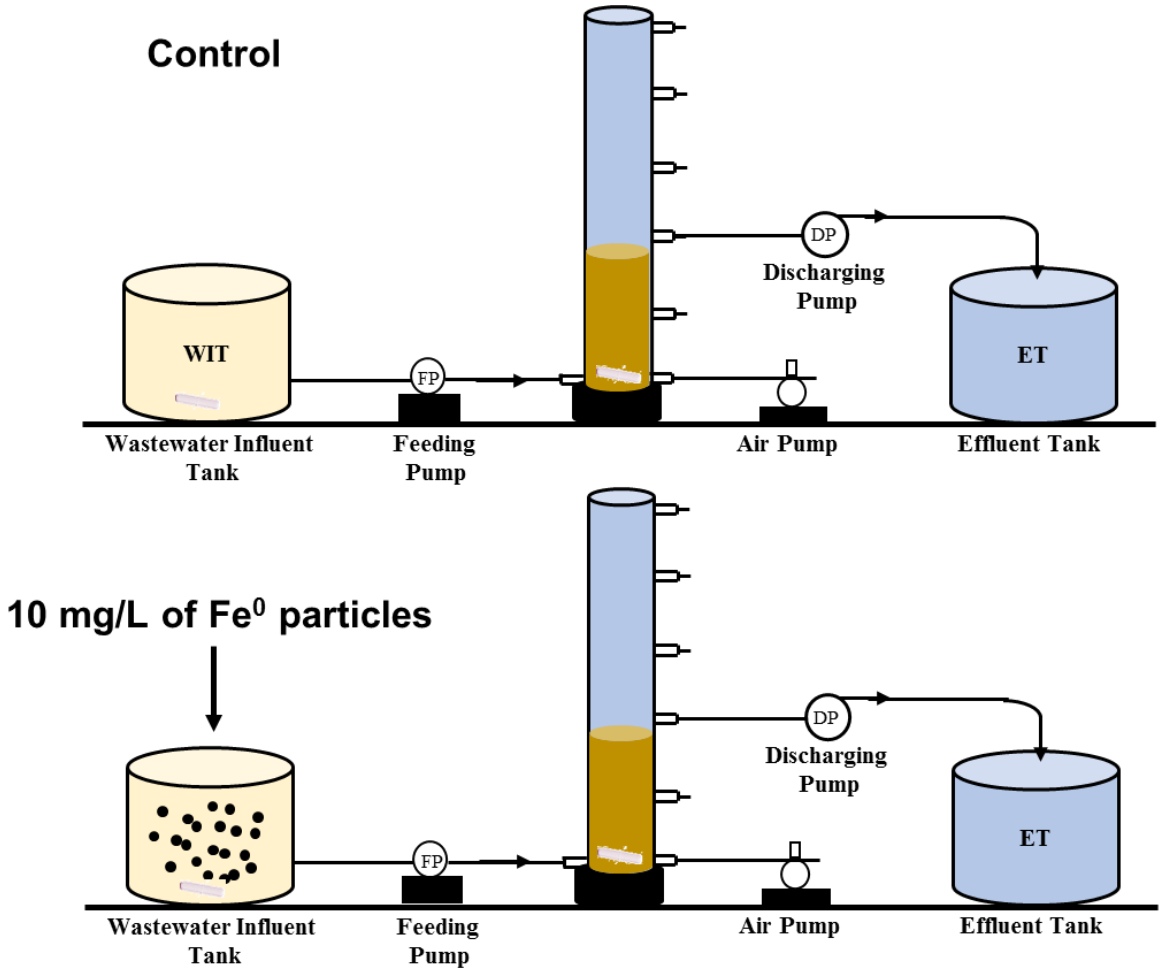

Fig. 5-1. Sequencing Batch Reactor system (SBRS) for wastewater treatment and aerobic granulation process

5.3. Assessment of the granulation process in the SBRs

This work was performed over 60 days to assess the formation process of aerobic granules using two sequencing batch reactors. The formation of aerobic granules was monitored by measuring the SVI, MLSS and MLVSS. The formation of aerobic granules supposed to be completed when the ratio of SVI30/SVI5 exceeds 90% and the granules clearly get formed in the reactors [94]. On the 52^{sd} day, the ratio of SVI_5/SVI_{30} reached 100% and the granules were clearly seen in SBR1 and SBR2.

Fig.5-4 shows the formed granules in the reactors on day 60. The granules in SBR2 were slightly heavier and denser than that granules in SBR, implying that the addition of Fe^0 had a slight effect on the formation of aerobic granules. For the formation time of granules, the addition of Fe^0 in SBR2 accelerated the formation of granules 15 days before that ones in SBR1 as shown in Fig.5-5. In addition, the MLSS and MLVSS were measured in SBR1 and SBR2 to evaluate the biomass content and the formation of aerobic granules in the reactors. During the first five days, the reactors had different concentrations of MLSS and MLVSS. Therefore, the very same concentration of MLSS set in the reactors on day 7.

It was noticed that the settling time of sludge in reactors highly correlated to the concentration of MLSS and MLVSS. When the settling time was decreased in the reactors, the MLSS and MLVSS decreased as well. When the settling time was decreased to two min, the sludge content has become stable in the reactors and the MLSS concentration started to increase due to the elevated microbial growth as shown in Fig.5-3.

The MLSS concentration in the effluent was relatively low and was not exceeded 200 mg L^{-1} at the end of the study. The MLSS and MLVSS concentrations play an important role in determining the performance of the SBRs towards the removal of contaminants [118].
MLSS and MLVSS consist the microorganisms that are necessary and responsible for the formationof aerobic granules and contaminants removal. Therefore, MLSS concentration should be as high as possible in the reactors.

As shown in Fig.5-3 MLSS concentration was slightly higher in SBR2 with respect to SBR1 after the addition of Fe^0, suggesting that Fe^0 particles contributed to increase the concentration of MLSS through the adsorption on the EPS, improving cell accumulation [119]. The results of granule size and size distribution in SBR1 and SBR2 were presented in Table 1. There were three populations of seed sludge granules including mean d (0.1) [small], mean d (0.5) [midsize] and mean d (0.9) [large]. The large granule size population was higher than the small and midsize population in both reactors and the average granule size was increased during the operation of the SBRs.

Moreover, the average granule size in the SBR2 was slightly higher than that size in SBR1 and that was only observed after the addition of Fe^0. For example, on day 37, 43 and 60, the average particle size in the SBR1 was 71.1, 67.2 and 548.8 µm, respectively, and was 90.8, 109.0 and 553.1 µm, in SBR2, respectively.

In addition, the light microscopy images were taken on day 55th, the images showed the filamentous bacteria in both reactors. The images showed that the filamentous bacteria in the SBR2 were surrounded by black Fe^0 particles. Yilmaz et al. [94], found the same structure when they used Fe^{2+} and Fe^{3+} as an additives in the SBR. This could interpret the increased EPSs content in SBR2 as Fe^0 particles serve as
a carrier or nuclei for the new generated cells.

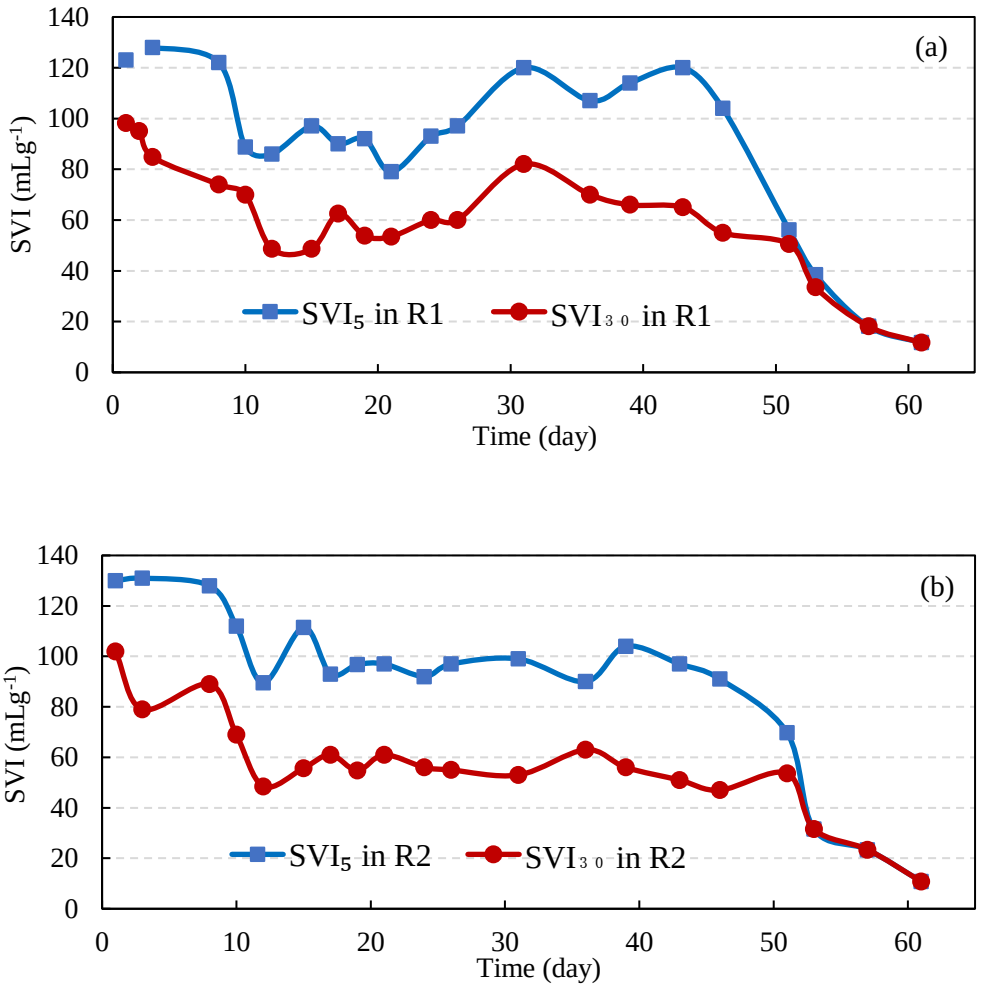

Fig. 5- 2. Variation in sludge volume index after 5 and 30 min of settling during the entire study (a) SBR1 and (b) SBR2.

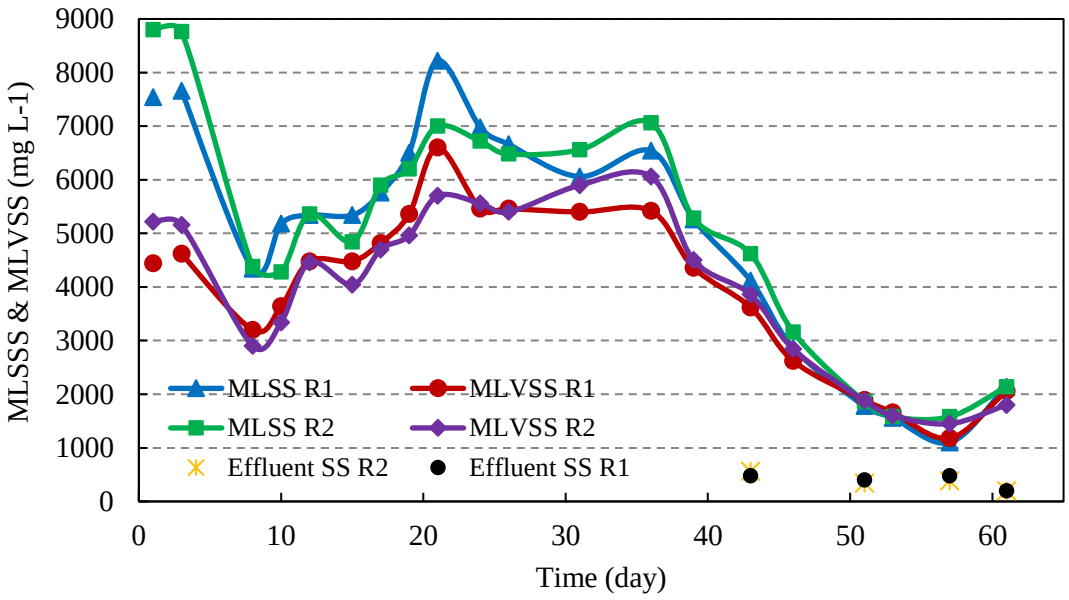

Fig. 5-3. Concentrations of MLSS, MLVSS and effluent SS during the entire study in SBR1 and SBR2

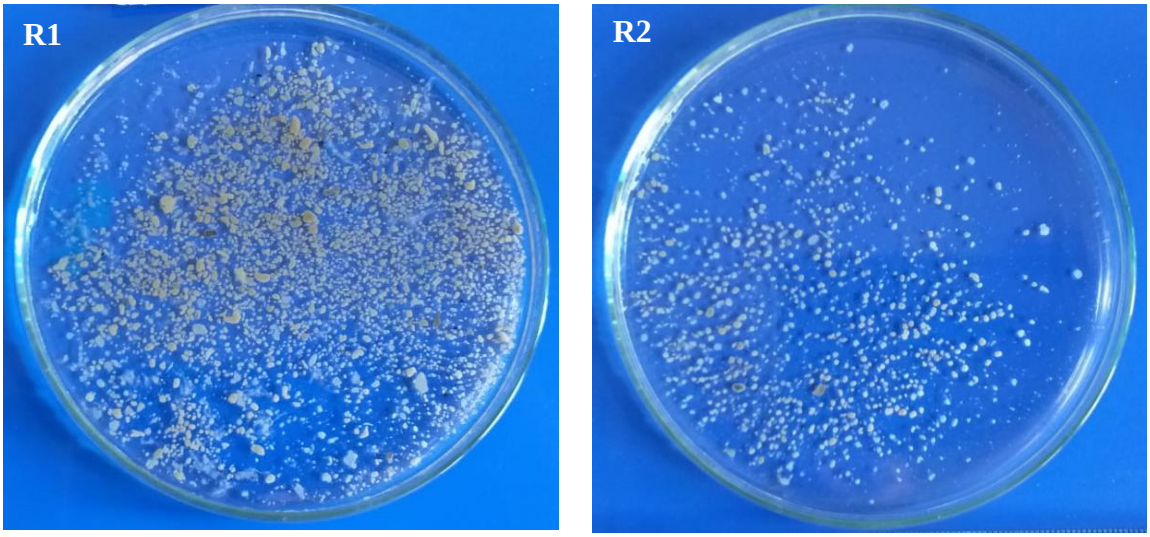

Fig. 5-4. Images of the formed granules in SBR1 and SBR2.

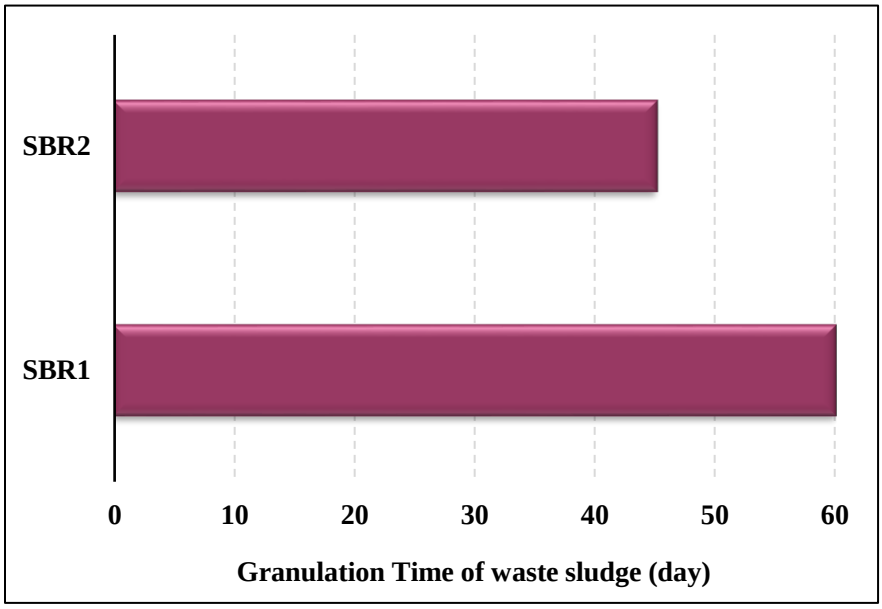

Fig. 5-5. Shows the granulation time of waste sludge in SBR1 and SBR2.

5.4. Extracellular polymeric substance (EPS)

EPSs are the metabolic products play a major role in forming the aerobic granules and help to estimate bacterial growth rate [101, 120]. EPSs are mainly composed of carbohydrates and protein substance that accumulate and embed the bacteria in a protective mucilage [120]. It was reported that the generated EPSs in the reactors help to accelerate the granulation process [101]. In this study, EPS content was measured on day 12, 30, 44 and 52. On day 12th, almost the same concentrations of carbohydrate and protein were detected in the reactors as shown in Fig.5-6a and b. Whilst, on day 30, carbohydrate and protein concentrations which extracted from the precipitate and supernatant (SMP) were increased in the reactors compared with that concentrations on day 12. Moreover, the carbohydrate and protein concentrations increased more in SBR2 with respect to SBR1. Therefore, EPS content was greater in SBR2 which attributed to the addition of Fe^0 particles.

Accordingly, Fe^0 particle had a positive effect on the production of EPSs. The addition of Fe^0 particles increased the EPS content through charge neutralization and double-layer compression. It has been reported that [107, 121], divalent ions such as Mg^{2+} and Ca^{2+} improve the microbial diversity and granulation process respectively. Similarly, Fe^{2+} ions produced by the corrosion reaction of Fe^0 interact with EPSs components by creating direct bonds with protein on the surface of bacteria, forming important molecules for the growth of negatively charged bacteria. Therefore, iron ions generated from the corrosion Fe^0 particles have a key role in improving cell aggregation due to the interaction with EPSs, implying that the iron ions contribute effectively for enhancing the granulation process.

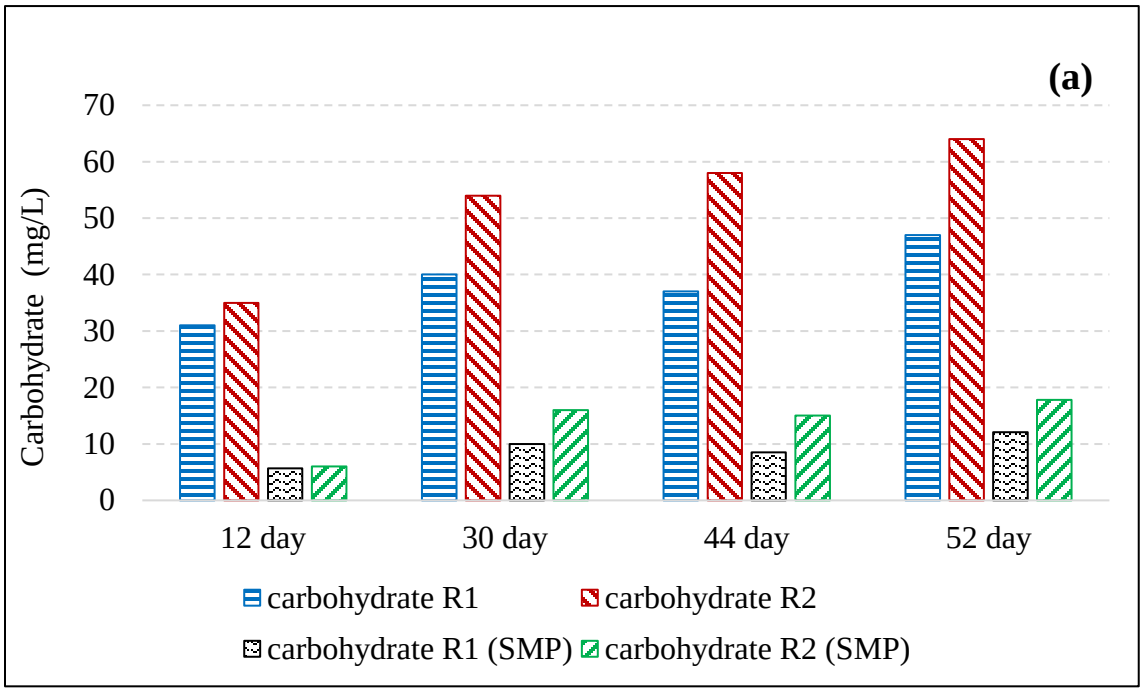

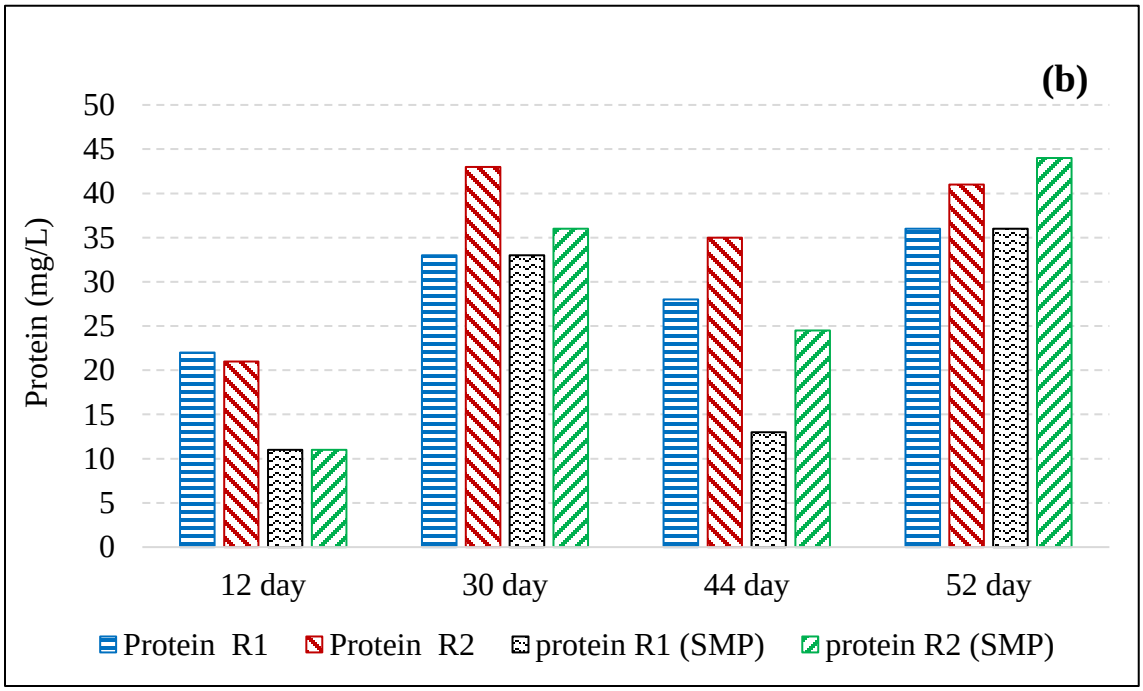

Fig. 5-6. Depicts the EPS content in SBR1 & SBR2 where; (a) carbohydrate concentration in SBR1& SBR2, and (b) protein concentration in SBR1 & SBR2.

5.5. Bacterial community structure

In total 38 orders were commonly found in activated sludge from 14 WWTPs including *Sphingobacteriales*, *Anaerolineales*, *Rhodocyclales*, *Burkholderiales*, *Rhizobiales* , *Xanthomonadales*, *Verrucomicrobiales*, *Clostridiales*, *Planctomycetales*, *Myxococcales*, etc. which accounted for 96 to 99% of the classified sequences [107, 121, 122]. Among them, *Rhizobiales, Clostridiales, Sphingobacteriales, Actinomycetales, Burkholderiales* and *Xanthomonadales* were found in our seed sludge by 14.7%, 11.1%, 8.1%, 7.6%, 5.3% and 4.9%, respectively, as shown in Table 5-1. Glycosphingolipid (GSL) -producing bacteria, namely *Sphingomonadales, Rhizobiales and Sphingobacteriia* were reported in membrane biofouling. GSL protects bacteria from a
dverse environmental conditions such as extreme pH, temperature, salinity and high pressure [123].

Rhizobiales were the most numerically dominate group during the entire study, and the percentage of *Rhizobiales* increased from 14.7% in seed sludge to 23.9% in SBR1 and 25% in SBR2 in a short period.

The high shear force and short settling time applied in AGS reactors probably led to this increase. *Xanthomonadales* were the second dominate order in SBR1 and SBR2 with 12% and 13.5% whereas these group of bacteria were only 4.9% in the seed sludge. *Xanthomonadales* are well known EPS producing bacteria [124].

Previous study demonstrated that suggested that the high shear force may select for bacteria with superior attachment ability and those that produce very sticky polysaccharides [123]. *Sphingobacteriales, Burkholderiales, Rhodocyclales, Actinomycetales and Rhizobiales* were found the fundamental organisms responsible for biofilm formation in other study [125]. Thus, the presence of *Actinomycetales* and *Burkholderiales* ranging from 8.8% to 4.9% throughout the study can be explained by their ability to form biofilm.

Seed Sludge		SBR1		SBR2	
Order	**%**	**Order**	**%**	**Order**	**%**
Rhizobiales	14.7	*Rhizobiales*	23.9	*Rhizobiales*	25.1
Clostridiales	11.1	*Xanthomonadales*	12.0	*Xanthomonadales*	13.5
Sphingobacteriales	8.1	*Actinomycetales*	8.8	*Bacteria unclassified*	9.9
Actinomycetales	7.6	*Bacteria unclassified*	6.4	*Actinomycetales*	7.5
Bacteria_unclassified	7.5	*Clostridiales*	6.2	*Burkholderiales*	4.9
Burkholderiales	5.3	*Burkholderiales*	5.1	*Clostridiales*	3.6
Xanthomonadales	4.9	*Sphingobacteriales*	1.2	*Sphingobacteriales*	1.2

Table 5-1. Microbial population in the used seed sludge, SBR1, and SBR2 at the end of the study.

Members of *Clostridiales* are responsible for the processes of hydrolysis and fermentation of organic matter during anaerobic digestion in UASBs treating wastewater, and they display an ability to become part of heterogeneous biofilms [126].
Clostridiales were detected as high as 11.1% in the seed sludge but decreased to 6.3% in SBR1 and 3.7% in SBR2.

The microbial community results demonstrated that the AGS operation conditions especially low settling time have the impact on the microbial diversity and population but, the addition of ZVI did not dramatically affect them.

5.6. Performance of the SBRs in contaminants removal

5.6.1. Phosphorus removal

Fig.5-7. shows the results of phosphate removal by analyzing the effluent of SBR1 and SBR2. The results showed that the reactors exhibited an excellent performance of phosphate removal especially after the formation of granules. It is the biological removal phosphate which gradually enhanced in both reactors with the time due do the elevated bacterial growth and the formation of aerobic granules. It was proved that the precipitation of phosphorus as inorganic phosphate ($Ca_3(PO_4)_2$ and $MgHPO_4$) is the maim removal mechanism of phosphate using aerobic granulation technology. It was observed that about 45% of the total phosphate removal using aerobic technology occurred by the direct precipitation within the aerobic granules [127].

Besides, phosphate precipitation within the EPS could be one of the biological removal pathways of phosphate. It was reported that about 17.6 % of the total removal of phosphate was by the accumulation of phosphorus within the EPS [128]. Moreover, the concentration of Phosphate in the effluent of SBR2 was slightly lower than that in SBR1, which was attributed to the chemical adsorption of PO_4-P onto Fe^0 particles.

It has been reported that Fe^0 is one of the most efficient adsorbents for the removal of phosphate in aqueous solutions [25, 129]. Furthermore, Fe^0 particles can stimulate the growth of bacteria in the reactors which in turn improves their phosphate removal ability [104].

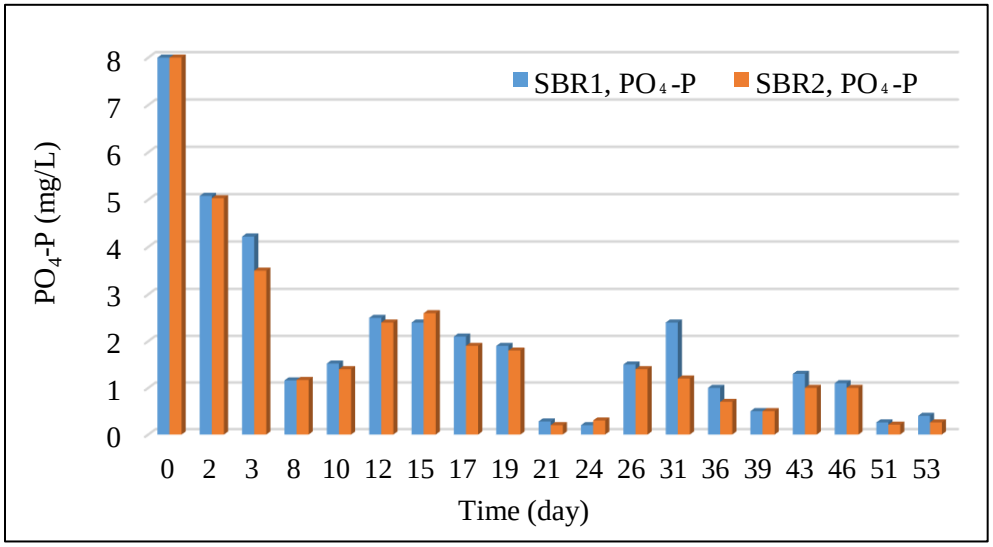

Fig.5-7. Phosphate concentrations in the effluent of SBR1 and SBR2

5.6.2. Nitrogen removal

Fig. 5-9 illustrates ammonia concentration in the effluent of SBR1 and SBR2 during the entire study. The removal of ammonia gradually increased, and a complete removal was observed when the aerobic granules were totally formed in the reactors. It was observed that the removal of ammonia was to some extent higher in SBR2 with respect to SBR1 which was compatible with the elevated nitrate concentration in SBR2 as shown in Fig.5-8, indicating a faster nitrification process in SBR2. The improved nitrification process in SBR2 could be ascribed to the added Fe^0 particles. Nitrite concentration was always less than 1 mg L^{-1} due to the fast oxidation process in the reactors. However, the reactors had a slow denitrification process as nitrate concentration increased in the effluent of the reactors. The reason could be attributed to the facultative heterotrophic bacteria which consume nitrate only when oxygen levels are depleted. Therefore, the biological reduction of nitrate (NO_3) to nitrogen gas (N_2) could not occurs under aerobic conditions. The pH value was monitored in the reactors and effluent tanks. During the nitrification process, bacteria use the alkalinity as a source of carbon [130]. Additionally, hydrogen ions and nitrous acid are produced during the oxidation of ammonia to nitrite [131].

Therefore, the nitrification process leads to a decrease in the pH value. In this study, despite of the higher nitrification process in SBR2 pH in the effluent of the SBR2 was 8.1 which is higher than pH value (7.7) in SBR1. The increased pH in SBR2 is attributed to the addition of Fe^0 which increases pH value according to the following equation.

$$3Fe^0 + O_2 + 4H_2O \rightarrow 6OH^- + 3Fe^{2+} + H_2 \quad (1)$$

Therefore, the addition of Fe^0 particles into the SBRs provide an alkaline medium which could stimulate the nitrification process by the ammonia-oxidizing bacteria (AOB).

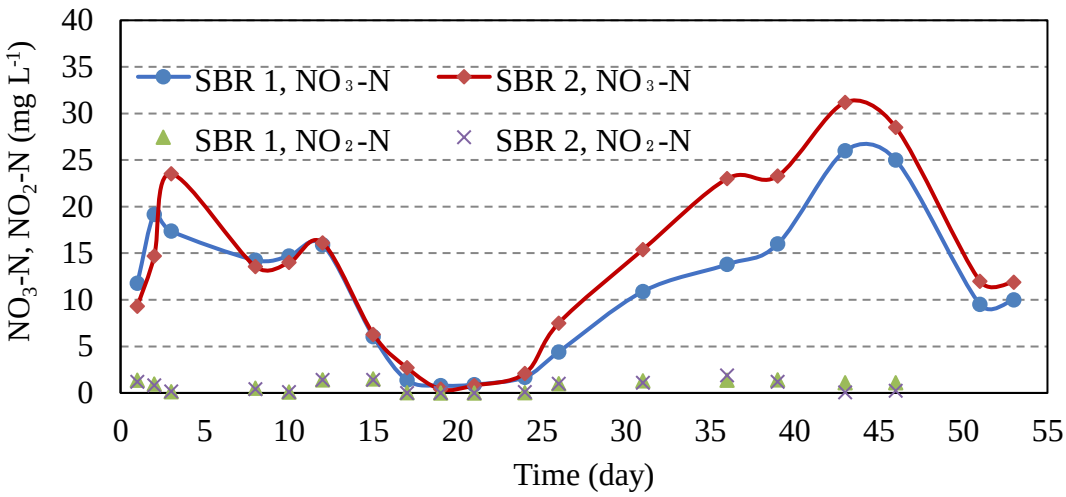

Fig. 5-8. Nitrate and nitrite concentrations in the effluent of SBR1 and SBR2.

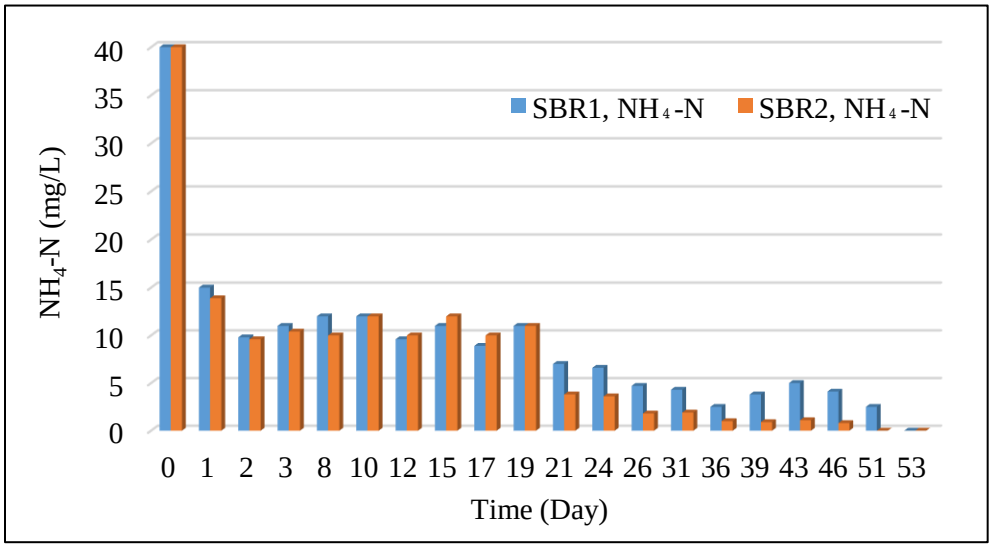

Fig. 5-9. Ammonia concentration in the effluent of the SBR1 and SBR2

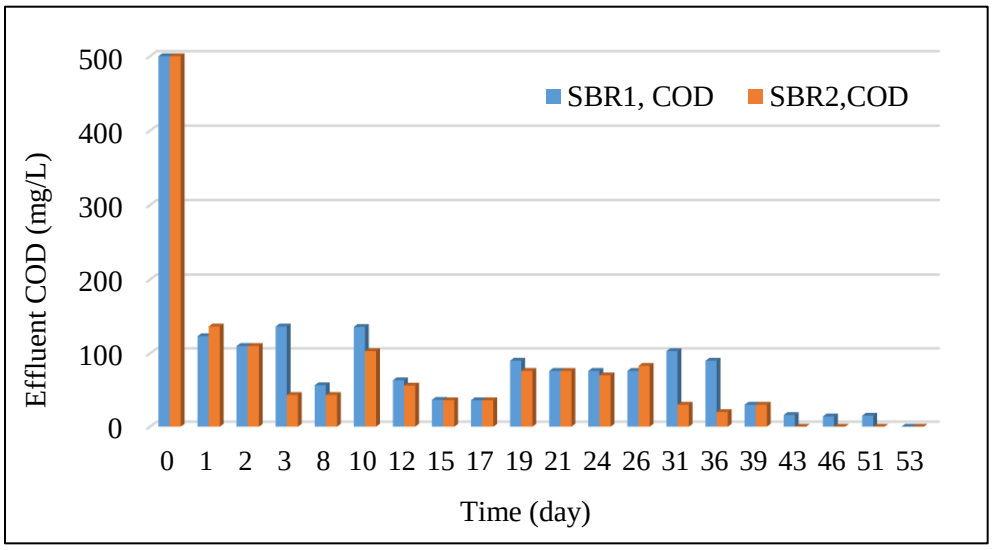

Fig. 5-10. COD concentrations in the effluent of SBR1 and SBR2

5.6.3. COD removal

The performance of the SBRs in removing organic matter was assessed by monitoring the COD concentration in the effluent of the reactors. The removal efficiency of COD in both reactors reached 88.7 % on day 12 and kept increasing significantly which reached 100 % at the end of the study as shown in Fig. 5-10.

The complete removal of COD was observed after the full formation of aerobic granules. After the addition of Fe^0 particles on day 24, a remarkable decrease in COD concentration was observed in the SBR2 where COD removal improved in R2 by 15 % compared to SBR1. The removal of COD remained better in R2 after the addition of Fe^0 until the end of the study.

The removal of COD using aerobic granular technology occurs by the direct decomposition by bacteria. Moreover, COD can be removed by the direct adsorption within the formed granules in the form of inorganic carbon compounds such as $CaCO_3$, $NaCO_3$, $MgCO_3$, K_2CO_3, H_2CO_3, HCO_3 and CO_2.

It was reported that a large amounts of $CaCO_3$ were found inside the aerobic granules and the crystalline form of $CaCO_3$ was the major mineral content in the aerobic granules [132]. These observations confirm the removal of carbon using aerobic granular technology as inorganic forms.

In addition, Fe^0 was found in our previous report to be an efficient adsorbent to remove the carbon from wastewater [133]. Moreover, the addition of Fe^0 stimulated bacterial growth which resulting in to improve the removal of COD by bacteria

5.7. Cycle study of the SBRs

To evaluate the performance of the operation stages or phases of the SBRs, a typical cycle study was conducted on the day 50. Samples were taken from the middle of the reactors throughout the cycle time.

The COD profiles in Fig. 5-11a and b. show the removal of COD during the four phases in SBR1 and SBR2. It was observed that the removal of COD mostly occurred in the static feeding phase (the first phase of operation). A complete COD removal was achieved in the reaction or aeration phase and the removal efficiency reached 100 % at the decanting phase. It was noticed that the removal of COD was faster in SBR2 during the cycle time as presented in Fig.5-11a and b.

Concerning phosphate removal during the cycle in SBR1, 40 % of phosphate was removed during the static feeding phase and increased to 60 % during the aeration/reaction phase and further increase was observed in the decanting phase which reached 78%.

Interestingly, the removal efficiency of phosphate reached 66% during the static feeding phase in SBR2 and increased to 81% during the aeration phase and finally reached 87% during the discharging phase, confirming that the removal of phosphate was much higher in SBR2 which may be attributed to the addition of Fe^0 particles.

The removal of ammonia reached 37% in the reactors during the static feeding phase. and the highest removal of ammonia was achieved during the aeration/reaction phase where it reached 57 % in the SBR1 and 77 % in the SBR2 during the aeration phase.

A complete removal of ammonia (100 %) was observed at the decanting phase in the effluent of SBR2. On the other hand, ammonia removal was 92 % in the effluent of SBR1. The ammonia cycle study proved that the removal of ammonia in the SBR2 was slightly higher and faster than that of the SBR.

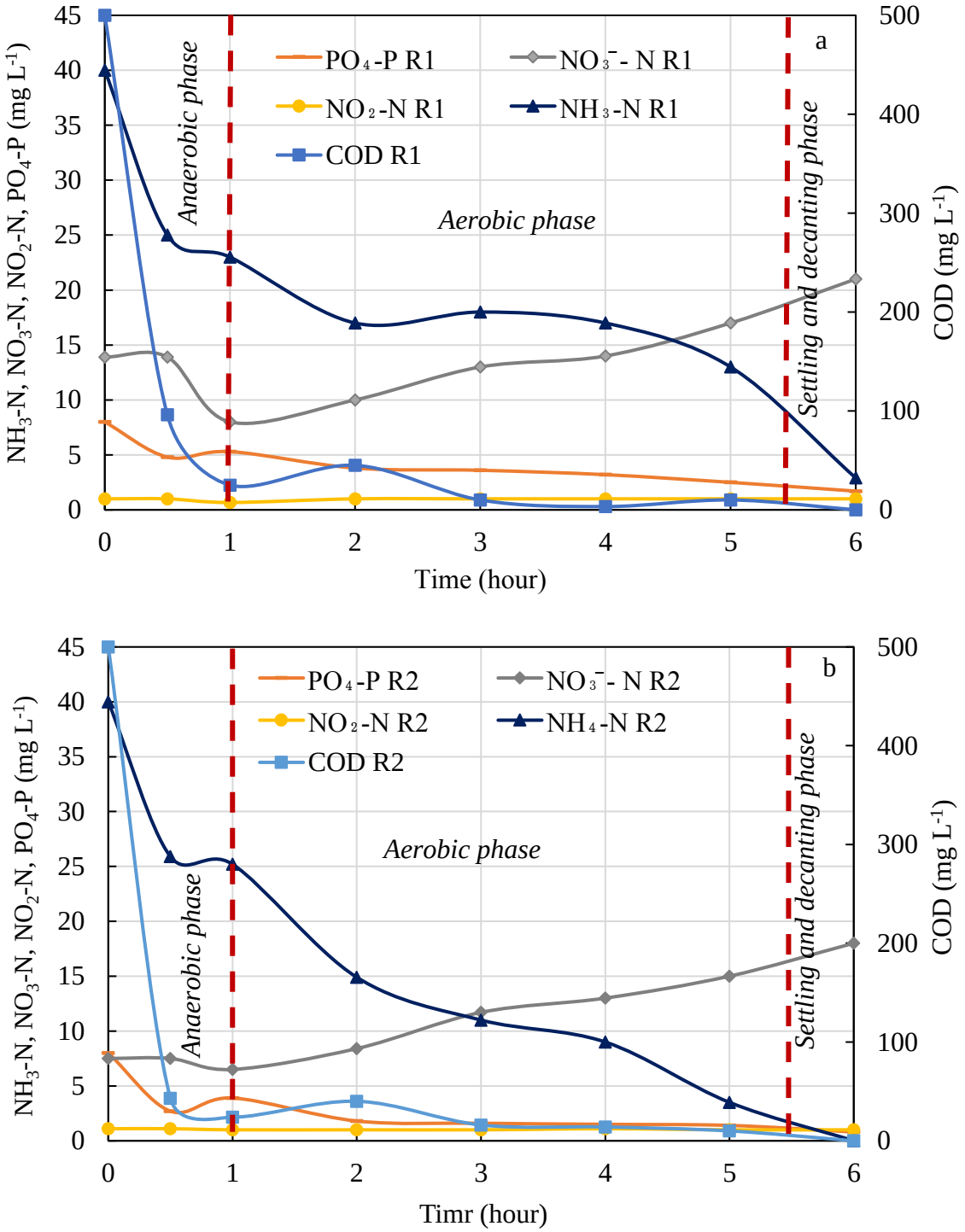

Fig. 5-11. Typical cycle study in (a) SBR1 and (b) SBR2 at the day of 50 depicts the removal behavior of NH_3-N, NO_3-N, NO_2-N, PO_4-P and COD in each pha

5.8. Conclusions

- In this study, the wastewater was efficiently treated, and the waste sludge totally converted to aerobic granules by developing two sequencing batch reactors.
- The removal of COD, NH_4-N, and PO_4-P increased with the time in the reactors, and a complete removal was observed after the formation of aerobic granules.
- The addition of Fe0 to R2 on day 24th slightly enhanced the removal of COD, PO4-P, and NH4-N by 8.12 %, 3.78%, and 7.1%, respectively.
- The addition of Fe0 into SBR2 significantly improved the generation of Carbohydrate and Protein by microbes, the main components of EPS, by 42% and 23%, respectively.
- Microbial community analysis confirmed that the addition of Fe^0 into SBR2 stimulated some bacterial types such as Rhizobiales and Xanthomonadales and inhibited others such as Clostridiales, confirming that the effect of Fe^0 on the bacterial growth was species dependent.
- The reactor which was augmented with Fe^0 had a start-up time of aerobic granulation (45 days) that was notably less than that for a reactor without augmentation (60 days).

CHAPTER 6

CONCLUSIONS AND RECOMMENDATIONS

Chapter 6: Conclusions and Recommendations

This chapter presents the significant findings obtained from three projects on water treatment and energy generation. Additionally, the chapter displays the future research plan, expected results, and impacts.

6.1. Major Findings and Recommendations

This thesis was grown based on the achieved research points and the new findings obtained from the implemented projects. The main achieved points in each project are summarized as follows:

In the first project which was related to the use of iron-based nanoparticles in water treatment

- The Fe^0 particles were successfully synthesized, stabilized, characterized, and tested for nitrate and phosphorus removal from contaminated water under different conditions.
- The stabilization of Fe^0 particles significantly improved their characteristics, appearing from the separated, and unaggregated particles.
- The stabilization of Fe^0, particularly with CMC, decreased the particle size from 100 to 10 nm.
- The stabilization of Fe^0 particles using four different polymers significantly improved the particle reactivity towards nitrate reduction as shown in following order; PVP/Fe^0 (238.9 mg/g) > PAA/Fe^0 (237.6 mg/g) > PSM/Fe^0 (233 mg/g) > CMC/Fe^0 (216 mg/g) > bare/Fe^0 (133 mg/g). This is one of the significant conclusions in this project that demonstrated PVP as an excellent polymer for Fe^0 stabilization, especially for reducible contaminants such as nitrate.
- The stabilization of Fe^0 particles, only with PAA, significantly enhanced phosphorus removal as presented in the following order; PAA/Fe^0 (78 mg/g) > bare/Fe^0 (61 mg/g) > PSM/Fe^0 (60 mg/g) > PVP/Fe^0 (58.4 mg/g) > CMC/Fe^0 (56.8 mg/g).
- This is another good conclusion obtained from this project that presented PAA as an excellent polymer for Fe^0 stabilization, especially for the adsorbable contaminants such as phosphorus

- The results of this research confirmed PVP/Fe^0 as the best stabilized type of iron for nitrate removal, but in case of phosphorus removal PAA was the best.
- In general, when it comes to remove both nitrate and phosphorus, the stabilized PAA/Fe^0 was the most efficient stabilized type of iron over the rest for simultaneous removal of nitrate and phosphorus with excellent removal rate at a wide range of pH, implying that PAA was the best polymer that improved both reduction and adsorption mechanisms of Fe^0 particles.

In the second project which was related to energy/methane generation

- The bare/Fe^0 particles were successfully coated using $Mg(OH)_2$ as a coating layer by following thermal deposition method.
- The bare and coated Fe^0 particles fully characterized using different techniques and the results confirmed the coating process of Fe^0 particles.
- The coated Fe^0 particles with $Mg(OH)_2$, synthesized at different coating ratios 5, 50, and 100% of Mg to Fe^0) were applied in the anaerobic digesters to increase methane generation from waste sludge.
- In the batch test experiments, the coated Fe^0 improved biogas and methane production by 25% and 46.6%, respectively at the optimum coating ratio of Mg to Fe (Mg/Fe^0:0.5) and at the optimum dosage (25 mg/gVS).
- Due to its high reactivity, which could be indicated by the high corrosion reaction, the addition of bare/Fe^0 particles in anaerobic digesters did not improve biogas/methane generation.
- The coating of bare/Fe^0 particles with $Mg(OH)_2$ reduced their corrosion rate in aqueous conditions, thereby decreased the released rate of iron ions and reduced the reductive force of Fe^0 particles, making them suitable additive for enhancing methane production during the anaerobic digestion process.
- The investigations from this project proved that the coated/Fe^0 enhanced the production of biogas and methane by increasing bacterial growth rate and serving as a buffering agent in the reactors

- Long-term investigation of methane generation was implemented using lab-scale semi-continuous system and the results proved the great performance of Mg/Fe^0 nanoparticles, coated at the optimum coating ratio based on batch test results (Mg/Fe^0:0.5), in improving methane generation rate. Methane production was enhanced two times in the presence of Mg/Fe^0 nanoparticles with respect to the control.

In the third project which was related to the use of Fe^0 nanoparticles in wastewater treatment and granulation process of waste sludge.

- The wastewater was treated, and the waste sludge totally converted to granules by developing two sequencing batch reactors.
- In the process, the reactors were simultaneously and automatically operated in a cyclic mode for sixty days with adding 10 mg/L of Fe^0 particles to the wastewater influent tank of reactor 2, whereas reactor 1 was operated as a control.
- In this project, the removal efficiency of COD, ammonia and phosphate increased with the time in the reactors, and almost complete removal was observed after the formation of aerobic granules.
- The addition of Fe^0 to reactor 2 on day 24th slightly increased the removal efficiency of contaminants from wastewater and stimulated the production of Extracellular Polymeric Substances (EPS), including protein and carbohydrate generation.
- The addition of Fe^0 to reactor 2 accelerated the formation of aerobic granules 15 days.
- The effect of Fe^0 particles on bacterial species in the reactor was genera dependent, for instance the addition of Fe^0 increased the growth of Rhizobiales and Xanthomonadales and decreased Clostridiales.

6.2. Future work

6.2.1. Purpose of proposed future research

✓ **Background of proposed research plan and Problem statement**

- Anaerobic digestion of waste activated sludge and other feedstocks is a promising technology and an alternative path to the non-environmentally friendly resources. Anaerobic digestion was, is and will be an efficient approach to convert organic matters (COD) of waste activated sludge and many other resources to energy (CH_4).
- Anaerobic digestion of activated sludge or any other feedstock consists three straight stages, first, hydrolysis of biological polymers with subsequent production of H_2, acetate, and other VFAs; second, conversion of these VFAs to H_2 and acetate by syntrophic bacteria under a low hydrogen partial pressure and finally conversion of acetate and H_2 to methane.
- The hydrolysis stage is recognized as the rate-limiting step in the anaerobic digestion. Therefore, problems such as slow hydrolysis process of organic matter and lower energy conversion efficiencies should be solved.
- Lower energy conversion efficiencies and slow hydrolysis processes of anaerobic digestion are the main obstruct to its actual application.

✓ **Purpose of proposed research**

The title of the proposed research is

"Two Stage Anaerobic Digestion Reactor for Efficient and Continues Methane Generation"

- The first purpose of the proposed research is to increase the production amount of methane by increasing the utilization of organic matter in anaerobic digestion reactor.
- The second purpose is to explore a new feedstock from the Crassulacean Acid Metabolism plants (CAMP). The new feedstock of CAMP will be mixed with the activated sludge to be used as a co-digestion feedstock. In this point of research, we are aiming to select one of the CAMP to be used as a co-digestion due to the following advantages of CAMP.
    1. CAMP have low lignin content; lignin is a key inhibitor of the cellulolytic activity for hydrolysis and the rate-limiting stage during the anaerobic digestion proses

The low lignin content of CAMP will make the hydrolysis process faster and easier than other plant species, therapy, improving the whole anerobic digestion process.

2. Furthermore, lignin and its derivatives can be highly toxic to methanogenic bacteria, so the low lignin content of CAM species offers some potential and significant advantages in terms of microbial conversion of plant biomass to biogas and other high-value products.
3. CAMP possess a specialized mode of photosynthesis systems that allows the stomata on the shoot surfaces to be closed during the day, thereby reducing water loss with CO_2 uptake from the atmosphere occurring mainly at night. This feature enable CAMP to grow relatively well in dry and poor-quality lands (deserts). Therefore, vast areas could be cultivated with CAMP to be a potential feedstocks for biogas and methane generation.

- The third purpose is to accelerate the hydrolysis step of the anaerobic digestion using special additives as trace elements necessary for the methanogenesis bacteria. Here, we will investigate the effect of special necessary nanoparticles on the anaerobic digestion process. The reason for using theses nanoparticles is to speed up the hydrolysis process, increase the soluble content of carbohydrate and protein, and improve the overall performance of the anaerobic digestion reactors.
- The fourth purpose is to design a two-stage anaerobic reactor using different microbiomes for each stage. The second stage which is fed with the liquid output stream from the former stage targets CH_4 and CO_2 generation. While the first stage aims to produce H_2, CO_2, and volatile fatty acids species. The first stage will contain the hydrolytic and fermentative microorganisms and the later stage will compose methanogens and fermentative microorganisms. The advantage of this design will allow H_2-producing bacteria to work in the first stage and H_2-consuming bacteria in the second stage. It is preferable to keep H_2-producing bacteria separate from H_2-consuming bacteria in the second reactor as the conversion of volatile fatty acids to H_2 and acetate requires a low hydrogen partial pressure.

Moreover, the production of volatile fatty acids and other acid types decreases pH value to less than 5 which could inhibit methane production as it requires a neutral pH from 6.6 – 7.8. Therefore, it is preferable to separate the acidogenic phase from the methanogenic phase. Furthermore, hydrolysis and acidogenic phases of anaerobic digestion can be enhanced by increasing the operating temperature; however, acetogenesis is adversely affected by high operating temperatures. Therefore, it is preferable to separate the acidogenic and methanogenic phases to optimize the temperature effect as described in Fig. 6-1.

- The fifth purpose is to develop and use a mathematical model to determine methane production potential and the maximum methane production rate for a two-stage anaerobic digestion reactor.

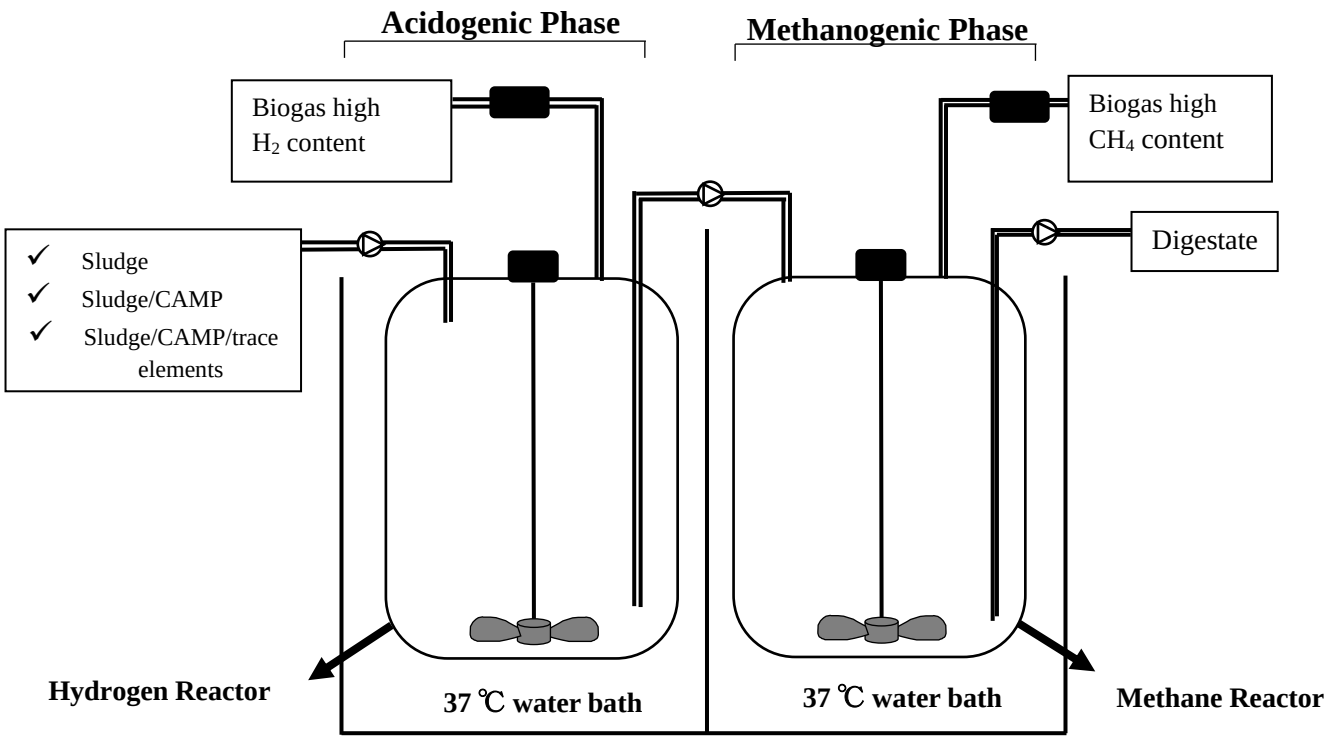

Fig.6-1 Two Stage Anerobic Digestion Reactor for Efficient and Continues Methane Generation

6.2.2. Proposed future research

The proposed plan is composed of several tasks as follows:

1. Review and preparation:
   - Review latest developments in anerobic digestion via literature survey, purchase and prepare essential materials for experimental works
2. Screening the potential of using CAMP as valuable feedstocks using the batch mode of anaerobic digestion and propose the most effective types for later investigations using two-stage anaerobic digestion mode.
3. Experimental setup and design of a two-stage anaerobic digestion reactor system for efficient and continuous generation of methane and operate it using the optimized mixture of activated sludge and CAMP.
4. Optimizing the reactor parameters such as temperature, pH, Hydraulic retention time (HRT), Organic loading rate (OLR) and determine the kinetic of microorganisms based on the HRT.
5. Discovering the role of adding special trace elements to the acidogenic phase and/or methanogenic phase in accelerating the hydrolysis process, microorganism kinetic rate and methane production.
6. Simulate and compare the results by developing a mathematical model.
7. Writing and submitting the research output to journals and conferences.

6.2.3. Expected results and impacts

1. Discovering a new feedstock competes with typical feedstocks for anaerobic digestion form Crassulacean Acid Metabolism plants.
2. Improving energy generation by separating the anaerobic digestion process, not only due to the energy produced as hydrogen but also because of the higher methane content.
3. Accelerating the methane generation process by feeding the hydrolyzed output of stage 1 to stage 2.
4. Demonstrating the optimal operating conditions of a two-stage anaerobic digestion reactor.
5. Improving the anaerobic digestion mechanism by adding special, cheap, and necessary trace elements for methanogens.
6. Developing a mathematical model to describe and predict the maximum methane production rate for a two-stage reactor.
7. The output of this work will offer solutions for the slow generation process of methane using different feedstocks, in addition, to provide lab-scale continues system of methane generation that could be applied on the large scale to effectively generate a clean source of energy, contributing to solving one of the global problems using methane as an alternative source of energy.

References

[1] F. Fu, D.D. Dionysiou, H. Liu, The use of zero-valent iron for groundwater remediation and wastewater treatment: a review, Journal of hazardous materials 267 (2014) 194-205.

[2] W.M. Lewis Jr, W.A. Wurtsbaugh, H.W. Paerl, Rationale for control of anthropogenic nitrogen and phosphorus to reduce eutrophication of inland waters, Environmental science & technology 45 (2011) 10300-10305.

[3] R.F. Follett, J.L. Hatfield, Nitrogen in the environment: sources, problems, and management, The Scientific World Journal 1 (2001) 920-926.

[4] A.M. Khalil, F.A. Memon, T.A. Tabish, D. Salmon, S. Zhang, D. Butler, Nanostructured porous graphene for efficient removal of emerging contaminants (pharmaceuticals) from water, Chemical Engineering Journal 398 (2020) 125440.

[5] L. El Hanache, L. Sundermann, B. Lebeau, J. Toufaily, T. Hamieh, T.J. Daou, Surfactant-modified MFI-type nanozeolites: Super-adsorbents for nitrate removal from contaminated water, Microporous and Mesoporous Materials 283 (2019) 1-13.

[6] E. Eroglu, V. Agarwal, M. Bradshaw, X. Chen, S.M. Smith, C.L. Raston, K.S. Iyer, Nitrate removal from liquid effluents using microalgae immobilized on chitosan nanofiber mats, Green Chemistry 14 (2012) 2682-2685.

[7] M.A. Tofighy, T. Mohammadi, Nitrate removal from water using functionalized carbon nanotube sheets, Chemical Engineering Research and Design 90 (2012) 1815-1822.

[8] Y. Liu, J. Wang, Reduction of nitrate by zero valent iron (ZVI)-based materials: A review, Science of The Total Environment (2019).

[9] A.M. Khalil, O. Eljamal, S. Jribi, N. Matsunaga, Promoting nitrate reduction kinetics by nanoscale zero valent iron in water via copper salt addition, Chemical Engineering Journal 287 (2016) 367-380.

[10] N.A. Khan, S.U. Khan, S. Ahmed, I.H. Farooqi, A. Dhingra, A. Hussain, F. Changani, Applications of nanotechnology in water and wastewater treatment: A review, Asian Journal of Water, Environment and Pollution 16 (2019) 81-86.

[11] L. Otero-González, J.A. Field, R. Sierra-Alvarez, Inhibition of anaerobic wastewater treatment after long-term exposure to low levels of CuO nanoparticles, Water research 58 (2014) 160-168.

[12] H. Mu, Y. Chen, Long-term effect of ZnO nanoparticles on waste activated sludge anaerobic digestion, Water research 45 (2011) 5612-5620.

[13] H. Mu, Y. Chen, N. Xiao, Effects of metal oxide nanoparticles (TiO2, Al2O3, SiO2 and ZnO) on waste activated sludge anaerobic digestion, Bioresource technology 102 (2011) 10305-10311.

[14] N.M. Duc, Effects of CeO2 and ZnO nanoparticles on anaerobic digestion and toxicity of digested sludge, Thailand: Asian Institute of Technology (2013).

[15] E. Casals, R. Barrena, A. García, E. González, L. Delgado, M. Busquets‐Fité, X. Font, J. Arbiol, P. Glatzel, K. Kvashnina, Programmed iron oxide nanoparticles disintegration in anaerobic digesters boosts biogas production, Small 10 (2014) 2801-2808.

[16] F. He, D. Zhao, Preparation and characterization of a new class of starch-stabilized bimetallic nanoparticles for degradation of chlorinated hydrocarbons in water, Environmental science & technology 39 (2005) 3314-3320.

[17] S. Laurent, D. Forge, M. Port, A. Roch, C. Robic, L. Vander Elst, R.N. Muller, Magnetic iron oxide nanoparticles: synthesis, stabilization, vectorization, physicochemical characterizations, and biological applications, Chemical reviews 108 (2008) 2064-2110.
[18] Y. Zhang, Y. Li, J. Li, L. Hu, X. Zheng, Enhanced removal of nitrate by a novel composite: nanoscale zero valent iron supported on pillared clay, Chemical Engineering Journal 171 (2011) 526-531.
[19] Y.H. Liou, S.-L. Lo, C.-J. Lin, W.H. Kuan, S.C. Weng, Chemical reduction of an unbuffered nitrate solution using catalyzed and uncatalyzed nanoscale iron particles, Journal of Hazardous Materials 127 (2005) 102-110.
[20] D. Sparis, C. Mystrioti, A. Xenidis, N. Papassiopi, Reduction of nitrate by copper-coated ZVI nanoparticles, Desalination and Water Treatment 51 (2013) 2926-2933.
[21] Y.-P. Sun, X.-Q. Li, W.-X. Zhang, H.P. Wang, A method for the preparation of stable dispersion of zero-valent iron nanoparticles, Colloids and Surfaces A: Physicochemical and Engineering Aspects 308 (2007) 60-66.
[22] A.M. Khalil, O. Eljamal, T.W. Amen, Y. Sugihara, N. Matsunaga, Optimized nano-scale zero-valent iron supported on treated activated carbon for enhanced nitrate and phosphate removal from water, Chemical Engineering Journal 309 (2017) 349-365.
[23] H. ZHANG, Z.-h. JIN, H. Lu, C.-h. QIN, Synthesis of nanoscale zero-valent iron supported on exfoliated graphite for removal of nitrate, Transactions of Nonferrous Metals Society of China 16 (2006) s345-s349.
[24] R. Mokete, O. Eljamal, Y. Sugihara, Exploration of the reactivity of nanoscale zero-valent iron (NZVI) associated nanoparticles in diverse experimental conditions, Chemical Engineering and Processing-Process Intensification 150 (2020) 107879.
[25] S. Takami, O. Eljamal, A.M. Khalil, R. Eljamal, N. Matsunaga, Development of continuous system based on nanoscale zero valent iron particles for phosphorus removal, Journal of JSCE 7 (2019) 30-42.
[26] Y. Cho, S.-I. Choi, Degradation of PCE, TCE and 1, 1, 1-TCA by nanosized FePd bimetallic particles under various experimental conditions, Chemosphere 81 (2010) 940-945.
[27] S.H. Joo, D. Zhao, Destruction of lindane and atrazine using stabilized iron nanoparticles under aerobic and anaerobic conditions: effects of catalyst and stabilizer, Chemosphere 70 (2008) 418-425.
[28] F. He, D. Zhao, C. Paul, Field assessment of carboxymethyl cellulose stabilized iron nanoparticles for in situ destruction of chlorinated solvents in source zones, Water research 44 (2010) 2360-2370.
[29] C. Su, R.W. Puls, T.A. Krug, M.T. Watling, S.K. O'Hara, J.W. Quinn, N.E. Ruiz, A two and half-year-performance evaluation of a field test on treatment of source zone tetrachloroethene and its chlorinated daughter products using emulsified zero valent iron nanoparticles, Water research 46 (2012) 5071-5084.
[30] R. Eljamal, O. Eljamal, A.M. Khalil, B.B. Saha, N. Matsunaga, Improvement of the chemical synthesis efficiency of nano-scale zero-valent iron particles, Journal of environmental chemical engineering 6 (2018) 4727-4735.

[31] Y.-b. Hu, M. Zhang, R. Qiu, X.-y. Li, Encapsulating nanoscale zero-valent iron with a soluble Mg (OH) 2 shell for improved mobility and controlled reactivity release, Journal of Materials Chemistry A 6 (2018) 2517-2526.
[32] J. Luo, L. Feng, Y. Chen, X. Li, H. Chen, N. Xiao, D. Wang, Stimulating short-chain fatty acids production from waste activated sludge by nano zero-valent iron, Journal of biotechnology 187 (2014) 98-105.
[33] A. Ferrari, S. Lombardi, A. Signoroni, Bacterial colony counting with convolutional neural networks in digital microbiology imaging, Pattern Recognition 61 (2017) 629-640.
[34] J. Wu, H.-m. Zhou, H.-z. Li, P.-c. Zhang, J. Jiang, Impacts of hydrodynamic shear force on nucleation of flocculent sludge in anaerobic reactor, Water research 43 (2009) 3029-3036.
[35] B. Fr, T. Griebe, P. Nielsen, Enzymatic activity in the activated-sludge floc matrix, Applied microbiology and biotechnology 43 (1995) 755-761.
[36] O.H. Lowry, N.J. Rosebrough, A.L. Farr, R.J. Randall, Protein measurement with the Folin phenol reagent, Journal of biological chemistry 193 (1951) 265-275.
[37] W.E. Federation, A. Association, Standard methods for the examination of water and wastewater, American Public Health Association (APHA): Washington, DC, USA (2005).
[38] A. American Public Health, A. American Water Works, F. Water Environment, Standard methods for the examination of water and wastewater, APHA-AWWA-WEF, Washington, D.C., 1998.
[39] H. Pyenson, P. Tracy, A 1, 10—phenanthroline method for the determination of iron in powdered milk, Journal of dairy science 28 (1945) 401-412.
[40] O. Eljamal, K. Sasaki, T. Hirajima, Sorption kinetic of arsenate as water contaminant on zero valent iron, (2013).
[41] C.-B. Wang, W.-x. Zhang, Synthesizing nanoscale iron particles for rapid and complete dechlorination of TCE and PCBs, Environmental science & technology 31 (1997) 2154-2156.
[42] G. Sheng, P. Yang, Y. Tang, Q. Hu, H. Li, X. Ren, B. Hu, X. Wang, Y. Huang, New insights into the primary roles of diatomite in the enhanced sequestration of UO22+ by zerovalent iron nanoparticles: an advanced approach utilizing XPS and EXAFS, Applied Catalysis B: Environmental 193 (2016) 189-197.
[43] M. Stefaniuk, P. Oleszczuk, Y.S. Ok, Review on nano zerovalent iron (nZVI): from synthesis to environmental applications, Chemical Engineering Journal 287 (2016) 618-632.
[44] O. Eljamal, A.M. Khalil, Y. Sugihara, N. Matsunaga, Phosphorus removal from aqueous solution by nanoscale zero valent iron in the presence of copper chloride, Chemical Engineering Journal 293 (2016) 225-231.
[45] H. Song, E.R. Carraway, Catalytic hydrodechlorination of chlorinated ethenes by nanoscale zero-valent iron, Applied Catalysis B: Environmental 78 (2008) 53-60.
[46] Q. Zhang, D. Zhao, S. Feng, Y. Wang, J. Jin, A. Alsaedi, T. Hayat, C. Chen, Synthesis of nanoscale zero-valent iron loaded chitosan for synergistically enhanced removal of U (VI) based on adsorption and reduction, Journal of colloid and interface science 552 (2019) 735-743.

[47] X. Zhao, W. Liu, Z. Cai, B. Han, T. Qian, D. Zhao, An overview of preparation and applications of stabilized zero-valent iron nanoparticles for soil and groundwater remediation, Water research 100 (2016) 245-266.
[48] F. He, D. Zhao, Manipulating the size and dispersibility of zerovalent iron nanoparticles by use of carboxymethyl cellulose stabilizers, Environmental science & technology 41 (2007) 6216-6221.
[49] Y.T. Lin, Y.W. Liu, Y.J. Cheng, H.Y. Huang, Analyses of sulfonamide antibiotics by a successive anion - and cation - selective injection coupled to microemulsion electrokinetic chromatography, Electrophoresis 31 (2010) 2260-2266.
[50] W. Jiao, Y. Song, D. Zhang, G. Chang, H. Fan, Y. Liu, Nanoscale zero-valent iron modified with carboxymethyl cellulose in an impinging stream-rotating packed bed for the removal of lead (II), Advanced Powder Technology 30 (2019) 2251-2261.
[51] B. Liang, Y. Xie, Z. Fang, E.P. Tsang, Assessment of the transport of polyvinylpyrrolidone-stabilised zero-valent iron nanoparticles in a silica sand medium, Journal of nanoparticle research 16 (2014) 1-11.
[52] O. Eljamal, I.P. Thompson, I. Maamoun, T. Shubair, K. Eljamal, K. Lueangwattanapong, Y. Sugihara, Investigating the design parameters for a permeable reactive barrier consisting of nanoscale zero-valent iron and bimetallic iron/copper for phosphate removal, Journal of Molecular Liquids 299 (2020) 112144.
[53] A. McPherson, M. Goltz, A. Agrawal, Pollutant Degradation by Nanoscale Zero Valent Iron (nZVI): Role of Polyelectrolyte Stabilization and Catalytic Modification on nZVI Performance, Interactions of Nanomaterials with Emerging Environmental Contaminants, ACS Publications2013, pp. 159-191.
[54] S. Sepehri, M. Heidarpour, J. Abedi-Koupai, Nitrate removal from aqueous solution using natural zeolite-supported zero-valent iron nanoparticles, Soil and Water Research 9 (2014) 224-232.
[55] Z. Jiang, L. Lv, W. Zhang, Q. Du, B. Pan, L. Yang, Q. Zhang, Nitrate reduction using nanosized zero-valent iron supported by polystyrene resins: role of surface functional groups, Water research 45 (2011) 2191-2198.
[56] R. Chitrakar, S. Tezuka, A. Sonoda, K. Sakane, K. Ooi, T. Hirotsu, Phosphate adsorption on synthetic goethite and akaganeite, Journal of colloid and interface science 298 (2006) 602-608.
[57] L. Zeng, X. Li, J. Liu, Adsorptive removal of phosphate from aqueous solutions using iron oxide tailings, Water research 38 (2004) 1318-1326.
[58] J. Xiong, Z. He, Q. Mahmood, D. Liu, X. Yang, E. Islam, Phosphate removal from solution using steel slag through magnetic separation, Journal of hazardous materials 152 (2008) 211-215.
[59] T. Almeelbi, A. Bezbaruah, Aqueous phosphate removal using nanoscale zero-valent iron, Nanotechnology for Sustainable Development, Springer2012, pp. 197-210.
[60] J. Adusei-Gyamfi, V. Acha, Carriers for nano zerovalent iron (nZVI): Synthesis, application and efficiency, RSC advances 6 (2016) 91025-91044.
[61] B. Kamarehie, E. Aghaalib, S. Musavic, S. Hashemid, A. Jafaria, Nitrate removal from aqueous solutions using granular activated carbon modified with iron nanoparticles, atmosphere 1 (2018) 4.

[62] H. Dong, K. Ahmad, G. Zeng, Z. Li, G. Chen, Q. He, Y. Xie, Y. Wu, F. Zhao, Y. Zeng, Influence of fulvic acid on the colloidal stability and reactivity of nanoscale zero-valent iron, Environmental Pollution 211 (2016) 363-369.
[63] L. Wang, T.N. Aziz, L. Francis, Determining the limits of anaerobic co-digestion of thickened waste activated sludge with grease interceptor waste, Water research 47 (2013) 3835-3844.
[64] J. Ariunbaatar, A. Panico, G. Esposito, F. Pirozzi, P.N. Lens, Pretreatment methods to enhance anaerobic digestion of organic solid waste, Applied energy 123 (2014) 143-156.
[65] X. Fonoll, S. Astals, J. Dosta, J. Mata-Alvarez, Anaerobic co-digestion of sewage sludge and fruit wastes: evaluation of the transitory states when the co-substrate is changed, Chemical Engineering Journal 262 (2015) 1268-1274.
[66] Y.Y. Choong, I. Norli, A.Z. Abdullah, M.F. Yhaya, Impacts of trace element supplementation on the performance of anaerobic digestion process: A critical review, Bioresource technology 209 (2016) 369-379.
[67] M.A. Ganzoury, N.K. Allam, Impact of nanotechnology on biogas production: a mini-review, Renewable and Sustainable Energy Reviews 50 (2015) 1392-1404.
[68] A. García, L. Delgado, J.A. Torà, E. Casals, E. González, V. Puntes, X. Font, J. Carrera, A. Sánchez, Effect of cerium dioxide, titanium dioxide, silver, and gold nanoparticles on the activity of microbial communities intended in wastewater treatment, Journal of hazardous materials 199 (2012) 64-72.
[69] J. Gonzalez-Estrella, R. Sierra-Alvarez, J.A. Field, Toxicity assessment of inorganic nanoparticles to acetoclastic and hydrogenotrophic methanogenic activity in anaerobic granular sludge, Journal of hazardous materials 260 (2013) 278-285.
[70] S. Karri, R. Sierra ‐ Alvarez, J.A. Field, Zero valent iron as an electron ‐ donor for methanogenesis and sulfate reduction in anaerobic sludge, Biotechnology and Bioengineering 92 (2005) 810-819.
[71] F. Suanon, Q. Sun, M. Li, X. Cai, Y. Zhang, Y. Yan, C.-P. Yu, Application of nanoscale zero valent iron and iron powder during sludge anaerobic digestion: Impact on methane yield and pharmaceutical and personal care products degradation, Journal of hazardous materials 321 (2017) 47-53.
[72] S. Jiang, S. Park, Y. Yoon, J.-H. Lee, W.-M. Wu, N. Phuoc Dan, M.J. Sadowsky, H.-G. Hur, Methanogenesis facilitated by geobiochemical iron cycle in a novel syntrophic methanogenic microbial community, Environmental science & technology 47 (2013) 10078-10084.
[73] X.-q. Li, D.G. Brown, W.-x. Zhang, Stabilization of biosolids with nanoscale zero-valent iron (nZVI), Journal of nanoparticle research 9 (2007) 233-243.
[74] L. Su, X. Shi, G. Guo, A. Zhao, Y. Zhao, Stabilization of sewage sludge in the presence of nanoscale zero-valent iron (nZVI): abatement of odor and improvement of biogas production, Journal of Material Cycles and Waste Management 15 (2013) 461-468.
[75] Y. Yang, J. Guo, Z. Hu, Impact of nano zero valent iron (NZVI) on methanogenic activity and population dynamics in anaerobic digestion, Water research 47 (2013) 6790-6800.

[76] T.W. Amen, O. Eljamal, A.M. Khalil, Y. Sugihara, N. Matsunaga, Methane yield enhancement by the addition of new novel of iron and copper-iron bimetallic nanoparticles, Chemical Engineering and Processing-Process Intensification 130 (2018) 253-261.
[77] K. Chaithawiwat, A. Vangnai, J.M. McEvoy, B. Pruess, S. Krajangpan, E. Khan, Impact of nanoscale zero valent iron on bacteria is growth phase dependent, Chemosphere 144 (2016) 352-359.
[78] M.L. Sacca, C. Fajardo, M. Martinez-Gomariz, G. Costa, M. Nande, M. Martin, Molecular stress responses to nano-sized zero-valent iron (nZVI) particles in the soil bacterium Pseudomonas stutzeri, Plos one 9 (2014) e89677.
[79] C. Lee, J.Y. Kim, W.I. Lee, K.L. Nelson, J. Yoon, D.L. Sedlak, Bactericidal effect of zero-valent iron nanoparticles on Escherichia coli, Environmental science & technology 42 (2008) 4927-4933.
[80] Y.-X. Huang, J. Guo, C. Zhang, Z. Hu, Hydrogen production from the dissolution of nano zero valent iron and its effect on anaerobic digestion, Water research 88 (2016) 475-480.
[81] Y. Wu, S. Wang, D. Liang, N. Li, Conductive materials in anaerobic digestion: From mechanism to application, Bioresource technology 298 (2020) 122403.
[82] X. Hao, J. Wei, M.C. van Loosdrecht, D. Cao, Analysing the mechanisms of sludge digestion enhanced by iron, Water research 117 (2017) 58-67.
[83] H. Watling, D. Collinson, D. Shiers, C. Bryan, E. Watkin, Effects of pH, temperature and solids loading on microbial community structure during batch culture on a polymetallic ore, Minerals Engineering 48 (2013) 68-76.
[84] M. Zhang, J. Li, Y. Wang, Impact of biochar-supported zerovalent iron nanocomposite on the anaerobic digestion of sewage sludge, Environmental Science and Pollution Research 26 (2019) 10292-10305.
[85] M.I. Tanimu, T.I.M. Ghazi, M.R. Harun, A. Idris, Effect of feed loading on biogas methane production in batch mesophilic anaerobic digesters treating food waste, International Journal 5 (2014).
[86] R.Z. Gaur, S. Suthar, Anaerobic digestion of activated sludge, anaerobic granular sludge and cow dung with food waste for enhanced methane production, Journal of Cleaner Production 164 (2017) 557-566.
[87] M. Sun, B. Liu, K. Yanagawa, N.T. Ha, R. Goel, M. Terashima, H. Yasui, Effects of low pH conditions on decay of methanogenic biomass, Water research 179 (2020) 115883.
[88] C. Zhao, H. Mu, Y. Zhao, L. Wang, B. Zuo, Microbial characteristics analysis and kinetic studies on substrate composition to methane after microbial and nutritional regulation of fruit and vegetable wastes anaerobic digestion, Bioresource technology 249 (2018) 315-321.
[89] Y. Wei, R.T. Van Houten, A.R. Borger, D.H. Eikelboom, Y. Fan, Minimization of excess sludge production for biological wastewater treatment, Water Research 37 (2003) 4453-4467.
[90] S.S. Adav, D.-J. Lee, K.-Y. Show, J.-H. Tay, Aerobic granular sludge: recent advances, Biotechnology advances 26 (2008) 411-423.

[91] C. Wan, P. Zhang, D.-J. Lee, X. Yang, X. Liu, S. Sun, X. Pan, Disintegration of aerobic granules: role of second messenger cyclic di-GMP, Bioresource technology 146 (2013) 330-335.
[92] T. Seviour, B.C. Donose, M. Pijuan, Z. Yuan, Purification and conformational analysis of a key exopolysaccharide component of mixed culture aerobic sludge granules, Environmental science & technology 44 (2010) 4729-4734.
[93] B.P. Moy, J.H. Tay, S.K. Toh, Y. Liu, S.L. Tay, High organic loading influences the physical characteristics of aerobic sludge granules, Letters in Applied Microbiology 34 (2002) 407-412.
[94] G. Yilmaz, U. Bozkurt, K.A. Magden, Effect of iron ions (Fe 2+, Fe 3+) on the formation and structure of aerobic granular sludge, Biodegradation 28 (2017) 53-68.
[95] G. Lettinga, J. Field, J. Van Lier, G. Zeeman, L.H. Pol, Advanced anaerobic wastewater treatment in the near future, Water Science and Technology 35 (1997) 5-12.
[96] G. Lettinga, A. Van Velsen, S.d. Hobma, W. De Zeeuw, A. Klapwijk, Use of the upflow sludge blanket (USB) reactor concept for biological wastewater treatment, especially for anaerobic treatment, Biotechnology and bioengineering 22 (1980) 699-734.
[97] J.R. Campos, E. Foresti, R.D. Camacho, Anaerobic wastewater treatment in the food processing industry: two case studies, Water Science and Technology 18 (1986) 87-97.
[98] L. Nunez, B. Martinez, Anaerobic treatment of slaughterhouse wastewater in an expanded granular sludge bed (EGSB) reactor, Water Science and Technology 40 (1999) 99-106.
[99] W.-Q. Guo, N.-Q. Ren, X.-J. Wang, W.-S. Xiang, Z.-H. Meng, J. Ding, Y.-Y. Qu, L.-S. Zhang, Biohydrogen production from ethanol-type fermentation of molasses in an expanded granular sludge bed (EGSB) reactor, International Journal of Hydrogen Energy 33 (2008) 4981-4988.
[100] X. Quan, M. Zhang, P.G. Lawlor, Z. Yang, X. Zhan, Nitrous oxide emission and nutrient removal in aerobic granular sludge sequencing batch reactors, Water research 46 (2012) 4981-4990.
[101] Y. Liu, J.-H. Tay, State of the art of biogranulation technology for wastewater treatment, Biotechnology advances 22 (2004) 533-563.
[102] J. Zhu, P.A. Wilderer, Effect of extended idle conditions on structure and activity of granular activated sludge, Water Research 37 (2003) 2013-2018.
[103] C. Wan, X. Yang, D.-J. Lee, X.-Y. Wang, Q. Yang, X. Pan, Aerobic granulation of aggregating consortium X9 isolated from aerobic granules and role of cyclic di-GMP, Bioresource Technology 152 (2014) 557-561.
[104] Q. Kong, H.H. Ngo, L. Shu, R.-s. Fu, C.-h. Jiang, M.-s. Miao, Enhancement of aerobic granulation by zero-valent iron in sequencing batch airlift reactor, Journal of hazardous materials 279 (2014) 511-517.
[105] J.-H. Tay, S. Pan, Y. He, S.T.L. Tay, Effect of Organic Loading Rate on Aerobic Granulation. I: Reactor Performance, Journal of Environmental Engineering 130 (2004) 1094-1101.
[106] L.S. Clesceri, A.E. Greenberg, A.D. Eaton, E.W. Rice, M.A.H. Franson, Standard methodsfor the examination of water and wastewater, 2005.

[107] H.-L. Jiang, J.-H. Tay, Y. Liu, S.T.-L. Tay, Ca 2+ augmentation for enhancement of aerobically grown microbial granules in sludge blanket reactors, Biotechnology letters 25 (2003) 95-99.
[108] S. Wang, W. Shi, S. Yu, X. Yi, X. Yang, Formation of aerobic granules by Mg 2+ and Al 3+ augmentation in sequencing batch airlift reactor at low temperature, Bioprocess and biosystems engineering 35 (2012) 1049-1055.
[109] L. Liu, D.-W. Gao, M. Zhang, Y. Fu, Comparison of Ca2+ and Mg2+ enhancing aerobic granulation in SBR, Journal of Hazardous Materials 181 (2010) 382-387.
[110] X.M. Li, Q.Q. Liu, Q. Yang, L. Guo, G.M. Zeng, J.M. Hu, W. Zheng, Enhanced aerobic sludge granulation in sequencing batch reactor by Mg2+ augmentation, Bioresour Technol 100 (2009) 64-67.
[111] W. Hao, Y. Li, J. Lv, L. Chen, J. Zhu, The biological effect of metal ions on the granulation of aerobic granular activated sludge, Journal of Environmental Sciences 44 (2016) 252-259.
[112] H.Q. Yu, H.H.P. Fang, J.H. Tay, Effects of Fe2+ on sludge granulation in upflow anaerobic sludge blanket reactors, Water Science and Technology 41 (2000) 199-205.
[113] J.E. Burgess, J. Quarmby, T. Stephenson, Role of micronutrients in activated sludge-based biotreatment of industrial effluents, Biotechnol Adv 17 (1999) 49-70.
[114] O. Eljamal, K. Sasaki, T. Hirajima, Numerical simulation for reactive solute transport of arsenic in permeable reactive barrier column including zero-valent iron, Applied Mathematical Modelling 35 (2011) 5198-5207.
[115] I. Maamoun, O. Eljamal, A.M.E. Khalil, Y. Sugihara, N. Matsunaga, Phosphate Removal Through Nano-Zero-Valent Iron Permeable Reactive Barrier; Column Experiment and Reactive Solute Transport Modeling, Transport in Porous Media (2018).
[116] M.M. Scherer, S. Richter, R.L. Valentine, P.J. Alvarez, Chemistry and microbiology of permeable reactive barriers for in situ groundwater clean up, Critical reviews in microbiology 26 (2000) 221-264.
[117] W. Zhang, L. Chen, H. Chen, S.-Q. Xia, The effect of Fe0/Fe2+/Fe3+ on nitrobenzene degradation in the anaerobic sludge, Journal of hazardous materials 143 (2007) 57-64.
[118] N. Rosman, Efficiency of aerobic granulation technology in treating high strength soy sauce wastewater, Sains Malays 43 (2014) 1485-1490.
[119] H. Dong, L. Li, Y. Lu, Y. Cheng, Y. Wang, Q. Ning, B. Wang, L. Zhang, G. Zeng, Integration of nanoscale zero-valent iron and functional anaerobic bacteria for groundwater remediation: a review, Environment international 124 (2019) 265-277.
[120] Z. Wang, L. Liu, J. Yao, W. Cai, Effects of extracellular polymeric substances on aerobic granulation in sequencing batch reactors, Chemosphere 63 (2006) 1728-1735.
[121] X.-M. Li, Q.-Q. Liu, Q. Yang, L. Guo, G.-M. Zeng, J.-M. Hu, W. Zheng, Enhanced aerobic sludge granulation in sequencing batch reactor by Mg2+ augmentation, Bioresource technology 100 (2009) 64-67.
[122] X. Wang, M. Hu, Y. Xia, X. Wen, K. Ding, Pyrosequencing analysis of bacterial diversity in 14 wastewater treatment systems in China, Appl. Environ. Microbiol. 78 (2012) 7042-7047.
[123] V. Nagaraj, L. Skillman, G. Ho, D. Li, A. Gofton, Characterisation and comparison of bacterial communities on reverse osmosis membranes of a full-scale desalination plant by bacterial 16S rRNA gene metabarcoding, NPJ biofilms and microbiomes 3 (2017) 13.

[124] C.H. Neoh, P.Y. Yung, Z.Z. Noor, M.H. Razak, A. Aris, M.F.M. Din, Z. Ibrahim, Correlation between microbial community structure and performances of membrane bioreactor for treatment of palm oil mill effluent, Chemical Engineering Journal 308 (2017) 656-663.
[125] J. Luo, P. Lv, J. Zhang, A.G. Fane, D. McDougald, S.A. Rice, Succession of biofilm communities responsible for biofouling of membrane bio-reactors (MBRs), PloS one 12 (2017) e0179855.
[126] K. Calderón, B. Rodelas, N. Cabirol, J. González-López, A. Noyola, Analysis of microbial communities developed on the fouling layers of a membrane-coupled anaerobic bioreactor applied to wastewater treatment, Bioresource technology 102 (2011) 4618-4627.
[127] A. Mañas, B. Biscans, M. Spérandio, Biologically induced phosphorus precipitation in aerobic granular sludge process, Water research 45 (2011) 3776-3786.
[128] W. Huang, W. Huang, H. Li, Z. Lei, Z. Zhang, J.H. Tay, D.-J. Lee, Species and distribution of inorganic and organic phosphorus in enhanced phosphorus removal aerobic granular sludge, Bioresource technology 193 (2015) 549-552.
[129] O. Eljamal, J. Okawauchi, K. Hiramatsu, Removal of phosphorus from water using marble dust as sorbent material, Journal of Environmental Protection 3 (2012) 709.
[130] E. Padan, E. Bibi, M. Ito, T.A. Krulwich, Alkaline pH homeostasis in bacteria: new insights, Biochimica et biophysica acta (BBA)-biomembranes 1717 (2005) 67-88.
[131] D. Cheddie, Ammonia as a hydrogen source for fuel cells: a review, Hydrogen energy-challenges and perspectives, IntechOpen2012.
[132] Y.-Q. Liu, G.-H. Lan, P. Zeng, Excessive precipitation of CaCO 3 as aragonite in a continuous aerobic granular sludge reactor, Applied microbiology and biotechnology 99 (2015) 8225-8234.
[133] T.W. Amen, O. Eljamal, A.M. Khalil, N. Matsunaga, Evaluation of sulfate-containing sludge stabilization and the alleviation of methanogenesis inhibitation at mesophilic temperature, Journal of Water Process Engineering 25 (2018) 212-221.